國立臺灣大學工學院化學工程研究所

博士論文

Department of Chemical Engineering

College of Engineering

National Taiwan University

Doctoral Dissertation

利用第一原理計算預測純物質與混合物
之熱力學性質與相平衡
First-Principles Predictions of Thermodynamic Properties
and Phase Equilibria for Pure and Mixture Fluids

謝介銘

Chieh-Ming Hsieh

指導教授: 林祥泰 博士

Advisor: Shiang-Tai Lin, Ph.D.

中華民國 99 年 7 月

July, 2010

國立臺灣大學博士學位論文

口試委員會審定書

利用第一原理計算預測純物質與混合物
之熱力學性質與相平衡
First-Principles Predictions of Thermodynamic Properties and
Phase Equilibria for Pure and Mixture Fluids

本論文係 謝介銘 君（F93524068）在國立臺灣大學化學
工程研究所完成之博士學位論文，於民國 99 年 7 月 21 日承
下列考試委員審查通過及口試及格，特此證明

口試委員：

_____（簽名）

（指導教授）

系主任、所長 _____（簽名）

I

誌　　謝

　　由衷的感謝我的指導老師林祥泰教授，在我這個六年的碩士班與博士班生涯的指導與教誨，使得研究工作可以順利進行，進而完成此論文。六年的時間，看似漫長，卻在轉眼間就過了，很慶幸的，我遇到了一個個性平和與深具耐心的老師，對於我研究上的遭遇的問題，總是能不厭其煩的與我深入討論，追求真相與合理的解答，讓我深刻感受到一位學者對研究的熱情，也讓我學習到做研究與做事情的方法與態度。除了研究外，在人生的課題上遭遇的問題，也能與老師分享，老師也樂於聆聽並從不同的觀點來提供意見。我想，這六年來，若我有任何的進步與成長，不論是研究上或是待人處世上，大半都該歸功於我的指導老師。

　　也感謝這六年來，來來去去的研究室夥伴，除了課業研究上互相砥礪外，也充實且完整了我的研究生生涯。與我並肩奮鬥六年的小董，雖然晚期見面談天的時間較少，還是無法抹去一起奮鬥的過去。從大學時代一起奮鬥的到研究所的夥伴阿竹、崇民與旻璁，一起討論研究，一起在羽球場上揮灑汗水，讓我的研究生生涯更添樂趣，特別是崇民與阿竹，一位是從高中到大學的同班同學，一位是大學四年的室友，深厚的情誼不是三言兩語可以道盡的。小傑、小剛、舒潔、展嘉、孟廷、少儂的優秀的表現，也激勵著我，讓我在研究上絲毫不敢懈怠。穎銘、小容容與阿牛，我不會忘記我們的夏天，特別是阿牛，跟我同時畢業一起感受寫論文的艱辛。信傑、乃元、書書與阿光，桌球不是我的強項，我們還是聊聊研究或是閒話家常就好。君毅、書漢與奕霈，雖然相處時間不長，但曾經共處一室做研究，相信我們也培養出特別的情感。大夥兒在研究生生涯中同甘共苦、編織夢想的日子，不是短短的一兩句話可以道盡的，感謝各位豐富精采了我的研究生生涯，也祝福各位都能有錦繡的前程。

　　感謝我的家人，雖然沒有將研究課題上的事情與你們分享，但是你們一直我最堅強的後盾，讓我沒有後顧之憂，今天能夠順順利利的有這麼點小小的成就，沒有父母的苦心栽培，與家人的鼓勵支持，是絕不可能的。

　　感謝蓋涵，從我大學時期準備研究所考試開始，不論快樂或是艱苦，一路陪伴我、鼓勵我、相信我、給予我正面的能量，慢慢的，讓我想要在各方面都要變

III

的更好。

　　感謝我的口試委員，台灣科技大學林河木名譽教授、李明哲教授，清華大學汪上曉教授，台灣大學陳延平教授、陳立仁教授、諶玉真教授，在百忙之中撥冗出席學生的口試，悉心的指導我的研究與論文，提供許多寶貴的建議，使論文更加完善。

　　另外，也特別感謝在我申請直升博士班時，幫我寫推薦信的王大銘教授，您的首肯無疑是給學生的最大肯定與鼓勵。也感謝社會學系孫中興教授，您的妙語如珠總是讓我期待又害怕，與您聊天，總能讓學生對生活有另一番新的見解。

　　在成長的路上，一路走來要感謝的人太多，即便是任何一點點微不足道的幫助，甚至不是幫助，我都由衷感謝著。最後，要再一次感謝我的指導教授林祥泰老師，感謝您六年來的悉心指導與諄諄教導。

摘　　要

　　本研究主要透過結合量子力學原理溶合自由能計算以及Peng-Robinson狀態方程式，預測純物質與混合流體之相行為。以往使用 Peng-Robinson 狀態方程式描述純流體性質時，必須先有該流體的臨界性質及離心因子，以計算分子間吸引力參數 $a(T)$及分子體積 b 參數。對於混合流體，則還需要搭配混合律及使用適當的二元相互作用參數，才能得到較佳的相行為描述。對實驗數據的依賴大幅地限制了此類狀態方程式的應用範圍。在本研究中，我們透過統計力學理論的推導，建立溶合自由能計算中吸引力與狀態方程式中的能量參數 $a(T,\underline{x})$間的關係，並以溶合計算中使用的分子體積與流體組成來估算狀態方程式中的體積參數 $b(\underline{x})$。此方法結合 Peng-Robinson 狀態方程式與以溶合理論為基礎的 COSMO-SAC 模型(在本研究中稱為 PR+COSMOSAC)，不需要任何與物質有關的參數或不同物質間的二元相互作用參數，即可用來預測純物質的蒸氣壓、液相密度與臨界性質，更能應用在預測混合流體的液-氣、液-液與氣-液-液相平衡。此方法應用在預測 1296 個純物質的臨界壓力、臨界溫度、臨界體積、蒸氣壓(常壓沸點下)、液體密度(常壓沸點下)的平均相對誤差分別為 10%、4%、5%、49%與 21%。此方法應用在預測混合流體的氣-液相平衡上，針對 230 個系統得到的系統總壓與氣相組成誤差分別為 28%與 5%。當系統中所有物質的實驗值(蒸氣壓或臨界性質與離心因子)可取得並用於溶合自由能計算中，此誤差可大幅減少至 6%與 2%。此方法應用在預測混合流體的液-液相平衡上，針對 68 個雙成分與 39 個三成分系統得到的液相組成的方均根誤差分別為 0.0689 (80%) 與 0.0775 (72%)。此方法對於混合流體之液-液與氣-液-液相行為的預測上，可與官能基貢獻法中最為廣泛應用的 Modified UNIFAC 得到相同的精確度。此方法應用於預測藥物在純溶劑與混合溶劑中的溶解度上，針對 52 種藥物於 37 種純溶劑與 156 種混合溶劑得到的方均根誤差分別為 1.78 (495%) 與 1.40 (304%)，此預測結果優於 COSMO-SAC 模型。當藥物在純溶劑中溶解度的實驗值可取得時，藥物於混合溶劑中溶解度的方均根誤差可大幅減少至 0.65 (91%)。由於此方法沒有缺少官能基定義或是參數的問題，因此可應用於新製程的研發，特別是在缺少實驗值或二元相互作用參數的情況下，現有其他方法皆無法使用。

關鍵字：Peng-Robinson 狀態方程式，COSMO-SAC 模型，溶合自由能，相平衡預測，第一原理計算。

Abstract

In this study, a novel approach combining quantum mechanical solvation free energy calculations and Peng-Robinson equations of state (PR EOS) is proposed for the prediction of phase equilibria of both pure and mixture fluids. For pure substances the critical properties and acentric factor must be used to determine the energy $a(T)$ and volume b parameters. An appropriate mixing rule and often the binary interaction parameters are necessary in order to have a better description of the phase behavior for mixtures. The application of PR EOS is therefore limited by the need of input of experimental data. In this study, we found that the temperature and composition dependence of the energy parameter $a(T,\underline{x})$ in the EOS can be derived from the attractive contribution of the solvation free energy. The volume parameter $b(\underline{x})$ is estimated to be the mole-fraction weighted average of the molecular solvation cavity. Combined with first-principle solvation calculations, both parameters $a(T,\underline{x})$ and $b(\underline{x})$ can be obtained without the use of any experimental data (e.g., critical properties or acentric factor) and binary interaction parameters. The Peng-Robinson EOS combined with a solvation model based on COSMO-SAC calculation, denoted as PR+COSMOSAC, contains neither species dependent parameter nor binary interaction parameters, and can be used to predict vapor pressure, liquid density, and critical properties of pure substances, and vapor-liquid equilibrium (VLE), liquid-liquid equilibrium (LLE), and vapor-liquid-liquid equilibrium (VLLE) of mixtures. It is found that the overall relative average error from PR+COSMOSAC is 49% in vapor pressure, 21% in liquid density at normal boiling point, 10% in critical pressure, 4% in critical temperature, and 5% in critical volume for 1296 pure substances; and 28% in total pressure, and 5% in vapor phase composition for 230 binary mixtures in vapor-liquid

equilibrium. The errors in binary VLE predictions can be reduced significantly down to 6% and 2% if experimental data (vapor pressures or critical properties and acentric factor) are used to correct for any error in the calculated charging free energy of pure species. The overall root-mean-square errors in the mutual solubility of 68 binary and 39 ternary mixtures predicted from PR+COSMOSAC are 0.0689 (80%) and 0.0775 (72%), respectively. This method provides the prediction of LLE and VLLE with accuracy similar to that from the widely used group contribution method, the modified UNIFAC model. The overall RMS errors of PR+COSMOSAC in drug solubility prediction of 52 drugs in 37 pure solvents and 156 mixture solvents are 1.78 (495%) and 1.40 (304%), respectively. This accuracy is better than that from COSMO-SAC model. The overall RMS of drug solubility prediction in mixture solvents can be greatly reduced to 0.65 (91%) when the experimental solubility of the drug in the relevant pure solvent is available. Since there is no issue of missing parameters or group definitions, this model is particular useful for the design of new processes involving chemicals whose interaction parameters are not available due to the lack of experimental data.

Keywords: Peng-Robinson equation of state, COSMO-SAC, solvation free energy, phase equilibrium prediction, first-principles calculation.

Index of Tables

Index of Figures

as in Figure 5.2-1.

Table of Content

Chapter 1. Introduction

The knowledge of thermodynamic properties and phase equilibria of pure and mixture fluids is of great importance in the design and optimization of chemical processes [1-2]. For example, the information regarding temperature, pressure and composition in vapor-liquid equilibrium (VLE) and liquid-liquid equilibrium (LLE) is crucial for the design of distillation and extraction processes [3-7]. For some special processes, such as extractive distillation, the capability of describing the more complex phase-behaviors such as the vapor-liquid-liquid equilibrium (VLLE) becomes necessary [8-12]. While it may be straightforward to acquire the needed data directly from experimental measurement, a reliable predictive model can significantly reduce the time, cost, and risk for problems involving extreme operation conditions and/or toxic chemicals.

Many thermodynamic models have been proposed and are proven useful for the correlation and/or prediction of the phase behaviors of fluids. Since van der Waals first proposed the two-parameter cubic equations of state (EOS) [5], such a type of EOS (e.g. the Redlich-Kwong (RK) [13], and the Soave-Redlich-Kwong (SRK) [14] and the Peng-Robinson (PR) EOS [15]) has been widely used in the industry for process design, simulation and optimization because of its accuracy and ease of use. Furthermore, EOS have proven to be a powerful tool for describing the properties of pure components and mixtures, including the vapor pressure [16-24], critical properties [20, 25-26], phase equilibrium [27-38], etc. However, these EOS are usually less accurate for associating fluids and liquid mixtures. Some of these issues are addressed in more recent, none cubic types of EOS such as SAFT [39-40], PC-SAFT [41], and CPA [42].

In general, a cubic equation of state has two compound-specific parameters: one

1

temperature-dependent interaction parameter $a(T)$ and one volume parameter b. For pure compounds, their values are typically determined from the critical properties (T_c, P_c) and the acentric factor (ω) of pure substances. (For mixtures a further condition, such as van der Waal one-fluid mixing rule [5], is needed to determine the composition dependence of these two parameters.) However, for some species there exists substantial inconsistency in the reported values of critical properties. For example, the critical temperature ranges from 629 to 664.3 K and the critical pressure from 3.85 to 4.60 MPa for the cyclohexanone [43-45]. In addition, experimental critical properties are not always available, for example, for newly synthesized compounds and for heavy organics that would decompose before reaching the critical point. It is therefore desirable to have a method for describing the phase behaviors without the need of experimental data, such as critical properties.

There have been efforts made to replace the use of experimental critical properties with other properties. For example, Coniglio and his co-workers [16-17] proposed a modified cubic EOS (PR-type with volume translated correction) which requires input of only one boiling point. Kontogeorgis [20] proposed a method to predict the critical properties from one experimental vapor pressure datum and the van der Waals surface area. There are also group contribution models [46-49] available. Such methods, when applicable, are very accurate, however, at the cost of having a large number of parameters and requiring special care for isomers and/or compounds containing multiple functional groups [50].

Another class of thermodynamic models focuses on the modeling of non-ideality, or the excess free energy (G^{ex}), in the liquid phase; that is the so called liquid models (LM) [3, 51-64]. Examples such as the Wilson [52], NRTL [53], UNIQUAC [54], UNIFAC [3], modified UNIFAC [55-59], COSMO-RS [60-61], and COSMO-SAC [62-64]

2

models have been implemented in many process simulators [65] for the correlation or prediction of low pressure VLE (with the assumption of gas phase being ideal) and LLE of mixtures. Parameters in liquid models usually depend on the experimental data used in the regression. For example, parameters obtained from fitting to VLE experimental data cannot describe LLE behaviors very well [66-68], or vice versa. For the same reason, the original UNIFAC parameters usually fails to describe LLE, and an additional parameter set, UNIFAC-LLE parameter table [66], was developed specifically for LLE [69]. Therefore, these models should be used with caution as the origin of parameters may affect the design strategy for new processes [1]. Some of these problems are removed in the modified UNIFAC model [55-59], whose parameter set was optimized against thousands of experimental data (including both VLE and LLE). Unfortunately, there are still many missing parameters in the parameter matrix for modified UNIFAC [58] which severely limit its applications to new processes.

A third class is the combination of a cubic equation of state (EOS) with a liquid model through the use of a G^{ex}-based mixing rule [70-75]. This approach has the advantages of both the EOS (accurate description for pressure-volume-temperature relation) and liquid models (accurate description for liquid phase nonideality). Even though the underlying idea of G^{ex}-based mixing rules that the EOS should behave like a LM at some limiting condition breaks down [76], this kind of approach can successfully describes VLE for a wide range of temperature and pressure [77]. Escobedo-Alvarado and Sandler [78] and Matsuda et al. [79] have demonstrated the prediction of high pressure LLE using parameters determined from low pressure LLE data. Nevertheless, there has been no study regarding the description of LLE and VLE using the same set of parameters.

In this study, a different approach based on quantum mechanical solvation

calculations is suggested to overcome two aforementioned issues: (1) the need for experimental critical properties and ancetric factor as input of equation of state and (2) the description of various types of phase behaviors (VLE, LLE, and VLLE) over a wide range of temperature and pressure for both pure and mixture fluids using a single set of parameters. In this method, the energy parameter $a(T,\underline{x})$ and volume parameter $b(x)$ in the Peng-Robinson EOS are obtained from the solvation charging free energy $\Delta \underline{G}^{*chg}$ and the cavity volume for molecular solvation. This approach, denoted as PR+COSMOSAC (because a solvation model based on COSMO-SAC [62-64] calculations is used for $\Delta \underline{G}^{*chg}$), has the advantages that, using the molecular structure as the only input, both pure fluid properties (such as vapor pressure, liquid density, and critical properties) [25] and phase behavior of mixtures [such as VLE, LLE, VLLE, and solid-liquid equilibria (such as drug solubility)] [36-38] can be obtained using one common set of non-species-dependent parameters in the solvation model. Furthermore, depending on availability, experimental data (vapor pressure or critical properties) of pure substances can be incorporated to increase the accuracy in the description of mixture properties, especially for VLE and VLLE. More importantly, there is no issue of missing parameters in this method because it utilizes the results from first principle solvation calculations and no species dependent parameter is required. We believe that this method is ideal for the initial design of new processes, where some or all the needed experimental data are not immediately available.

Chapter 2. Theory

In this chapter, we establish the theoretical basis for determining the parameters in a pressure-volume-temperature-composition (P-T-$\underline{V}$-x) equation of state from quantum mechanical calculations. In particular, we are interested in obtaining these parameters from the perspective of molecular solvation.

2.1 Solvation Free Energy from Equation of state (EOS)

The solvation free energy ΔG^{*sol}, as defined by Ben-Naim [80], is the work needed for transferring of a molecule (solute) from an ideal gas phase to a solution (solvent) under constant temperature T and pressure P. Such a free energy is commonly computed from a hypothetical two-step process: (1) creating a cavity to size of the solute (the corresponding work is referred to as the cavity formation free energy ΔG^{*cav}) and (2) placing the solute into the cavity (the corresponding work referred to as the solvation charging free energy ΔG^{*chg}), that is, (as illustrated in Figure 2.1-1)

$$\Delta G^{*sol} = \Delta G^{*cav} + \Delta G^{*chg} \tag{2.1-1}$$

Lin et al. [81] have shown that the solvation free energy is related to the configuration Helmholtz free energy A^{CONF} (sometimes called the residual property [82]) as

$$\Delta \underline{G}^{*sol} = \underline{A}^{\mathrm{CONF}} + (z - 1)RT \tag{2.1-2}$$

where R is the ideal gas constant and $\underline{A}^{\mathrm{CONF}}$ is the difference in $\underline{A}$ between a real system and a ideal gas system at the same molar volume $\underline{V}$, temperature T (and composition), i.e., $\underline{A}^{\mathrm{CONF}} = \underline{A}(\underline{V},T) - \underline{A}^{\mathrm{IG}}(\underline{V},T)$. Abbott and Prausnitz [82] also showed an important connection between the statistical thermodynamics ($\underline{A}^{\mathrm{CONF}}$) and the classical thermodynamics (z), that is,

$$\underline{A}^{CONF}(\underline{V},T) = RT \int_{\underline{V}=\infty}^{\underline{V}} \frac{(1-z)}{\underline{V}} d\underline{V} \tag{2.1-3}$$

where the compressibility factor can be obtained from a EOS describing P-$\underline{V}$-T relationship. Substituting $\underline{A}^{CONF}$ in Eq. (2.1-2) with Eq. (2.1-3), one has

$$\frac{\Delta \underline{G}^{*sol}(\underline{V},T)}{RT} = (z-1) + \int_{\underline{V}=\infty}^{\underline{V}} \frac{(1-z)}{\underline{V}} d\underline{V} \tag{2.1-4}$$

This equation provides a key connection between the novel solvation theory and the classical equation of state.
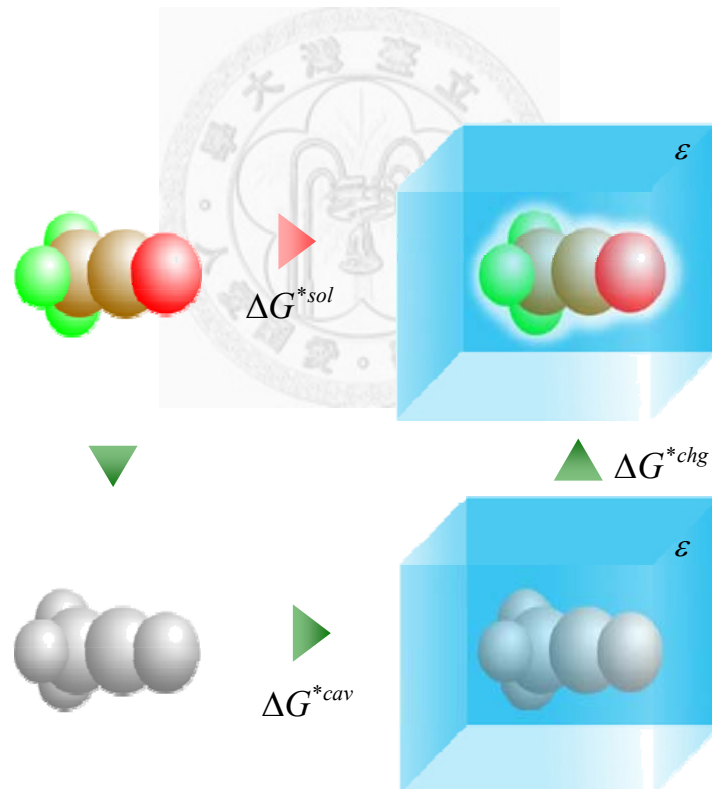
Figure 2.1-1. The solvation process can be separated into two steps: (1) creating a cavity to size of the solute (ΔG^{*cav}) and (2) placing the solute into the cavity (ΔG^{*chg}).

2.2 Parameters of Equation of State from Solvation Charging Free Energy

In section 2.1, the solvation free energy of a solution obtained from the compressibility is derived. In this study, assume that the fluids obey the Peng-Robinson EOS [15]

$$z = \frac{\underline{V}}{\underline{V}-b} - \frac{a}{RT}\frac{\underline{V}}{\underline{V}(\underline{V}+b)+b(\underline{V}-b)} \tag{2.2-1}$$

where a and b are the energy and volume parameters, respectively. For a pure substance, the energy parameter is a temperature-dependent parameter, and the volume parameter is a constant corresponding to the molecular volume of the chemical substance. These parameters become composition-dependent for mixtures. Substituting z in Eq. (2.1-4) with Eq. (2.2-1), the solvation free energy becomes to

$$\frac{\Delta \underline{G}^{*sol}(T,\underline{V})}{RT} = (z-1) + \ln\frac{\underline{V}}{\underline{V}-b} + \frac{a}{bRT}\left[\frac{1}{2\sqrt{2}}\ln\frac{\underline{V}+b(1-\sqrt{2})}{\underline{V}+b(1+\sqrt{2})}\right] \tag{2.2-2}$$

The free energy of cavity formation can be equated to the contribution by the repulsive term. Therefore, the cavity formation free energy is

$$\frac{\Delta \underline{G}^{*hccav}}{RT} = \left(\ln\frac{\underline{V}}{\underline{V}-b} + \frac{b}{\underline{V}-b}\right) \tag{2.2-3a}$$

or in the repulsive limit, in which case the compressibility factor $z = 0$,

$$\frac{\Delta \underline{G}^{*hccav}(z=0)}{RT} = \left(\ln\frac{\underline{V}}{\underline{V}-b} - 1\right) \tag{2.2-3b}$$

According to Eq. (2.1-1), the difference between the solvation free energy and the cavity formation free energy is the solvation charging free energy

$$\frac{\Delta \underline{G}^{*chg}}{RT} = \frac{a}{bRT}\left[\frac{1}{2\sqrt{2}}\ln\frac{\underline{V}+b(1-\sqrt{2})}{\underline{V}+b(1+\sqrt{2})} - \frac{b\underline{V}}{\underline{V}^2+2b\underline{V}-b^2}\right] \tag{2.2-4a}$$

or in the repulsive limit,

$$\frac{\Delta \underline{G}^{*chg}(z=0)}{RT} = \frac{a}{bRT}\left[\frac{1}{2\sqrt{2}}\ln\frac{\underline{V}+b(1-\sqrt{2})}{\underline{V}+b(1+\sqrt{2})}\right] \tag{2.2-4b}$$

From Eq. (2.2-4) the energy parameter $a(T,\underline{x})$ can be expressed in terms of the solvation charging free energy as

$$a(T,\underline{x}) = \frac{b(\underline{x})}{C_{PR}}\Delta \underline{G}^{*chg}(T,\underline{V},\underline{x}) \tag{2.2-5}$$

where the value of C_{PR} (the subscript PR denotes that this parameter depends on the EOS used), defined as the terms in the square brackets in Eq. (2.2-4), can be determined if the ratio $\underline{V}/b$ is known. It was first set to be -1.123 [25] [from Eq. (2.2-4a) with $\underline{V}/b=1$]. Another possible choice is the repulsive limit in which case $C_{PR} = -0.623$ [from Eq. (2.2-4b) with $\underline{V}/b=1$]. It should be noted that the ratio $\underline{V}/b = 1$ is only used in the determination of C_{PR}. The choice of the pressure for C_{PR} and the expression of $\Delta\underline{G}^{*chg}$ should be consistent with the pressure used in the evaluation of the charging free energy. However, the solvation model (COSMO solvation model) that will be introduced later does not provide such information. We find that the repulsive limit condition (at a certain pressure) provides a much better vapor-liquid equilibrium (VLE) description for mixtures [36]; therefore, $C_{PR} = -0.623$ is used throughout this study.

The volume parameter b can be assumed to be the same as the volume of the solvation cavity. For a pseudo-pure fluid, it can be approximated from the mole fraction average of pure component contributions, i.e.,

$$b(\underline{x}) = \sum_i x_i b_i \tag{2.2-6}$$

Therefore, together with Eq. (2.2-6) for $b(\underline{x})$, Eq. (2.2-5) provides a way to estimate the temperature and composition dependence of parameter $a(T,\underline{x})$ from the solvation charging free energy, whose value is determined from a solvation model described in the next section.

2.3 Determination of the Solvation Charging Free Energy

Among the many approaches to determine the solvation charging free energy [83-87], we choose here the implicit solvation quantum mechanical calculations [83, 88-90]. Of particular interest here is the Conductor-like Screening Model (COSMO), pioneered by Klamt and others [63, 85, 90-93]. In this method, a solute is initially placed in a conductor so that it is perfectly screened. The screening charges are then removed so that the environment is restored to the real solution state. Based on such a process Lin et al. [63] determined the charging free energy from the sum of four contributions, i.e.,

$$\Delta \underline{G}_{i/j}^{*chg}(T,\underline{x}) = \Delta \underline{G}_i^{*is} + \Delta \underline{G}_i^{*cc} + \Delta \underline{G}_{i/j}^{*res}(T,\underline{x}) + \Delta \underline{G}_i^{*dsp}(T) \qquad (2.3-1)$$

where the superscripts *is*, *cc*, *res*, and *dsp* denote ideal solvation, charge-averaging correction, restoring, and dispersion contribution to the solvation charging free energy; the subscript *i/j* denotes the molecule *i* solvated into solution *j*. The first three terms on the right-hand side in Eq. (2.3-1) are based on the results of COSMO calculation; the temperature-dependent dispersion term is determined from the exposed surface area of molecule *i*.

The ideal solvation term is the difference in energy when the solute is in the ideal gas and in the conductor state

$$\Delta \underline{G}_i^{*is} = E_i^{COSMO} - E_i^{IG} \qquad (2.3-2)$$

where E_i^{IG} and E_i^{COSMO} are the total energy of molecule *i* in the ideal gas and ideal conductor states determined from first-principles quantum mechanical (QM) and COSMO solvation calculations [90]. Although E_i^{IG} and E_i^{COSMO} are the results of single molecule state, an assumption that the kinetic energies in these two states are the same is made. Thus, the kinetic energy will be cancelled when considering the energy difference between these two states. Figures 2.3-1 illustrates the optimal conformations

from QM calculations and the screening charge distribution on molecular cavity from COSMO calculations for three selected compounds.

(a) 1-Butanol   (b) Water   (c) Hexane
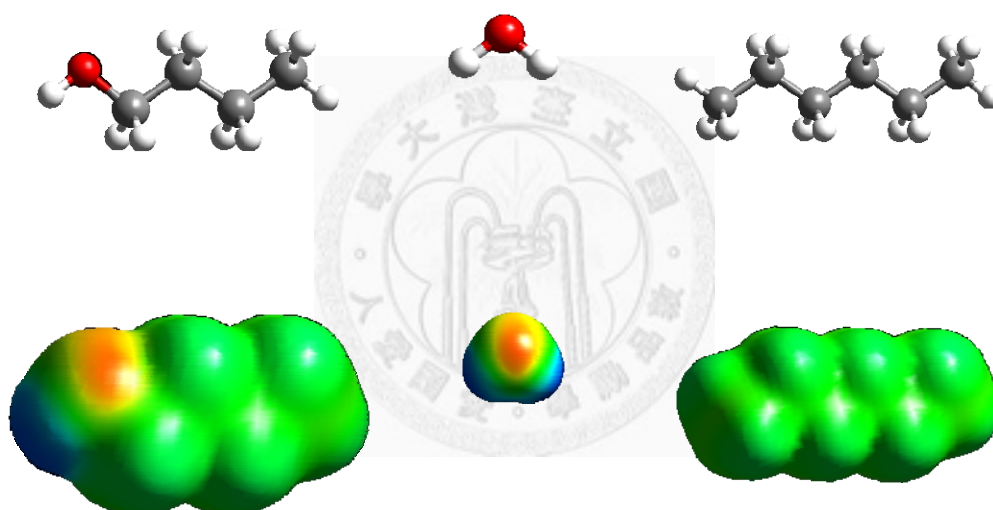
Figure 2.3-1. Molecular structure and screening charge distribution on molecular cavity (intensity of charge density: -0.025 ■■■■■■■ 0.025) obtained from quantum mechanical geometry optimization and COSMO calculation, respectively, for three selected molecules: 1-butanol, water, and hexane.

In the COSMO-based methods [60-64, 94], the work related to the removal of screening charges is determined from consideration of the electrostatic interactions between surface segments (each possesses certain amount of screening charges) when brought in contact. A fundamental assumption in these methods is that the segment pairs in contact are independent from one another (i.e., no interactions between any segment pairs). For this purpose, a charge averaging process was suggested [95]

$$\sigma_m = \frac{\sum\limits_n \sigma_n^* \dfrac{r_n^2 r_{eff}^2}{r_n^2 + r_{eff}^2} \exp\left(-f_{decay}\dfrac{d_{mn}^2}{r_n^2 + r_{eff}^2}\right)}{\sum\limits_n \dfrac{r_n^2 r_{eff}^2}{r_n^2 + r_{eff}^2} \exp\left(-f_{decay}\dfrac{d_{mn}^2}{r_n^2 + r_{eff}^2}\right)} \tag{2.3-3}$$

where d_{mn} is the distance between segments m and n, the parameter f_{decay} (set to 3.57) was introduced to balance the different units (between Bohr and angstroms) [95], $r_n = \sqrt{a_n/\pi}$ is the radius of segment n, and $r_{eff} = \sqrt{a_{eff}/\pi}$ (a_{eff} = 7.50 Å^2) is the radius of a standard surface segment. As a result, it is necessary to consider the energy shift associated with the charge averaging process

$$\Delta\underline{G}_i^{*cc} = f_{pol}^{1/2}\left[E_{diel}(\underline{q}) - E_{diel}(\underline{q}^*)\right] \tag{2.3-4}$$

where f_{pol} is the polarization factor (determined to be 0.6916 [63].); the dielectric energy is defined as $E_{diel}(\underline{q}) = \dfrac{1}{2}\sum\limits_v \phi_v q_v$, where q_v is the screening charge at some position v on the cavity surface and ϕ_v is the electrostatic potential due to the solute at position v. Both q_v and ϕ_v are obtained from the COSMO solvation calculation.

After charge averaging process, these screening charges are used to generate the sigma profile (or σ-profile), $p(\sigma)$, i.e., the probability of finding a surface segment with screening charge density σ. In order to better describe the hydrogen bonding interactions, the σ-profile is separated into non-hydrogen bonding $p^{nhb}(\sigma)$ and hydrogen

11

bonding components $p^{hb}(\sigma)$, i.e., $p(\sigma) = p^{nhb}(\sigma) + p^{hb}(\sigma)$ [25, 36, 62-63]. The hydrogen bonding σ-profile collects the surface segments on the hydrogen bonding acceptor (oxygen, nitrogen, and fluorine) and donor (hydrogen connects to O, N, and F) atoms. Only one type of hydrogen bonding interaction was considered. However, it is known that the strength of a hydrogen bond varies with the substances that form it. For example, the hydrogen bond strength between two alcohols (O—H····O in gas phase) ranges from 4.5~7.5 kcal/mol, that between two amines (N—H····N in gas phase) ranges from 3.4~4.4 kcal/mol, and that between a ketone and an amine (N—H····O in CCl₄ solvent) is about 3.9 kcal/mol [96]. To account for such differences, the hydrogen bonding σ-profile is further separated into three components.

$$p(\sigma) = p^{nhb}(\sigma) + p^{hydro}(\sigma) + p^{amino}(\sigma) + p^{other}(\sigma) \tag{2.3-5}$$

The first component $p^{hydro}(\sigma)$ collects the segments on the hydrogen fluoride and hydroxyl group, such as water or alcohol; the second one $p^{amino}(\sigma)$ collects segments on the amino groups of primary and secondary amines; the third one $p^{other}(\sigma)$ collects segments on other oxygen, nitrogen, and fluorine atoms which are not connected to any hydrogen atoms, such as NO₂. The refinement of the surface types of hydrogen bonding donors allows for a more specific description of interactions between different types of hydrogen bonds. Figure 2.3-2 illustrates the difference between σ-profile of four compounds in the original COSMO-SAC [62] and that in this study.

In a mixture, the σ-profile of the solution is calculated as the mole-fraction average from the contribution of the pure components

$$p_{mix}(\sigma) = \frac{\sum_i x_i n_i p_i(\sigma)}{\sum_i x_i n_i} = \frac{\sum_i x_i S_i p_i(\sigma)}{\sum_i x_i S_i} \tag{2.3-6}$$

where n_i, the number of surface segment for molecule i, is the ratio of molecular surface

area (S_i) and surface area of standard segment (a_{eff} = 7.5 Å); $p_i(\sigma)$, specific property of pure molecule, is the σ-profile of substance i. Examples of $p_{mix}(\sigma)$ for binary mixture benzene + water are shown in Figure 2.3-2. It should be noted that different settings in quantum mechanical COSMO calculations may affect the shape of the σ-profile [97-99].

(a) *nhb* component

(b) *hydro* component

(c) *amino* component

(d) *other* component
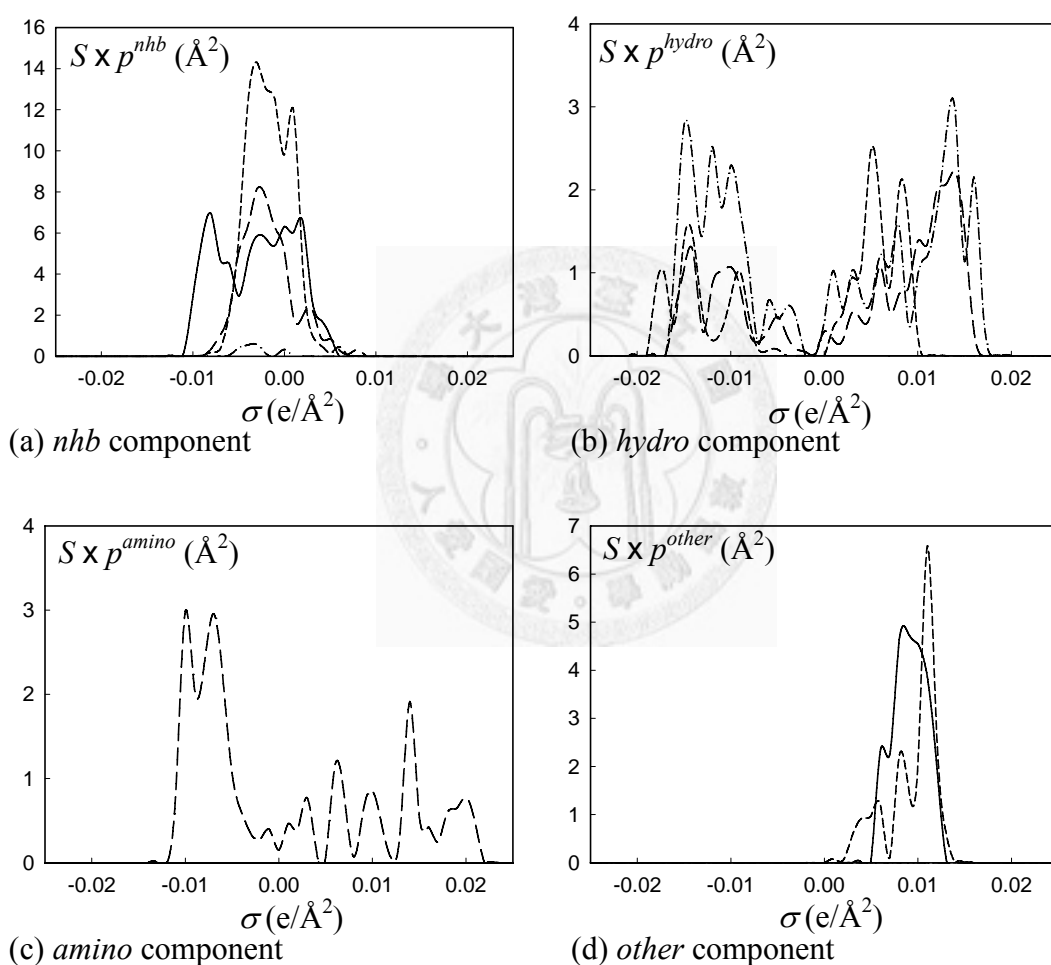
Figure 2.3-2. The sigma profiles for four representative compounds: acrylonitrile (solid line), monoethanolamine (long dashed line), isobutyric acid (short dashed line), and water (dashed-dotted line). S is the molecular surface area of species. The sum of $p^{hydro}(\sigma)$, $p^{amino}(\sigma)$, and $p^{other}(\sigma)$ is the $p^{hb}(\sigma)$ in the original COSMO-SAC model [62].
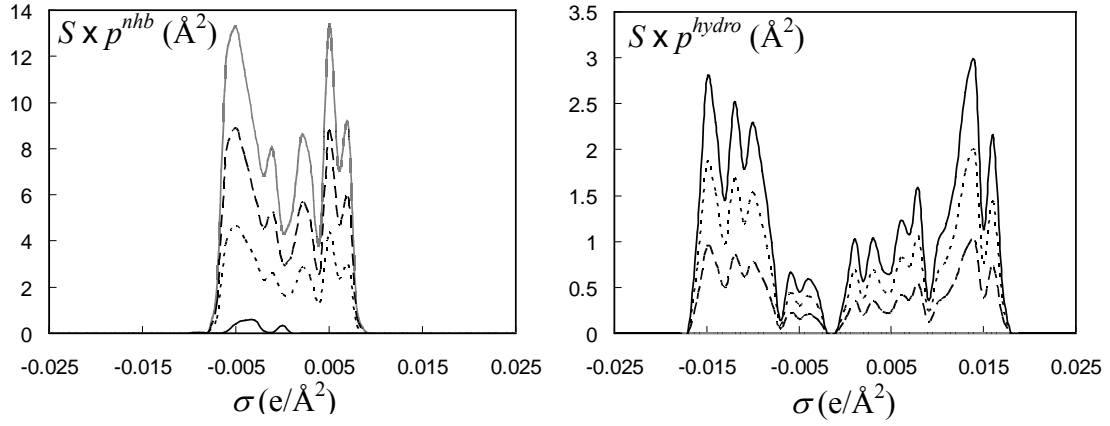
Figure 2.3-3. The sigma profiles of binary mixture benzene (1) + water (2) for four different concentrations: $x_1=0$ (solid line), $x_1=0.33$ (dotted line), $x_1=0.66$ (dashed line), and $x_1=1$ (gray line). Since water and benzene have only *nhb* and *hydro* segments, the other two s-profile components are omitted in this figure.

After generating the σ-profile (for each of the components and the mixture), the restoring contribution can be calculated from

$$\frac{\Delta\underline{G}_{i/j}^{*res}}{RT} = n_i \sum_{s}^{\substack{nhb,\,hydro,\\amino,\,other}} \left[\sum_{\sigma_m} p_i^s(\sigma_m^s) \ln\Gamma_j^s(\sigma_m^s) \right] \tag{2.3-7}$$

where $n_i = S_i/a_{eff}$ is number of segments of molecule i; the segment activity coefficient $\Gamma(\sigma)$ is determined from

$$\ln\Gamma_j^t(\sigma_m^t) = -\ln\left\{ \sum_{s}^{\substack{nhb,\,hydro,\\amino,\,other}} \sum_{\sigma_n} p_j^s(\sigma_n^s) \exp\left[\frac{-\Delta W(\sigma_m^t,\sigma_n^s)}{RT} + \ln\Gamma_j^s(\sigma_n^s) \right] \right\} \tag{2.3-8}$$

where the superscripts t and s can be *hydro*, *amino*, *other*, or *nhb*. The segment exchange energy ΔW is obtained from

$$\Delta W(\sigma_m^t,\sigma_n^s) = f_{pol}\frac{0.3 a_{eff}^{3/2}}{2\varepsilon_0}\left(\sigma_m^t + \sigma_n^s\right)^2 - c_{hb}(\sigma_m^t,\sigma_n^s)(\sigma_m^t - \sigma_n^s)^2 \tag{2.3-9}$$

where ε_0 is the permittivity of vacuum; $c_{hb}(\sigma_m^t, \sigma_n^s)$ is temperature-independent and its value is determined as

$$c_{hb}(\sigma_m^t, \sigma_n^s) = \begin{cases} c_{HH} & \text{if } s = t = \text{hydro and } \sigma_m^t \cdot \sigma_n^s < 0 \\ c_{AA} & \text{if } s = t = \text{amino and } \sigma_m^t \cdot \sigma_n^s < 0 \\ c_{OO} & \text{if } s = t = \text{other and } \sigma_m^t \cdot \sigma_n^s < 0 \\ c_{HA} & \text{if } s = \text{hydro, } t = \text{amino, and } \sigma_m^t \cdot \sigma_n^s < 0 \\ c_{HO} & \text{if } s = \text{hydro, } t = \text{other, and } \sigma_m^t \cdot \sigma_n^s < 0 \\ c_{AO} & \text{if } s = \text{amino, } t = \text{other, and } \sigma_m^t \cdot \sigma_n^s < 0 \\ 0 & \text{otherwise} \end{cases} \tag{2.3-10}$$

The values of these six parameters (c_{HH}, c_{AA}, c_{OO}, c_{HA}, c_{HO}, and c_{AO}) have been determined using experimental data of vapor pressures of selected pure substances and selected liquid-liquid equilibria and are summarized in Table 3-1.

The dispersion solvation free energy is considered to be proportional to the exposed surface area of the atom comprising the molecule [60-61, 63-64, 83, 100-102], that is,

$$\Delta \underline{G}_i^{*dsp}(T) = \sum_j s_j (A_{dsp,j} T + B_{dsp,j}) + \underline{G}_{HB}^{*dsp}(T) + \underline{G}_{RING}^{*dsp}(T) \tag{2.3-11}$$

where s_j is the total exposed surface area of atom type j, $A_{dsp,j}$ and $B_{dsp,j}$ are the dispersion parameters of atom type j, and $\underline{G}_{HB}^{*dsp}$ and $\underline{G}_{RING}^{*dsp}$ are the empirical corrections for hydrogen-bonding and cyclic (or aromatic) containing molecules. The expressions of these two terms are

$$\underline{G}_{HB}^{*dsp}(T) = \frac{1}{N_{HBH}} \left\{ \frac{A_{dsp,HB}}{1 + \exp\left[-\left(T - B_{dsp,HB}\right)/C_{dsp,HB}\right]} \right\} \tag{2.3-12}$$

$$\underline{G}_{RING}^{*dsp}(T) = N_{AR}(A_{dsp,RING} + B_{dsp,RING}) \tag{2.3-13}$$

where N_{HBH} and N_{AR} are the number of hydrogen-bonding donors (the hydrogen atoms connecting to either nitrogen, oxygen, or fluorine atom) and the number of atoms

involved in any ring-structure, respectively. All the parameters in the proposed model are determined by regression to experimental vapor pressure of selected compounds or experimental data of binary liquid-liquid equilibrium and summarized in Table 3-1.

Once the solvation charging free energy at some given temperature and solution composition is determined from Eqs. (2.3-1) to (2.3-13), the energetic parameter $a(T,\underline{x})$ in the PR EOS can be calculated from Eq. (2.2-5). This approach is referred to as PR+COSMOSAC hereafter.

2.4 Improvements in Prediction of Mixing Fluids When Some Experimental Data of Pure Substances are Available.

While the PR+COSMOSAC approach allows for the description of $P\underline{V}Tx$ relations of mixture fluids without input of experimental data, it is possible to increase its level of accuracy in the calculation of mixture properties, especially for vapor-liquid equilibrium predictions, by incorporating experimental data of pure substances, such as the vapor pressure or the critical properties. The method of inclusion of experimental data depends on the type of data available. Two methods will be introduced: the PR+COSMOSAC+P^{vap} method when the vapor pressures are available, and the PR+COSMOSAC+$T_cP_c\omega$ method when the critical properties and acentric factor are available.

If the vapor pressures of pure components are available, they are used to correct for any error in the charging free energy calculation of pure species

$$\Delta\underline{G}_{i/j}^{*chg} = \Delta\underline{G}_{i/j}^{*chg}\,[\text{Eq. (2.3-1)}] + \Delta\underline{G}_{i,\text{Corr}}^{*chg}(T) \tag{2.4-1}$$

where $\Delta\underline{G}_{i,\text{Corr}}^{*chg}(T)$ is a correction term and its value is adjusted so that correct vapor pressure of species i is obtained at temperature T. This approach, denoted as PR+COSMOSAC+P^{vap}, ensures correct pressures in the VLE phase diagram in the pure

fluid limits. However, it is not applicable for problems such as solubility of a gas in liquid because the system temperature is higher than the critical temperature of the gas (and no vapor pressure data is available).

When the critical properties (T_c and P_c) and acentric factor (ω) are available, they can be used to correct for the charging free energy as follows

$$\Delta \underline{G}_{i/j}^{*chg} = \Delta \underline{G}_{i/j}^{*chg} [\text{Eq. (2.3-1)}] - \Delta \underline{G}_{i/i}^{*chg} [\text{Eq. (2.3-1)}] + \frac{a_i C_{PR}}{b_i} \tag{2.4-2}$$

where $\Delta \underline{G}_{i/i}^{*chg}$ is the charging free energy of species i in its pure fluid, $a_i(T)$ and b_i are determined as those in the original PR EOS,

$$a_i(T) = 0.45724 \frac{R^2 T_{c,i}^2}{P_{c,i}} \left[1 + \kappa_i \left(1 - \sqrt{\frac{T}{T_{c,i}}} \right) \right]^2 \tag{2.4-3}$$

$$b_i = 0.07780 \frac{R T_{c,i}}{P_{c,i}} \tag{2.4-4}$$

with $\kappa_i = 0.37464 + 1.54226 \omega_i - 0.26992 \omega_i^2$, where $T_{c,i}$, $P_{c,i}$, and ω_i are critical temperature, critical pressure, and acentric factor, respectively. This approach, denoted as PR+COSMOSAC+$T_c P_c \omega$, ensures that the pure component vapor pressures will be the same as those determined from the original Peng-Robinson EOS. Comparing Eqs. (2.4-1) and (2.4-2), the pure fluid charging free energy correction is determined to be

$$\Delta \underline{G}_{i,\text{Corr}}^{*chg}(T) = \frac{a_i C_{PR}}{b_i} - \Delta \underline{G}_{i/i}^{*chg} [\text{Eq. (2.3-1)}] \tag{2.4-5}$$

in PR+COSMOSAC+$T_c P_c \omega$. It is noteworthy that, in order to obtain more accurate vapor pressures for pure substances, the expression for $a_i(T)$ as described in PRSV EOS (PR EOS modified by Stryjek and Vera [33]) can be used in replacement of Eq. (2.4-3).

2.5 Application in Prediction of Drug Solubility

The fundamental principle of solid-liquid equilibrium is

$$f_i^S = f_i^L \qquad (2.5\text{-}1)$$

where f_i^S is the fugacity of compound i in the solid phase. Since solid crystals are nearly pure, it is a good assumption to regard the solid phase as a pure phase. The fugacity of the solute in the liquid phase, f_i^L, can be determined from the product of the saturation mole fraction x_i; the activity coefficient at the saturation concentration γ_i, and the reference state fugacity f_i^{0L}. Thus, Eq. (2.5-1) can be rewritten as

$$f_i^S = x_i \gamma_i f_i^{0L} \qquad (2.5\text{-}2)$$

As shown by Prausnitz et al. [6], the change in fugacity of pure solid to liquid at the same temperature and pressure can be estimated from the data at the triple point

$$\ln \frac{f_i^{0L}}{f_i^S} = \frac{\Delta H_i^{fus}}{RT_{t,i}}\left(\frac{T_{t,i}}{T}-1\right) - \frac{\Delta c_{p,i}}{R}\left(\frac{T_{t,i}}{T}-1\right) + \frac{\Delta c_{p,i}}{R}\ln\frac{T_{t,i}}{T} \qquad (2.5\text{-}3)$$

where ΔH_i^{fus} is the enthalpy of fusion, $\Delta c_{p,i} = c_{p,i(\text{liquid})} - c_{p,i(\text{solid})}$ ($c_{p,i}$ is the normal pressure heat capacity), $T_{t,i}$ is triple point temperature of solute i. In order to simplify the calculation, two simplifications are made. First, the normal melting temperature T_m and the enthalpy of fusion at that temperature are used. This is because the difference between triple point temperature and normal melting temperature is small for most compounds and so does the difference between enthalpy of fusion at these two temperatures. Second, the first term on the RHS of Eq. (2.5-3) is the dominant term [6], so the remaing terms are neglected. The solubility of a solid non-electrolyte organic can thus be approximated by the following simplified equation

$$\ln x_i = \frac{\Delta H_i^{fus}}{R}\left(\frac{1}{T}-\frac{1}{T_{m,i}}\right) - \ln\gamma_i \qquad (2.5\text{-}4)$$

where the experimental values for enthalpy of fusion ΔH_i^{fus} and normal melting

18

temperature $T_{m,i}$ of the drug are used [103-104]. When experimental data are not available, the group contribution method, such as that of Chickos [105-106], can be used. The activity coefficient of solute i in mixture j is determined from

$$\gamma_{i/j}(T,P,\underline{x}) = \frac{\overline{f}_i^S(T,P,\underline{x})}{x_i f_i(T,P)} = \frac{\overline{\phi}_i^S(T,P,\underline{x})}{\phi_i(T,P)} \tag{2.5-5}$$

where $\overline{\phi}_i^S$ and ϕ_i are the fugacity coefficients of component i in the mixture (the superscript S denotes solution) and in its pure solvent.

In analogous to the corrections done in section 2.4 (where the accuracy of PR+COSMOSAC in VLE prediction can be improved significantly by using the experimental data of vapor pressures or critical properties and acentric factors), we propose a simple correction method to improve the accuracy of PR+COSMOSAC in prediction of drug solubility in mixture solvents by introducing the experimental data of drug solubility in the pure solvents. To achieve this, we assume that any error in the solubility calculation is a result of inaccurate description of dispersion contribution of solvation free energy. Therefore, the correction term is introduced only for the error in dispersion free energy of the solute in specified solvent and only for the solubility calculation,

$$\Delta\underline{G}_i^{*dsp} = \Delta\underline{G}_i^{*dsp} \text{ [Eq. (2.3-11)]} + \sum_k G_{ik}^{dsp,corr} X_k \tag{2.5-6}$$

where $G_{ik}^{dsp,corr}$ is the dispersion free energy correction coefficient for solute i in solvent k; X_k is the solvent fraction in the solute free solvent mixtures. In the case of a single solvent, Eq. (2.5-6) becomes

$$\Delta\underline{G}_i^{*dsp} = \Delta\underline{G}_i^{*dsp} \text{ [Eq. (2.3-11)]} + G_{ik}^{dsp,corr} \tag{2.5-7}$$

and the coefficient $G_{ik}^{dsp,corr}$ can be determined from fitting to experimental solubility data. This approach is denoted as PR+COSMOSAC+G^{dsporr}.

Chapter 3. Computational Method

3.1 PR+COSMOSAC model

The calculation of energy parameter a and volume parameter b in the Peng-Robinson EOS requires the computation of the solvation charging free energy. The computation consists of 8 steps as follows:

(1) The equilibrium geometry of the molecule in the ideal gas phase is obtained from molecular energy minimization using the quantum chemistry package. The molecular energy is determined from the density functional theory with non-local VWN-BP functional at the DNP (double numeric with polarization functions version 4.0.0 with a real space cutoff set to 5.50 Å) basis set level. The minimum energy of molecule in ideal gas E^{IG} can be found in the output file (extension *outmol*) [64].

(2) The COSMO calculation [90] (solvation calculation for a molecule in the conductor) at the same VWN-BP and DNP level (with default settings for all other parameters) is performed to obtain the energy in conductor E^{COSMO}, and the screening charges $\underline{q}^*$ on the molecular cavity surface (output file with extension *cosmo*). The molecular cavity is defined using the default atomic radii (listed in Table 3-1). The surface area (including the atom exposed surface area S_k) and volume of molecular cavity are obtained in the same calculation. (Note that there is a relatively comprehensive COSMO file databank [107-108], denoted as VT-database in this study, maintained by Liu's group at Virginia Polytechnic Institute and State University [109] and are directly used in this study.)

(3) The cavity volume of molecule i (multiplied by Avogadro's number) is taken as parameter b_i.

(4) The ideal solvation free energy $\Delta \underline{G}_i^{*is}$ is calculated using Eq. (2.3-2).

(5) For each species in the system, perform screening charge averaging using Eq. (2.3-3), determine the energy shift correction with Eq. (2.3-4), and generate the σ-profile $p_i(\sigma)$ (the details of this step can be found in the work of Lin and Sandler [63-64]).

(6) For a given mixture composition, the σ-profile of mixture $p_{mix}(\sigma)$ is determined from Eq. (2.3-6).

(7) For a given temperature, determine the restoring and dispersion free energy from Eqs. (2.3-7) and (2.3-11), respectively.

(8) Finally, the total solvation free energy, energy parameter $a(T,\underline{x})$, and volume parameter $b(\underline{x})$ are calculated from Eqs. (2.3-1), (2.2-5), and (2.2-6), respectively.

It should be noted here that steps 1 to 5 needs to be done only once for each chemical substance and then stored in a data base for further use, while steps 6 to 8 must be done at each temperature and mixture composition. Once parameters $a(T,\underline{x})$ and $b(\underline{x})$ are determined, the vapor-liquid and liquid-liquid equilibrium calculation can be done through the standard procedures [5, 7, 77] which are briefly summarized in the following sections. The equations for the calculation of critical properties are derived in Appendix A.

In PR+COSMOSAC+P^{vap}, the vapor pressure $P_i^{\text{vap}}(T)$ of pure substance i at T must be used to determine the charging free energy correction term $\Delta\underline{G}_{i,\text{Corr}}^{*chg}(T)$. The vapor pressure from PR+COSMOSAC is first calculated. The Newton-Ralphson method is then used to solve for $\Delta\underline{G}_{i,\text{Corr}}^{*chg}(T)$ so that the calculated vapor pressure equals to that from experiment. Once determined, the value of $\Delta\underline{G}_{i,\text{Corr}}^{*chg}(T)$ is used in Eq. (2.4-1) for all mixture calculations. Note that the correction term $\Delta\underline{G}_{i,\text{Corr}}^{*chg}(T)$ is temperature dependent and needs to be re-evaluated for all species when considering VLE at

different temperatures.

In PR+COSMOSAC+$T_c P_c \omega$, the pure fluid charging free energy $\Delta G_{i/i}^{*chg}$ [Eq. (2.3-1)], and $a_i(T)$ [Eq. (2.4-3)] and b_i [Eq. (2.4-4)] are determined for all species in the mixture. They are then used in Eq. (2.4-2) for mixture property calculations. Similar to the case of PR+COSMOSAC+P^{vap}, $\Delta G_{i/i}^{*chg}$ [Eq. (2.3-1)] and $a_i(T)$ need to be re-evaluated for each temperature of interest.

3.2 Procedure for Vapor-Liquid Equilibrium (VLE) Calculation

The procedure of isothermal VLE calculation follows the flow diagram algorithm for the bubble point pressure calculation using an equation of state in Sandler's textbook [5] and is shown in Figure 3.2-1.
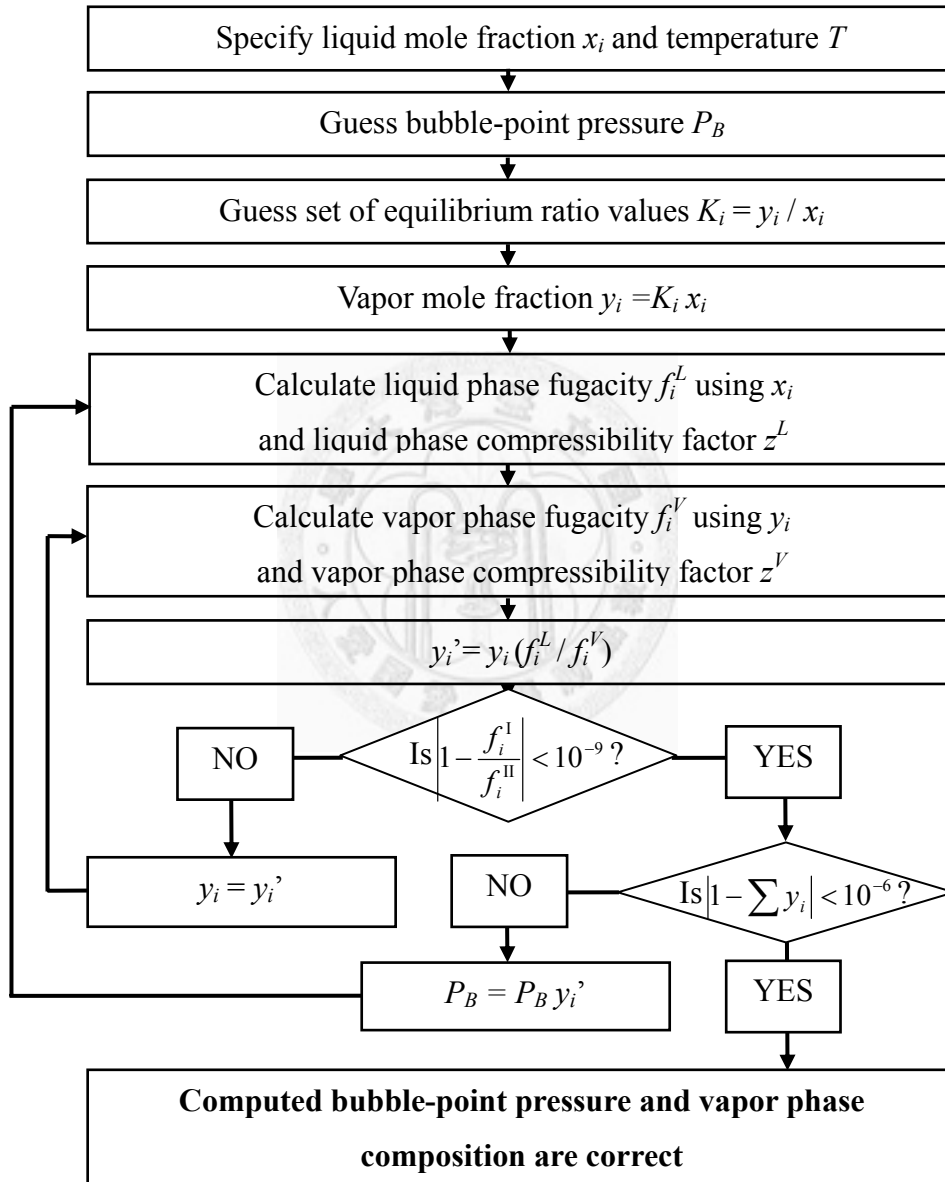
Figure 3.2-1. Flow diagram of an algorithm for the bubble-point pressure calculation using an equation of state.

3.3 Procedure for Liquid-Liquid Equilibrium (LLE) Calculation

The procedure of LLE calculation follows the flow diagram algorithm for the isothermal flash calculation using an equation of state in Sandler's textbook [5] and is shown in Figure 3.3-1.
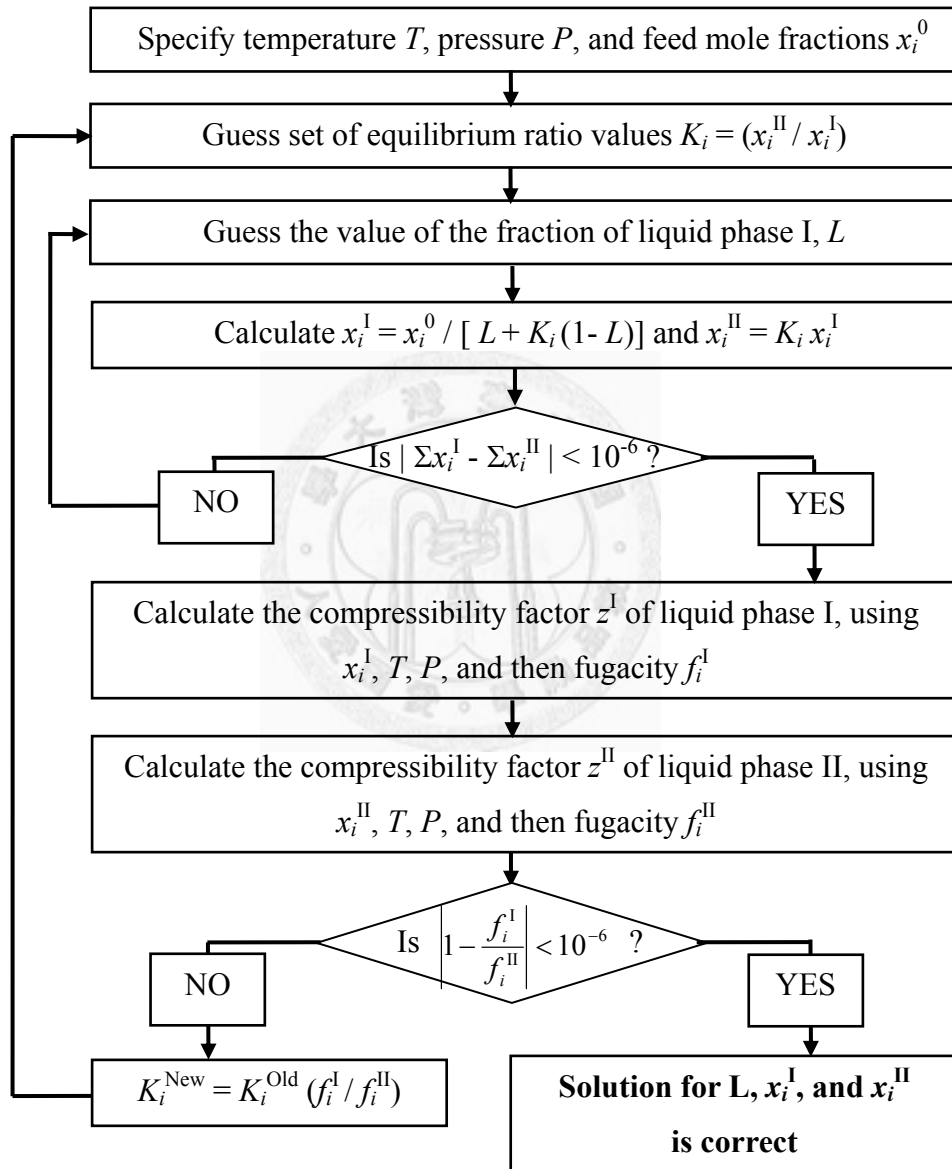
Figure 3.3-1. Flow diagram of an algorithm for the isothermal flash calculation using an equation of state.

3.4 Procedure for Vapor-Liquid-Liquid Equilibrium (VLLE) Calculation

For isobaric VLLE calculations, the procedure suggested by Iwakabe and Kosuge [67] is used. This calculation consists of four steps:

(1) For a given pressure P, the VLE over the whole composition range is calculated and the temperatures and compositions at the two turning points are recorded. (The turning points are the kinks in the dew point curves in the P-x-y diagram [67]. If VLLE exists, two turning points can be found in the VLE calculations.)

(2) The LLE calculation is then performed at the average temperature T from the two turning points. The compositions ($\underline{x}^{I}$, $\underline{x}^{II}$) of the two partially miscible liquids are recorded.

(3) Given pressure P and the liquid phase composition ($\underline{x}^{I}$ or $\underline{x}^{II}$), the temperature (T^{I} or T^{II}) and vapor phase composition ($\underline{y}^{I}$ or $\underline{y}^{II}$) are determined from isobaric VLE calculations.

(4) If the temperature in all these phases and vapor phase composition from the two isobaric calculations are the same ($|T\text{-}T^{I}|+|T\text{-}T^{II}|<10^{-3}$ K and $|\underline{y}^{I}\text{-}\underline{y}^{II}|<10^{-6}$), the VLLE calculation is converged. Otherwise, the average temperature ($0.5\text{x}(T^{I}+T^{II})$) is used as the new initial guess for T and steps (2) to (4) are repeated until convergence. The VLLE calculations usually converge within 10 iterations.

3.5 The 1-Octanol-Water Partition Coefficient

When a trace amount of solute i is added into the liquids of partially miscible 1-octanol and water, the ratio of the solute concentrations in the 1-octanol-rich phase (C_i^O) and the water-rich phase (C_i^W) is the 1-octanol-water partition coefficient of solute i, i.e., on a molar concentration basis

$$K_{\mathrm{OW},i} = \frac{C_i^O}{C_i^W} = \frac{C^O x_i^O}{C^W x_i^W} \tag{3.5-1}$$

, or on a mole fraction basis

$$K_{\mathrm{OW,X},i} = \frac{x_i^O}{x_i^W} \tag{3.5-2}$$

where C^O and C^W are the total molar concentrations of the 1-octanol-rich and water-rich phases, respectively; x_i^O and x_i^W are the mole fractions of solute i in the 1-octanol-rich and water-rich phases, respectively. According to the Gibbs phase rule, the degree of freedom of the system is 3 (= 3 species + 2 phases – 2), meaning that all the thermodynamics properties can be determined if the temperature, pressure, and the solute concentration in one of the phases are specified. In this work, the desired solute concentrations are determined with the initial more fraction 1.0×10^{-9} using the isothermal flash calculations [5] described in section 3.3.

3.6 The Infinite-Dilution Activity Coefficient.

The activity coefficient of component i in solution j can also be calculated from the ratio of fugacity coefficient of component i in the solution S ($\overline{\phi}_i^S$) and in its pure solvent (ϕ_i), i.e.

$$\gamma_{i/j}(T,P,\underline{x}) = \frac{\overline{f}_i^S(T,P,\underline{x})}{x_i f_i(T,P)} = \frac{\overline{\phi}_i^S(T,P,\underline{x})}{\phi_i(T,P)} \tag{3.6-1}$$

In order to determine the infinite dilution activity coefficient, we used $x_i = 0.0$ in the calculation of $\overline{\phi}_i^S$.

3.7 Procedure for Drug Solubility Calculation

The drug solubility calculation at specified temperature T and pressure P is performed following the flow diagram shown in Figure 3.7-1. The enthalpy of fusion and normal melting temperature of the drug are needed as input data in these calculations.
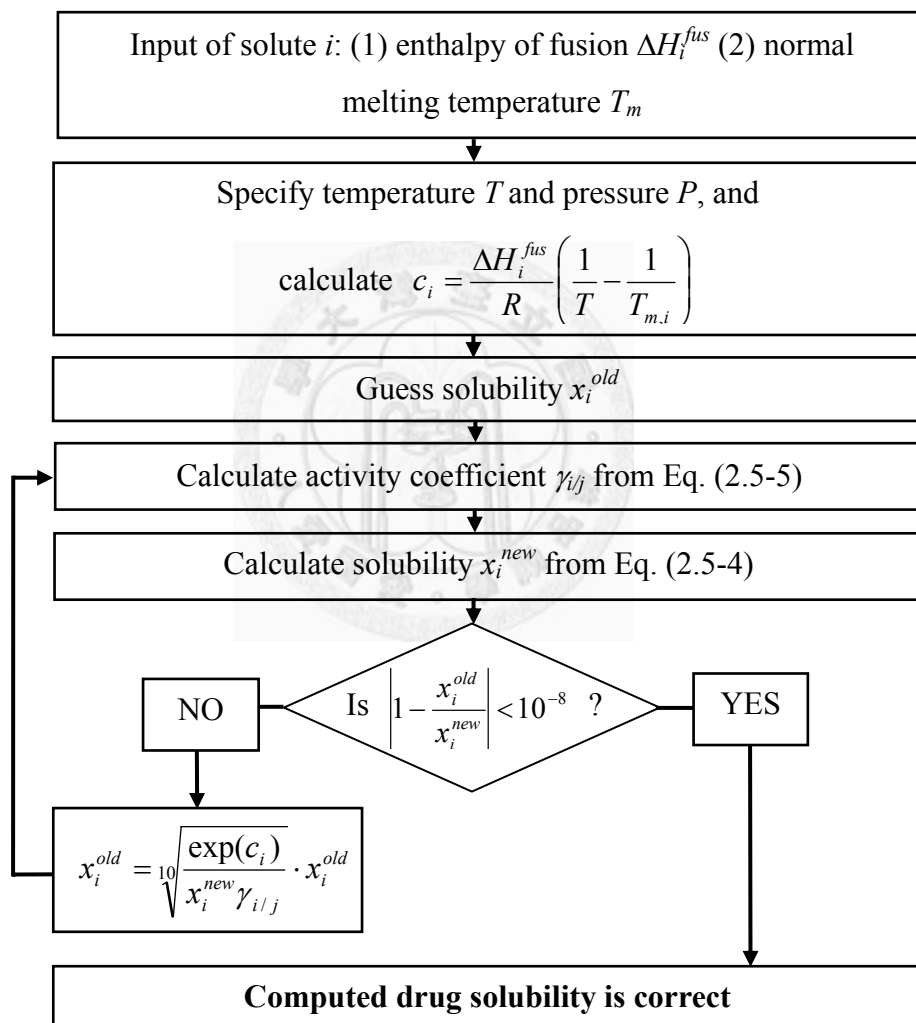
Figure 3.7-1. Flow diagram for the drug solubility calculation

3.8 Parameter Optimization

In the PR+COSMOSAC model, there are 15 global parameters and 3 parameters for each element [one for atomic radius (R_i) and two for calculation of dispersion energy ($A_{dsp,i}$ and $B_{dsp,i}$)], all of which are not system specific. Since all the organic compounds considered in this study are composed by only 6 atom types, there are currently a total of 33 (15+6×3) parameters in this model. Nine (a_{eff}=7.5 Å, f_{pol}=0.6916, f_{decay}=3.57, and R_i) of which are taken from Lin's work [63-64]. The remaining 24 parameters are optimized using experimental vapor pressure of selected compounds from the DIPPR database [43] (Note that for each compound, experimental vapor pressures at 3 different temperatures between the normal boiling point T_b and the critical point T_c are used.) or LLE of selected systems from the literature [110] with the following objective function

$$\text{Vapor pressure}:\text{Obj} = \left\{ \frac{1}{N} \sum_{j=1}^{N} \left[\ln P_j^{\text{vap}}(\text{calc}) - \ln P_j^{\text{vap}}(\text{expt}) \right]^2 \right\}^{1/2} \tag{3.8-1}$$

$$\text{LLE}:\text{Obj} = \left[\frac{1}{2M} \sum_{j=1}^{M} \sum_{k=1}^{2} \left(x_j^{k,\text{calc}} - x_j^{k,\text{expt}} \right)^2 \right]^{1/2} \tag{3.8-2}$$

where N is number of total data points; M is number of binary LLE tie-lines; superscript k indicates one of the two liquid phases in equilibrium; calc and expt represent the data from calculations and experiments.

The parameter optimization of these twenty-four parameters was performed stepwise as follows and once the parameters were optimized, these optimized parameters were fixed in the further optimization of other parameters.

(1) Linear alkanes (from ethane to dodecane) were used to optimize A_{dsp} and B_{dsp} for C and H atoms.

(2) Compounds that contain only C, H and O atoms (6 aldehydes, 11 ketones, 6 ethers, and 8 esters without branches) and do not have hydrogen bonding donor were

used to determine A_{dsp} and B_{dsp} for O.

(3) Fourteen linear alcohols were used to optimized c_{HH} (interaction between *hydro* groups) and c_{OO} (interaction between *other* groups) first and then the same set compounds were also used to determine the dispersion hydrogen bonding correction parameters ($A_{dsp,HB}$, $B_{dsp,HB}$, and $C_{dsp,HB}$).

(4) Compounds containing C, H, O, and N atoms (3 nitros and 3 nitriles) were used to optimize A_{dsp} and B_{dsp} of N.

(5) The dispersion correction parameters ($A_{dsp,RING}$ and $B_{dsp,RING}$) for ring structure involved in molecule were obtained from the optimization of 49 cycloalkane and aromatic compounds containing only C and H atoms.

(6) The A_{dsp} and B_{dsp} for Cl and F were then found using the data of 4 chlorine containing alkyl halides and 6 fluorine containing alkyl halides, respectively.

(7) c_{HO} (interaction between *hydro* and *other*) is optimized from 9 binary LLE.

(8) c_{AA} (interaction between *amino* groups) is optimized from vapor pressures of 20 amines.

(9) Two LLE systems are used to optimize c_{HA} (interaction between *hydro* and *amino*).

(10) c_{AO} (interaction between *amino* and *other*) is optimized from the vapor pressures of 12 selected compounds.

The compounds and LLE systems used in the parameter optimization are summarized in the Appendix B and the values of optimal parameters are summarized in Table 3-1. It should be noted that the values of hydrogen bonding interactions are very different each other. This reflects the fact that the interactions between different types of hydrogen bonding are different [96].

Table 3-1. Parameters and their values in the PR+COSMOSAC EOS

Universal Parameters

Parameter	Value	Parameter	Value
C_{PR}	-0.623	c_{HH} (kcal/mol).(Å^4/ e^2)	1757.9468
a_{eff}(Å^2)	7.50	c_{AA} (kcal/mol).(Å^4/ e^2)	1121.4047
f_{pol}	0.6916	c_{OO} (kcal/mol).(Å^4/ e^2)	1757.9468
f_{decay}	3.57	c_{HA} (kcal/mol).(Å^4/ e^2)	2462.3206
$A_{dsp,HB}$ (J/mol/K/Å^2)	-465876.8150	c_{HO} (kcal/mol).(Å^4/ e^2)	933.4108
$B_{dsp,HB}$ (J/mol/Å^2)	-429.5556	c_{AO} (kcal/mol).(Å^4/ e^2)	2057.9712
$C_{dsp,HB}$ (J/mol/K^2/Å^2)	-141.8436		
$A_{dsp,RING}$ (J/mol/K/Å^2)	-0.9181		
$B_{dsp,RING}$ (J/mol/Å^2)	-365.0667		

Atom Specific Parameters

atom type	R_i (Å)	$A_{dsp,i}$ (J/mol/K/Å^2)	$B_{dsp,i}$ (J/mol/Å^2)
H	1.30	0.1694	-191.4602
C	2.00	0.1694	-191.4602
N	1.83	0.4045	-207.9411
O	1.72	0.2701	-178.0767
F	1.72	0.1806	-125.7842
Cl	2.05	0.1566	-201.7754

Chapter 4. Predictions of Properties of Pure substances

In this section, the PR+COSMOSAC EOS is used to predict the vapor pressure, liquid density at the normal boiling point (T_b), critical properties (T_c, P_c, and $\underline{V}_c$), and normal boiling temperature (T_b) for 1296 pure substances. These compounds (which are composed by atoms C, H, O, N, Cl, and F) are all the common compounds that can be found in the VT-database [107-109] and DIPPR database [43]. The predicted results of vapor pressure at the normal boiling temperature, liquid density, and critical properties are compared with experimental values from DIPPR database. The accuracy of PR+COSMOSAC EOS is evaluated based either on average absolute relative deviation (AARD)

$$\text{AARD } p = \frac{1}{M} \sum_{i=1}^{M} \left| \frac{p_i^{\text{calc}} - p_i^{\text{expt}}}{p_i^{\text{expt}}} \right| \tag{4.0-1}$$

or the average absolute deviation (AAD)

$$\text{AAD } p = \frac{1}{M} \sum_{i=1}^{M} \left| p_i^{\text{calc}} - p_i^{\text{expt}} \right| \tag{4.0-2}$$

where p is the properties of interest (T_c, P_c, P, y_i, etc), M is the number of data points and the superscripts calc and expt denotes the value form either calculation or experiment, respectively. Table 4-1 summarizes the overall performance of PR+COSMOSAC EOS regarding the prediction of properties of pure substances.

Table 4-1. The overall average deviations for prediction of pure fluid properties

	N compounds[a]	AARD (%)
P_c (Pa)	346	9.7%
T_c (K)	431	4.1%
$\underline{V}_c$ (m³/mol)	270	5.2%
$P^{vap}(T_b)$ (Pa)[b]	1296	48.9%
Liquid density at T_b (kmol/m³)	1290	21.1%

a. A different number of compounds considered for each property is due to availability of experimental data in DIPPR database.

b. AARD estimated from the AAD of $\ln P^{vap}$.

4.1 Critical Properties

The overall AARD in the prediction of P_c, T_c, and $\underline{V}_c$ are 9.7% (0.39 MPa), 4.1% (22.34 K), and 5.2% (0.02 m³/kmol), respectively. Figures 4.1-1 to 4.1-3 illustrate the comparison of experimental and predicted critical properties for compounds whose experimental critical properties are available in the DIPPR database (346, 431, and 270 compounds in critical pressure P_c, critical temperature T_c, and critical volume $\underline{V}_c$, respectively). The critical volume is estimated from the volume of solvation cavity in COSMO calculation. The predicted $\underline{V}_c$ are in good agreement with experiment for small compounds (e.g., $\underline{V}_c$ < 0.6 m³/kmol). It has been observed previously that the critical volume is highly correlated with the molecular size [20]. We also found that there is an good linear correlation between the value of parameter b determined from the solvation cavity and that from T_c and P_c in the PR EOS (as shown in Figure 4.1-4). These results show that the atomic radii (Table 3-1) used in establishing the solvation cavity are

adequate for describing the volume parameter *b*. The larger deviations (underestimation) found for larger compounds could be attributed to the ignorance of conformation flexibility in current calculations (e.g., long chain alkanes are modeled as linear but they could be folded in reality) and/or the ignorance of molecular shape effects in the PR EOS (the cavity term in PR EOS is valid for spherical molecules [111]).

The deviations in T_c are less than 120 K, except for carbon monoxide and methacrylic acid, marked by A and B, respectively, in Figure 4.1-2. Once $\underline{V}_c$ and T_c are known, the critical pressure can be obtained from $P_c = z_cRT_c/\underline{V}_c$. While the PR EOS has a fixed value of critical compressibility factor ($z_c = 0.307$) for all compounds, experimental values of z_c range from 0.2 to 0.3 for most chemicals [43, 46]. Therefore, we have rescaled the calculated P_c by 0.26/0.307 in Figure 4.1-3 for better accuracy. [Note that the use of $z_c = 0.26$ is recommended for calculation of P_c only and is not used in any other property calculations (e.g. the vapor pressure).] The poorly predicted P_c found in Figure 4.1-3 (marked as C to K) are caused either by the constant critical compressibility factor ($z_c = P_cV_c/RT_c$) in the PR EOS or the error in the predicted T_c. For example, hydrogen fluoride (marked C) has $z_c = 0.117$ and ammonia (marked G) has $z_c = 0.242$ but has a deviation of 73 K in predicted T_c.
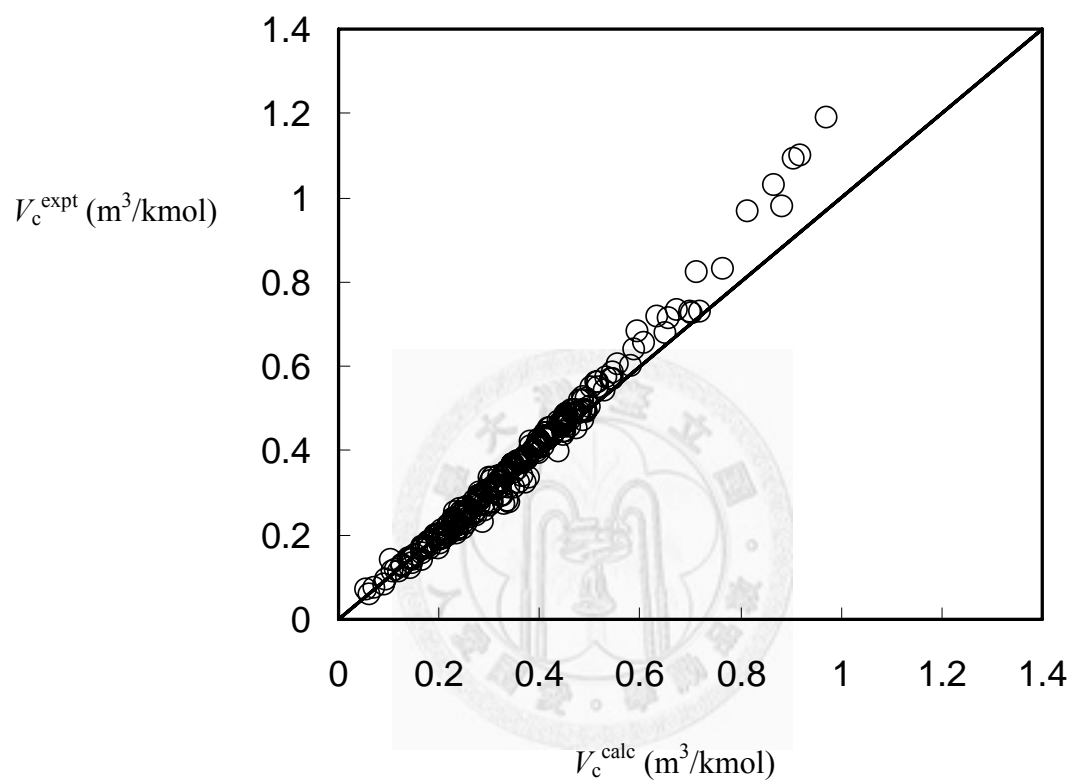
Figure 4.1-1. Comparison of critical volumes from experiments and predictions.
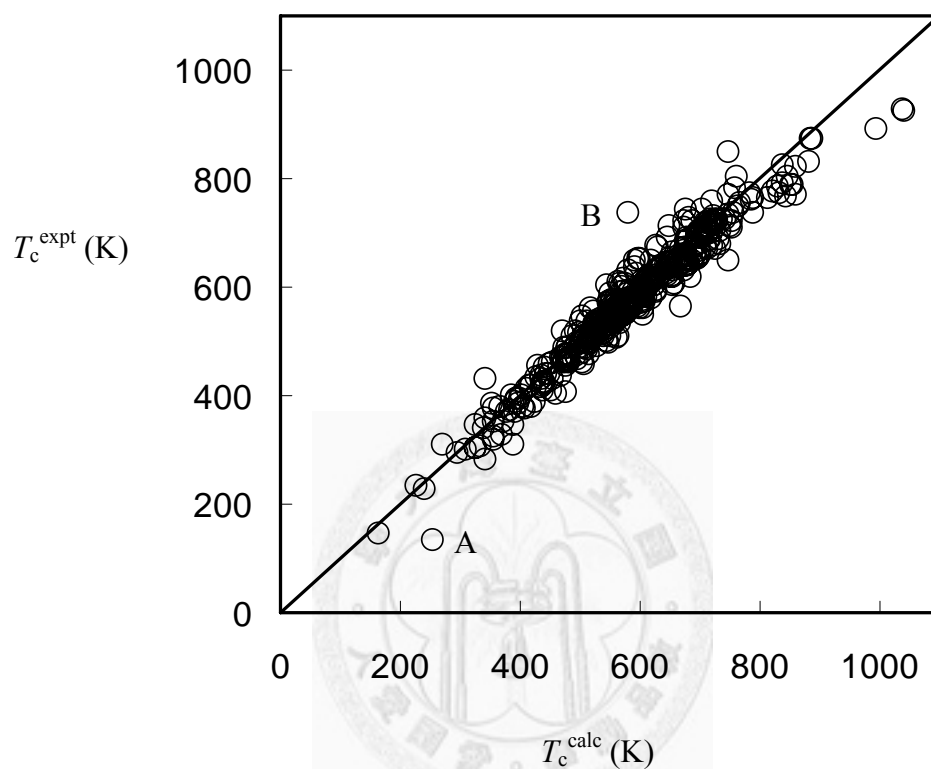
Figure 4.1-2. Comparion of critical temperatures from experiments and predictions. The marked species, whose absolute deviation are larger than 120 K, are (A) carbon monoxide and (B) methacrylic acid.
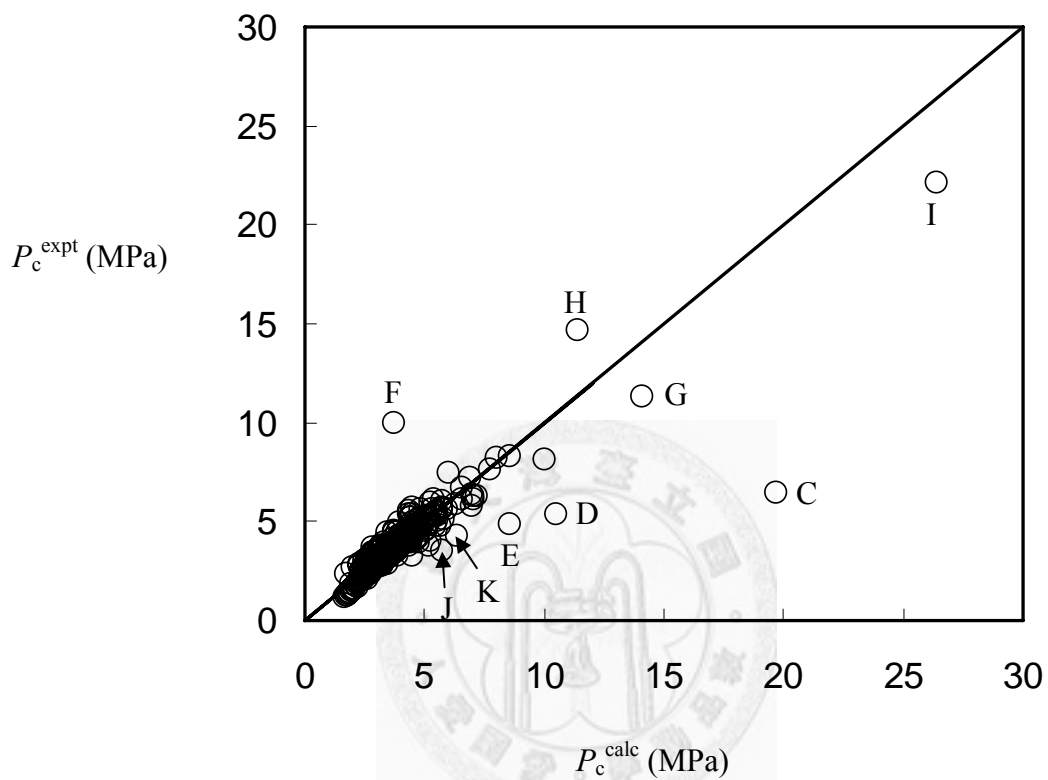
Figure 4.1-3. Comparison of critical pressures from experiments and predictions. The marked species, whose absolute deviations are larger than 2 MPa, are (C) hydrogen fluoride, (D) hydrogen cyanide, (E) acetonitrile, (F) nitrogen tetroxide, (G) ammonia, (H) hydrazine, (I) water, (J) carbon monoxide, and (K) propionitrile.
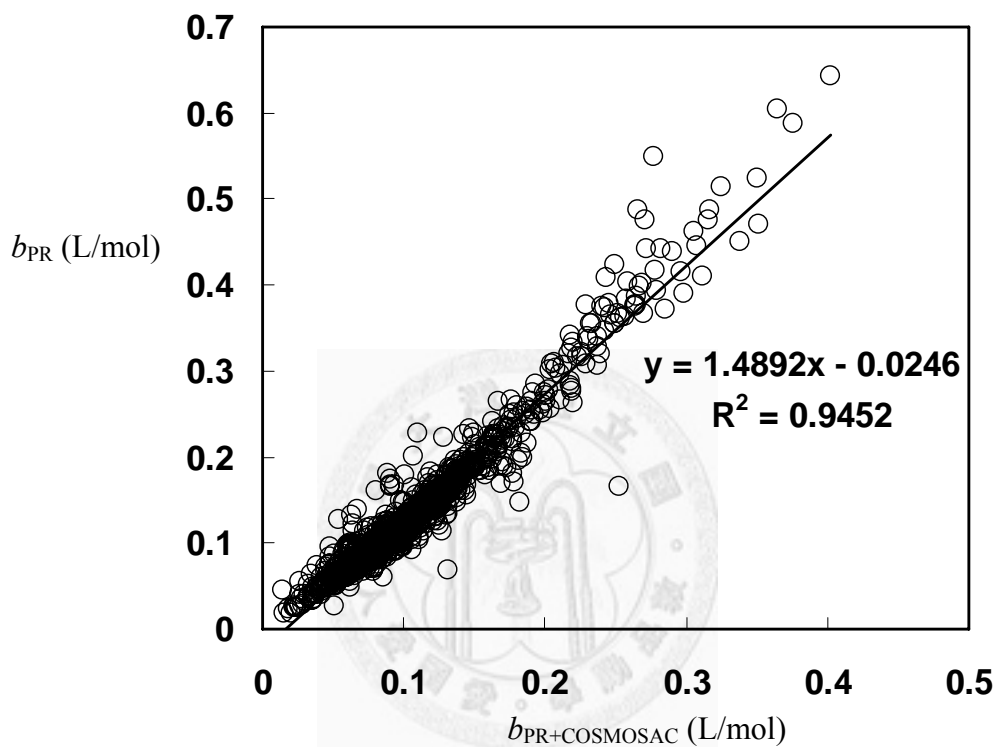
Figure 4.1-4. Comparison of values of volume parameter b for 1296 compounds in the original Peng-Robinson EOS and PR+COSMOSAC.

4.2 Vapor Pressure and Liquid Density at Normal Boiling Temperature

The results of vapor pressure at normal boiling point temperature (T_b) for a total of 1296 pure compounds are shown in Figure 4.2-1. Except for a total of 18 compounds having an error of 2 lnP unit (the worst predicted compound is carbon monoxide whose error in lnP is 6.77), predicted results for all the other compounds are acceptable. As listed in Table 4-1, the overall AARD of vapor pressure and liquid density at T_b are 48.9% (0.4 lnP unit) and 21.1%, respectively.

It seems that PR+COSMOSAC is unable to give a good prediction of vapor pressure for pure substance. This is because the prediction of vapor pressure of pure substances is a very challenging topic, especially when trying to use a single model without using any experimental data to predict a wide temperature range (from normal boiling point temperature to critical temperature). For example, some QSPR or artificial neural network models can provide much more accurate predictions, but they are restricted to predict the vapor pressure at a single temperature according to the experimental data used to get values of model parameters [112]. To our knowledge, the attempts on prediction of vapor pressures with a wide temperature range can be categorized into (a) COSMO-based methods and (b) methods that estimate the parameter values in an existing equation of state. The followings are examples of accuracy of existing models in prediction of vapor pressure of pure substances: (1) COSMO-RS: Eckert and Klamt [113] claimed that COSMO-RS can provide an absolute average deviation (AAD-ln$P$) less than 0.5 ln$P$ units (equals to absolute average relative deviation AARD-P <65%). (2) COSMO-SAC: Wang et al. [62] say that AARD-P for 1432 substances from COSMO-SAC is ~63% with the help of experimental liquid density. (3) Group contribution based equation of state: Emami et al. [114] use group contribution methods to estimate the values of parameters in Elliott-Suresh-Donohue

(ESD) EOS, SAFT EOS, and PC-SAFT EOS. The AARD-P for 878 compounds are 36% for ESD EOS, 65% for SAFT, and 32% for PC-SAFT. All these methods provide similar accuracy in prediction of vapor pressure of pure substances as PR+COSMOSAC.

To illustrate that the method proposed here can be used to describe the complete fluid phase diagram, in Figure 4.2-2 we present the pressure-volume and pressure-temperature diagrams for three chemical species having very different critical pressures: 1,3-propylene glycol (high P_c= 9.5 MPa), 1,1,2-trichloroethane (medium P_c= 4.83 MPa), cyclooctane (low P_c= 3.57 MPa). The solid and dashed lines are the results from the proposed method and the original PR EOS. The temperature dependence of the vapor pressure [Figure 4.2-2(a)] is well described for these compounds. The deviations of liquid molar volume and the gas molar volume from proposed model are similar to those from original PR EOS [(Figure 4.2-2(b)]. As listed in Table 4-1, the average absolute relative deviation in the liquid density for 1290 compounds at normal boiling point temperature (note there is no experimental data available in the DIPPR database for 6 of the 1296 compounds considered in this work) was found to be 21%. Although the agreement is not perfect, the present model shows how effectively a theoretically-based statistical mechanical model can describe the temperature-dependent parameter $a(T)$ in the PR EOS.
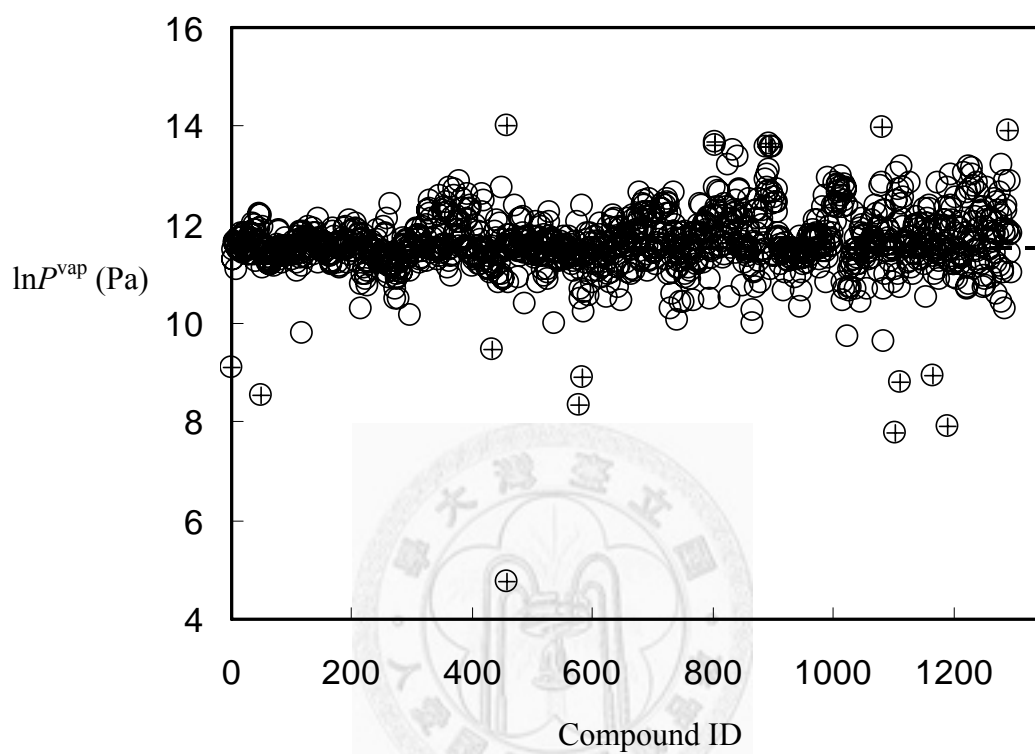
Figure 4.2-1. Predicted vapor pressure at normal boiling temperature for 1296 compounds. The dashed line presents 1 atm. The marked species, circle with cross, has an absolute deviations of $\ln P^{vap}$ larger than 2 lnP unit.

(a)
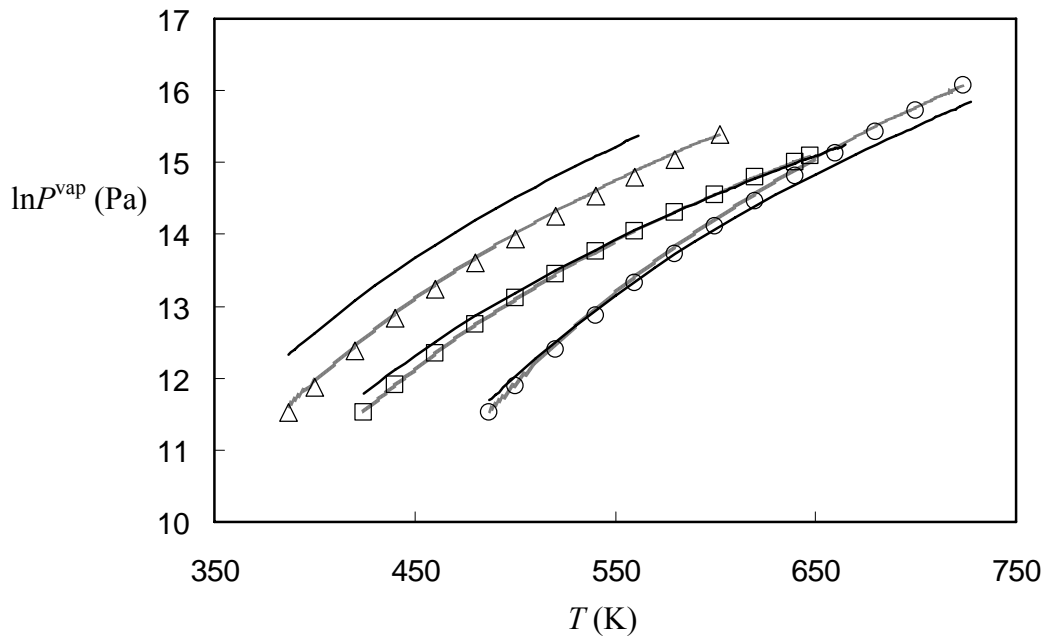
(b)
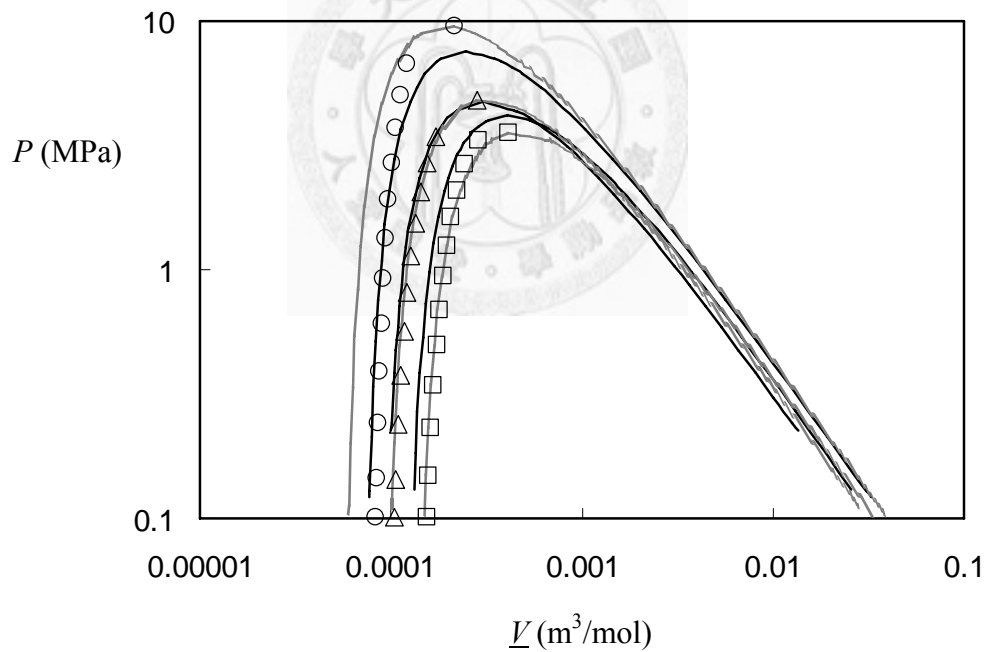
Figure 4.2-2. The pressure-temperature (a) and pressure-volume (b) diagrams from the original PR EOS (gray lines) and the PR+COSMOSAC with (solid lines) for cyclooctane, 1,1,2-trichloroethane, and 1,3-propylene glycol. The experimental data [43] are shown in triangles, squares, circles for the three compounds, respectively.

4.3 Normal Boiling Temperature (T_b) for environmentally important chemicals.

The normal boiling temperature of pure component is an essential property for many chemical, biochemical, and environmental studies. However, the experimental values of T_b for large, complex, or toxic species are very scarce. The determination of T_b is to determine the temperature at which the vapor pressure is 1atm. Wang et al. [115] showed the prediction of T_b for 86 environmentally important chemicals using the COSMO-SAC-BP model. It would be interesting to understand the accuracy of the proposed model in this application. Since there are 63 out of 86 compounds are included in VT-database, (It should be noted that cosmo-files of 5 compounds are taken from unpublished database which is the continuing work of VT-database and generated from Prof. Sandler's group), the prediction of T_b is performed only for these compounds.

The comparison of experimental and calculated T_b from COSMO-SAC-BP and PR+COSMOSAC is shown in Figure 4.3-1 and Table 4-2 (a comprehensive list can be found in Appendix C). The overall AAD-T and AARD-T are 17.7 K and 3.8% from the proposed model, which is more accurate than 22 K and 4.6% from COSMO-SAC-BP. Moreover, the maximum and the standard deviation of AAD are 75.7 K and 16.9 K from the PR+COSMOSAC and are also superior to 125.4 K and 25.2 K from COSMO-SAC-BP. Although the PR+COSMOSAC has more model parameters (33) than the COSMO-SAC-BP (23), the PR+COSMOSAC can provide a prior prediction while the COSMO-SAC-BP needs the liquid density as input.

Table 4-2. The comparison of overall deviation in normal boiling temperature for environmentally important chemicals (comprehensive list can be found in Appendix C).

	PR+COSMOSAC		COSMO-SAC-BP	
	AAD-T (K)	AARD-T (%)	AAD-T (K)	AARD-T (%)
Overall	17.7	3.8%	22.0	4.6%
Maximum	75.7	13.0%	125.4	20.5%
Standard deviation	16.9	--	25.2	--
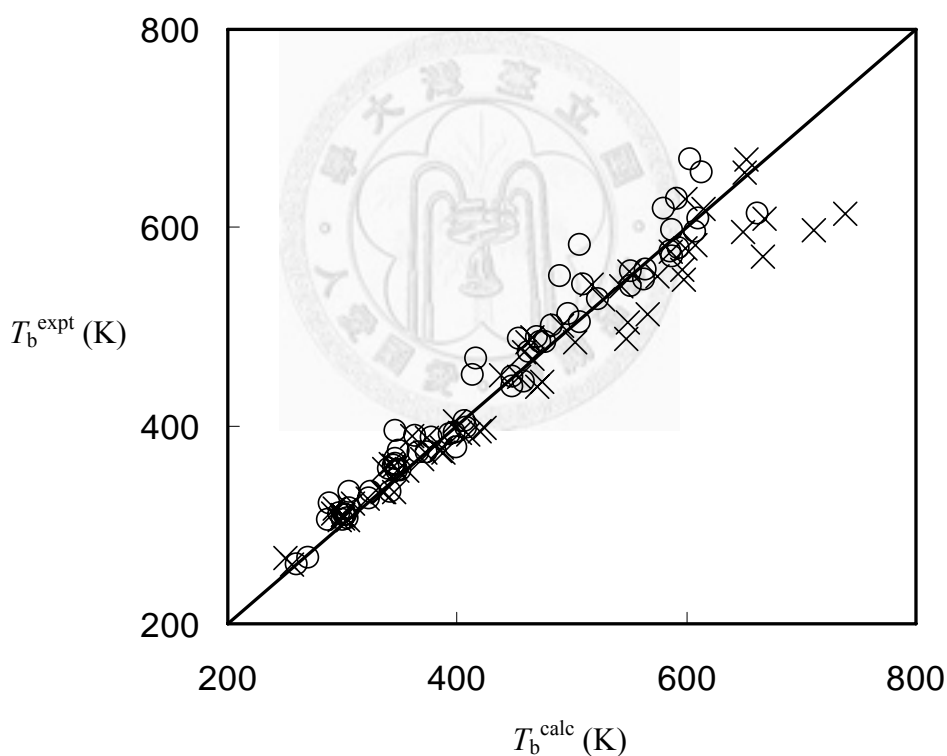
Figure 4.3-1. Comparison of normal boiling temperatures for environmentally important chemicals from experiments and predictions from PR+COSMOSAC (open circles) and COSMO-SAC-BP (crosses).

Chapter 5. Predictions of Phase Equilibria of Mixture Fluids

To facilitate the analysis of mixtures, the binary mixtures considered here are, according to the species involved in the formation of hydrogen bonds, classified into three groups [37, 78]:

(I) no hydrogen bond (e.g., nitroethane + hexane);

(II) hydrogen bonds between like species [e.g., pentane + water (hydrogen bonds between water only)];

(III) hydrogen bonds between unlike and like species [e.g., nitroethane + water (hydrogen bonds between nitroethane and water, and between water molecules)].

These three types of systems are denoted as type I, type II, and type III systems in the following discussions.

5.1 Vapor-Liquid Equilibrium (VLE)

In this study, vapor-liquid equilibrium data of 116 binary mixtures (including about 3000 data points with temperatures ranging from 255.37 K to 623.15 K and pressures from 0.03 KPa to 18.97 MPa) are used to examine the accuracy of PR+COSMOSAC. The overall absolute average errors from the proposed PR+COSMOSAC method are 28.2% [AARD determined from Eq. (4.0-1)] in pressure and 5.0% [AAD determined from Eq. (4.0-2)] in vapor phase composition (Table 5-1). The errors reduce significantly to 6.2% and 2.0% if the vapor pressures of pure components are used (PR+COSMOSAC+P^{vap}), and to 6.7% and 2.2% if critical properties and acentric factor of pure components are used (PR+COSMOSAC+$T_cP_c\omega$).

Figure 5.1-1 shows the *P-x-y* diagram for 2-methylpentane/3-methyl-2-butanol

binary mixtures. In this system the pure component vapor pressures are well predicted by PR+COSMOSAC and the predicted results from all three methods are almost identical. (Note that results from PR+COSMOSAC, PR+COSMOSAC+$T_cP_c\omega$, and PR+COSMOSAC+P^{vap} are shown in dashed, solid, and gray lines, respectively.) Figure 5.1-2 shows the *P-x-y* diagram for 1-hexene/ethyl acetate at three temperatures. At 313.15 K, the vapor pressures are well predicted from PR+COSMOSAC and the three methods behaves similarly. As the temperature increases, in which case the deviations in vapor pressure increases, larger deviations are observed in the mixture VLE as well. Similar phenomenon can be found in Figure 5.1-3. When the needed experimental data for PR+COSMOSAC+$T_cP_c\omega$ and PR+COSMOSAC+P^{vap} are available, these two methods reliably improves the accuracy in VLE regardless the mixture is ideal (e.g., Figure 5.1-4) or highly non-ideal (e.g., Figures 5.1-1, 5.1-2, 5.1-3, and 5.1-5). Therefore, while the completely predictive PR+COSMOSAC approach provides the general shape of VLE phase diagram, its accuracy in describing mixture VLE is limited by its capability of predicting pure component vapor pressures.

The applicability of the proposed method to high pressure systems is illustrated with 2-propanol/water binary mixtures in Figure 5.1-6. While the PR+COSMSAC method provides qualitative agreement with experiment, the inclusion of pure component properties (PR+COSMOSAC+$T_cP_c\omega$ and PR+COSMOSAC+P^{vap}) significantly improves the accuracy in predicted phase boundaries. Also note that the PR+COSMOSAC+P^{vap} is applicable only at temperatures below T_c of 2-propanol (~508 K), and both PR+COSMOSAC and PR+COSMOSAC+$T_cP_c\omega$ are applicable at all temperatures.

Table 5-1. The overall absolute average errors in equilibrium pressure and the liquid

phase composition from different methods

	PR+COSMOSAC			PR+COSMOSAC+P^{vap}			PR+COSMOSAC+$T_cP_c\omega$		
	AARD-P (%)	AAD-y_1 (%)	N-sys[a]	AARD-P (%)	AAD-y_1 (%)	N-sys	AARD-P (%)	AAD-y_1 (%)	N-sys
I	24.7	3.2	122	5.6	1.7	106	6.1	1.7	122
II	23.5	5.6	42	7.1	2.7	35	6.2	2.9	42
III	37.7	7.8	66	6.6	2.1	58	8.1	2.8	66
Overall	28.2	5.0	230	6.2	2.0	199[b]	6.7	2.2	230

a. N-sys: number of systems.

b. Fewer number of data points can be evaluated because some systems are at

temperatures higher than the critical temperature of one of the components in the

mixture.
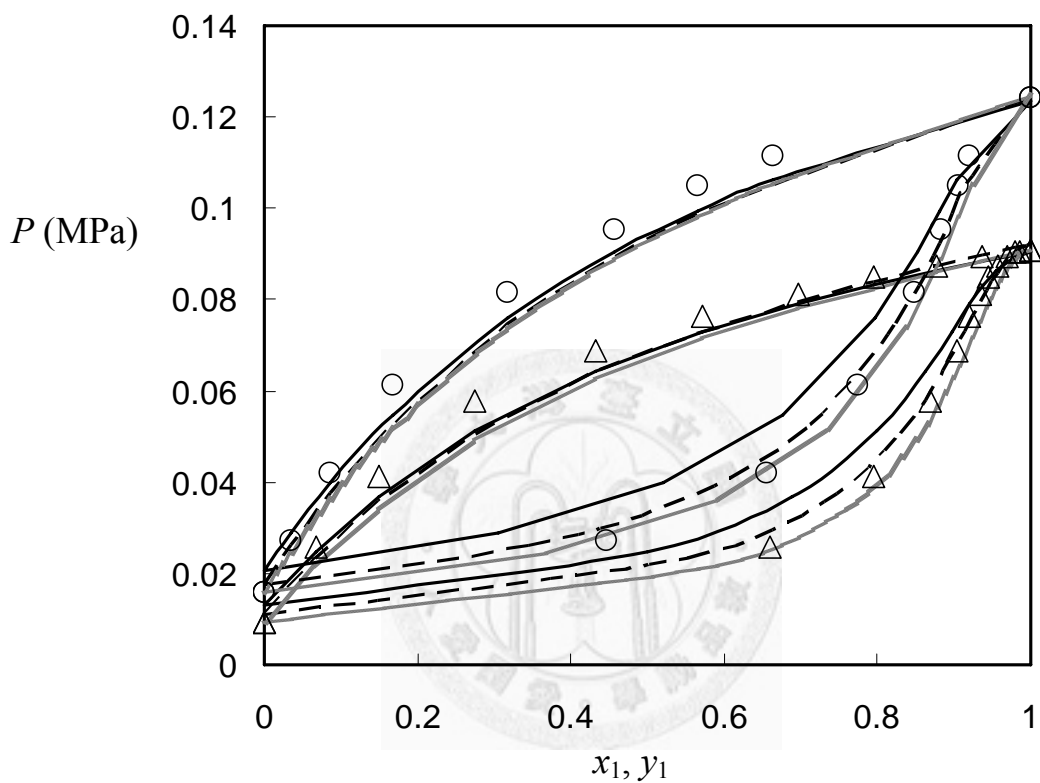
Figure 5.1-1. *P-x-y* phase diagram of vapor-liquid equilibrium for 2-methylpentane (1) + 3-methyl-2-butanol (2) (a type II system). The dashed, solid, and gray lines are predicted results from PR+COSMOSAC, PR+COSMOSAC+$T_cP_c\omega$, and PR+COSMOSAC+P^{vap}, respectively. The experimental data, taken from Psutka and Wichterle [116], are shown as open circles (340 K) and open triangles (330 K).
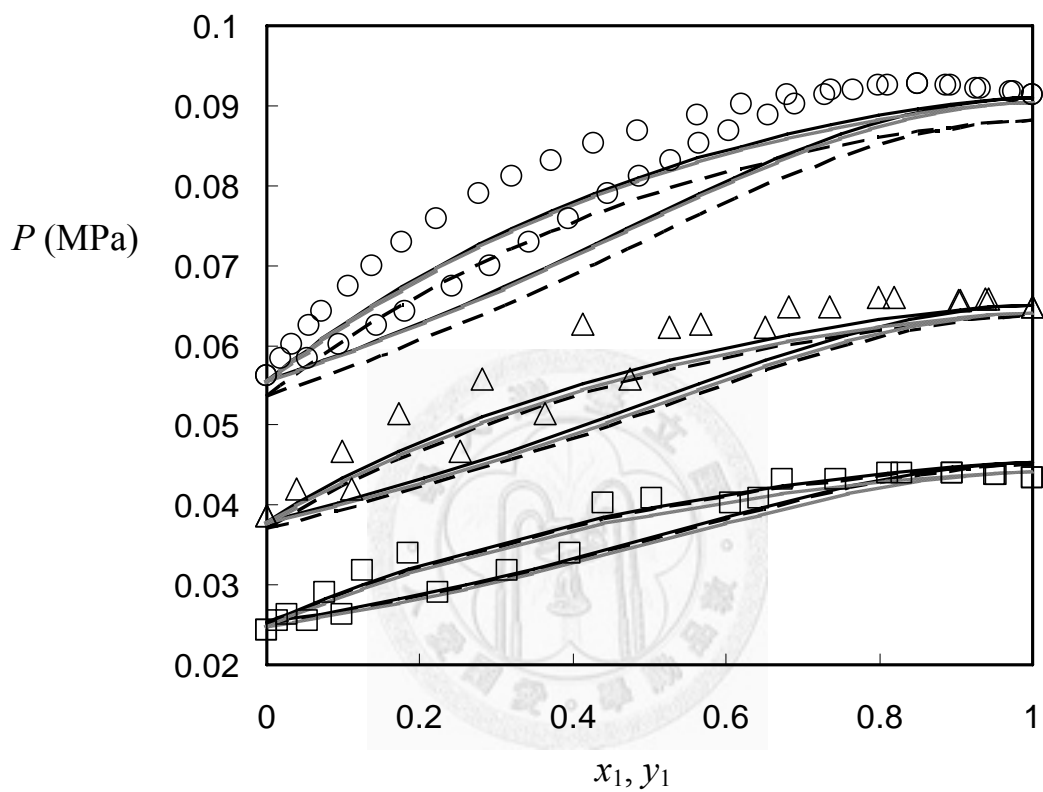
Figure 5.1-2. *P-x-y* phase diagram of vapor-liquid equilibrium for 1-hexene (1) + ethyl

acetate (2) (a type I system). The lines have the same meanings as in Figure 5.1-1. The

experimental data, taken from Campbell et al. [117], are shown as open circles (333.15

K) , open triangles (323.15 K), and open squares (313.15 K).
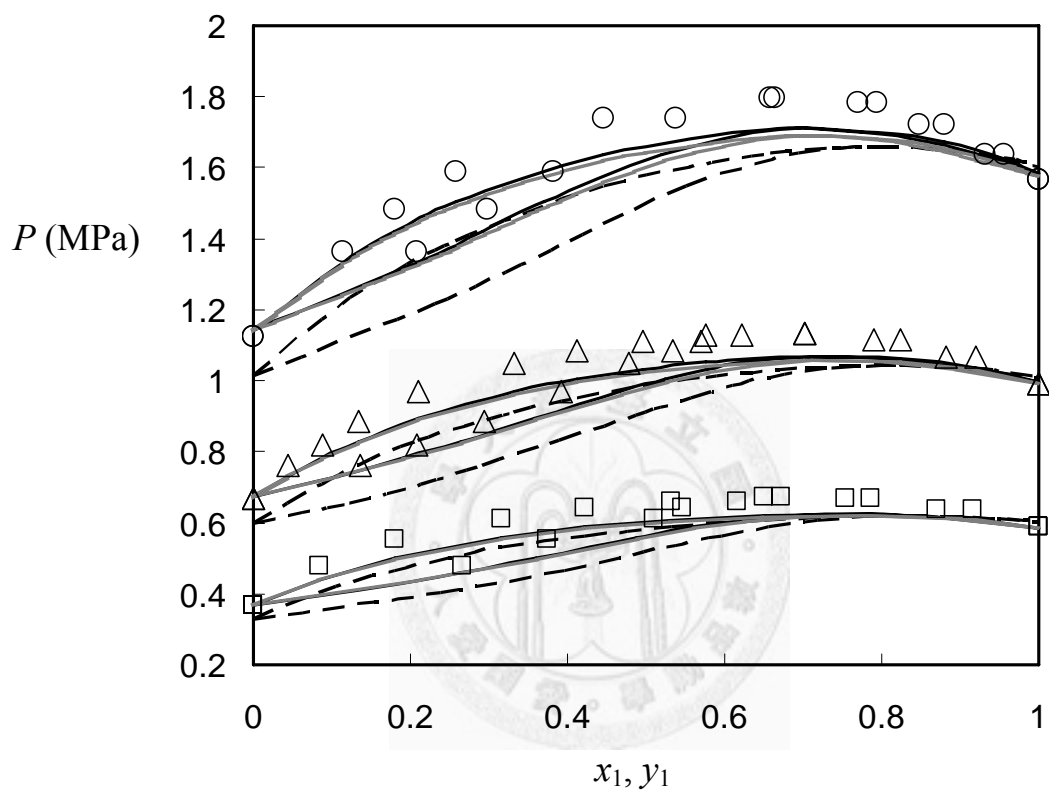
Figure 5.1-3. *P-x-y* phase diagram of vapor-liquid equilibrium for n-pentane (1) + acetone (2) (a type I system). The lines have the same meanings as in Figure 5.1-1. The experimental data, taken from Gmehling et al. [118], are shown as open circles (422.6 K) , open triangles (397.7 K), and open squares (372.7 K).
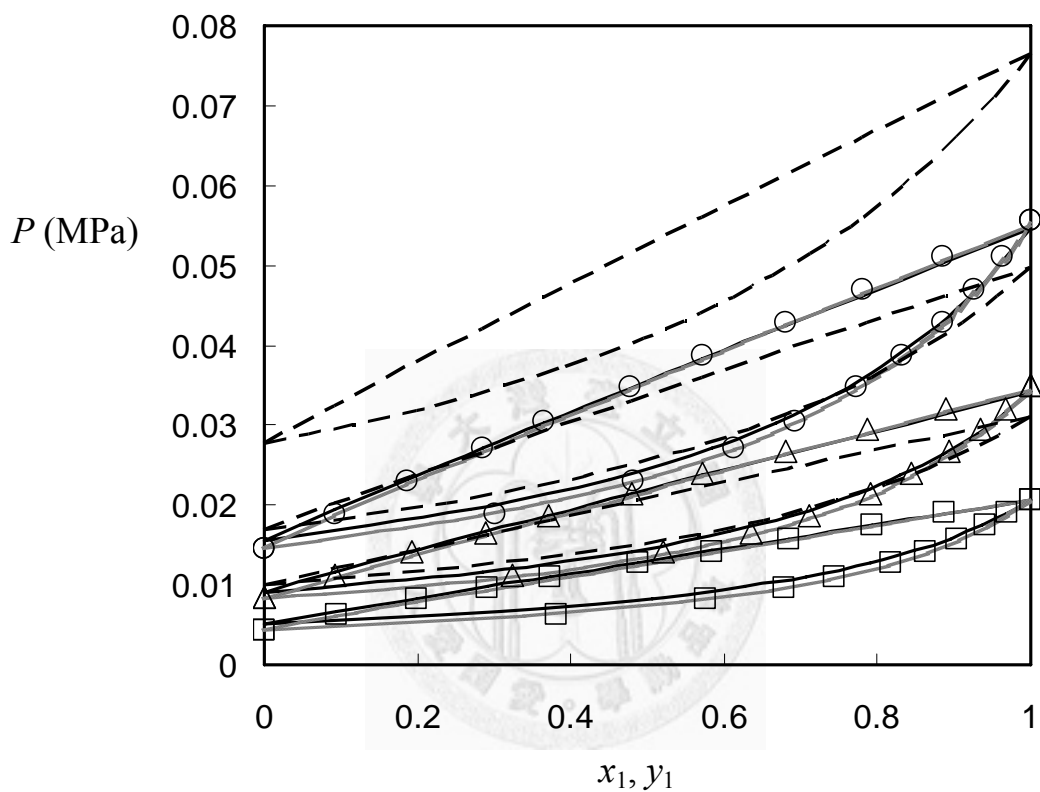
Figure 5.1-4. *P-x-y* phase diagram of vapor-liquid equilibrium for *p*-cresol (1) + 4-methoxyphenol (2) (a type III system). The lines have the same meanings as in Figure 5.1-1. The experimental data, taken from Hwang et al. [119], are shown as open circles (453.15 K) , open triangles (438.15 K), and open squares (423.15 K).
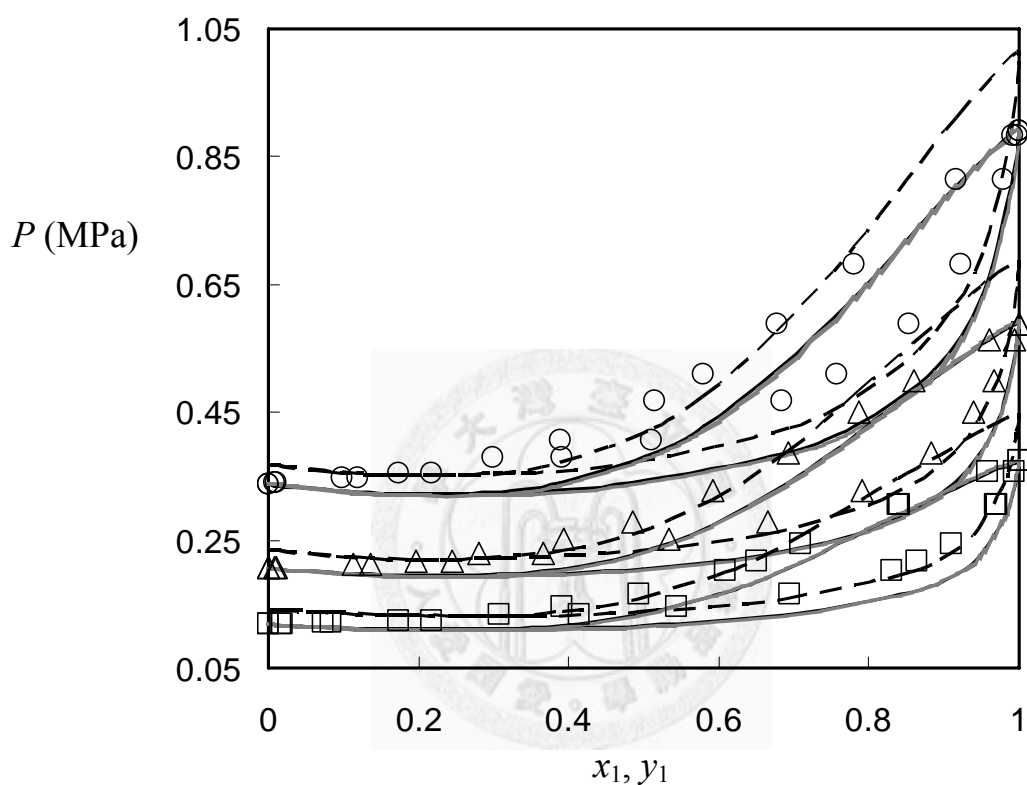
Figure 5.1-5. *P-x-y* phase diagram of vapor-liquid equilibrium for dimethyl ether (1) + 1,1,1,2,3,3-hexafluoropropane (2) (a type I system). The lines have the same meanings as in Figure 5.1-1. The experimental data, taken from Bobbo et al. [120], are shown as open circles (313.22 K) , open triangles (298.17 K), and open squares (283.12 K).
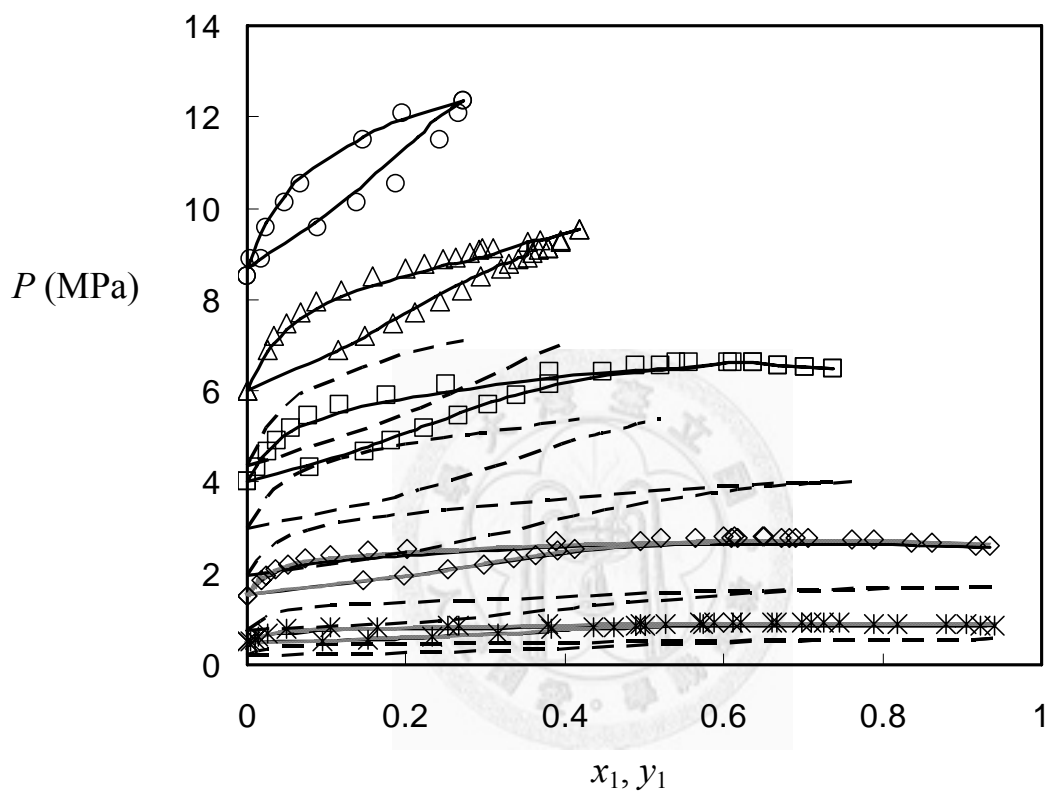
Figure 5.1-6. *P-x-y* phase diagram of vapor-liquid equilibrium for 2-propanol (1) + water (2) (a type III system). The lines have the same meanings as in Figure 5.1-1. The experimental data, taken from Barr-David and Dodge [121] and Sada and Morisue [122], are shown as open circles (573.15 K) , open triangles (548.15 K), open squares (523.15 K), open diamonds (473.15 K), and asterisks (423.15 K).

5.2 Liquid-Liquid Equilibrium (LLE)

In this study we consider a total of 68 binary and 39 ternary liquid-liquid equilibrium systems at atmospheric pressure and different temperatures. All the systems studied are highly non-ideal. Table 5-2 summarizes the predicted results from PR+COSMOSAC, modified UNIFAC [55], UNIFAC-LLE [66], and COSMO-SAC [62]. Note that in the case when several experimental data point are found at one temperature, the averaged experimental value in the literature [110] is used in the calculation of RMS. The overall deviation [determined from Eq. (3.8-2)] for binary LLE from PR+COSMOSAC is 0.0689 (corresponding to 80% in percentage error in mutual solubility) and similar accuracy is obtained from modified UNIFAC (0.0822 or 98%) and UNIFAC-LLE (0.0697 or 86%). These three approaches are more accurate than COSMO-SAC (0.1125 or 118%). Also shown in Table 5-2 are the numbers of systems in which a phase separation is successfully predicted. For example, 58 out of the total 68 binary mixture systems were successfully determined to exhibit LLE using the PR+COSMOSAC model proposed here. The corresponding numbers are 61 out of 68 systems, 55 out of 68 systems, and 48 out of 68 from the modified UNIFAC, UNIFAC-LLE, and COSMO-SAC model, respectively. Therefore, not one approach can describe all the 68 binary liquid-liquid equilibrium systems. For systems unable to be described the LLE phase separation, they are not included in the calculation of RMS error.

UNIFAC-LLE provides the lowest RMS for type I and II systems, but it sometimes fails to describe the temperature dependence of immiscible curve correctly (as illustrated in Figure 5.2-1). This is consistent with the observation that UNIFAC-LLE is suitable within a small temperature range from 10 to 40 $^{\circ}$C [66, 69]. As shown in Figures 5.2-1 and 5.2-2, both PR+COSMOSAC and modified UNIFAC are able to

describe well the temperature dependence of solubility curve.

Table 5-2. Comparison of root-mean-square (RMS) errors [Eq. (3.8-2)] from 4 different models in LLE prediction

	Expt.	PR+ COSMOSAC		Modified UNIFAC		UNIFAC-LLE		COSMO-SAC	
	$Nsys^a$	$Nsys^b$	RMS	$Nsys^b$	RMS	$Nsys^b$	RMS	$Nsys^b$	RMS
Binary^c	68	58	0.0689	61	0.0822	55	0.0697	48	0.1125
I	25	21	0.0967	23	0.0670	24	0.0729	21	0.0616
II	16	12	0.0235	15	0.0715	11	0.0376	13	0.0558
III	27	25	0.0674	23	0.1046	20	0.0835	14	0.2414
Ternary	39	39	0.0775	25	0.5150	23	0.0492	38	0.0779

a. number of mixture systems considered. Each system is a mixture of 2 (binary) or 3 (ternary) species.

b. number of systems (data points/tie-lines) that are predicted to show liquid-liquid phase separation.

c. The binary systems are categorized to three groups (I) no hydrogen bond, (II) hydrogen bonds between like species, and (III) hydrogen bonds between unlike and like species.
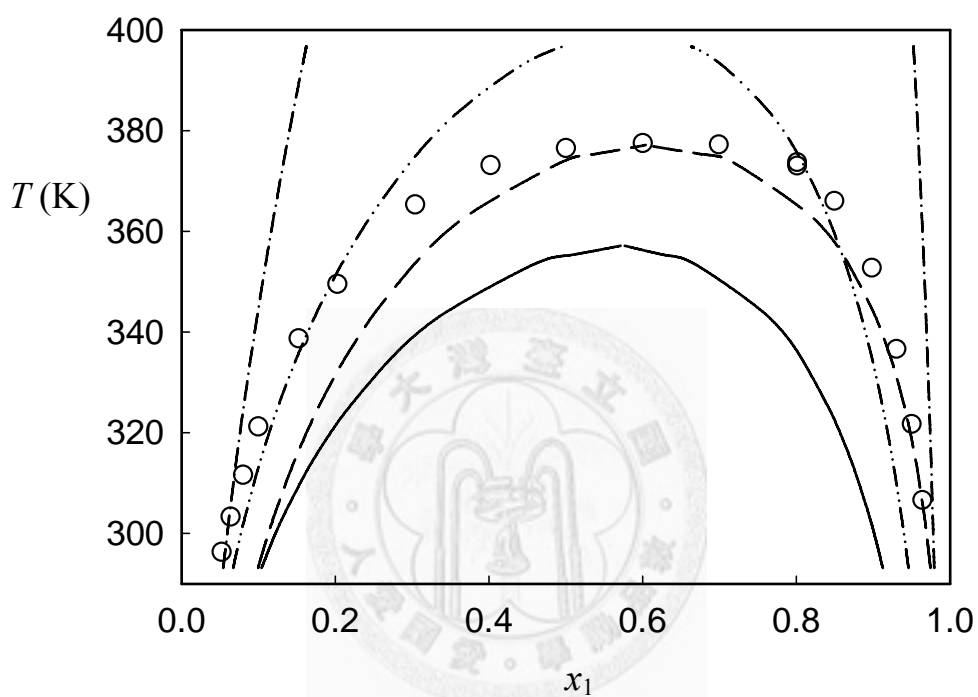
Figure 5.2-1. Comparison of predicted and experimental liquid-liquid equilibrium for furfural (1) + 2,2,5-trimethylhexane (2) (a type I system). The solid, dashed, dotted-dashed, dashed-dotted-dotted lines are predicted results from PR+COSMOSAC, modified UNIFAC, UNIFAC-LLE, and COSMO-SAC respectively. The open circles are the experimental data from Sørensen and Arlt [110].
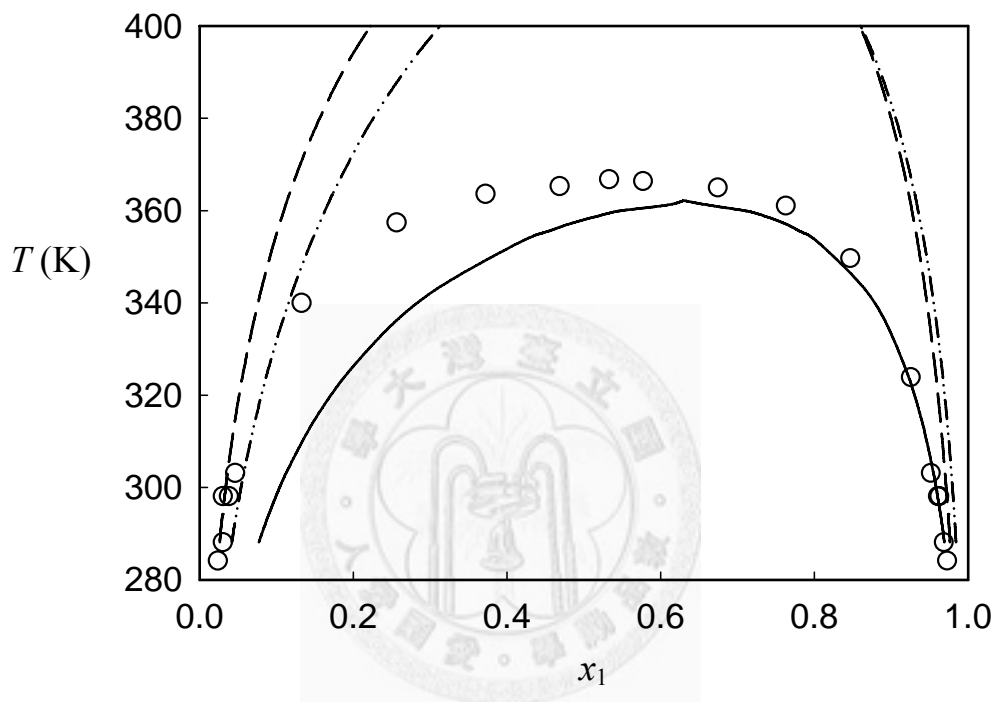
Figure 5.2-2. Comparison of predicted and experimental liquid-liquid equilibrium for nitromethane (1) + cyclohexane (2) (a type I system) [110]. The lines and symbols have the same meaning as in Figure 5.2-1. UNIFAC-LLE predicts no miscibility gap of this system.

The much smaller RMS obtained for type II system from PR+COSMOSAC and UNIFAC-LLE is because of well description of hydrocarbon + water systems, as illustrate in Figure 5.2-3. It is interesting to note that the PR+COSMOSAC EOS can describe the solubility both in the water-rich and the alkane-rich phases, while the UNIFAC-LLE is less accurate for the water-rich phase. The temperature variation in the mutual miscibility of water-alkane mixtures is better captured by the PR+COSMOSAC EOS.

Systems in type III are much more challenging because the hydrogen-bonding interaction exists not only between the same species but also between different species in the mixture. Taking the advantage of multiple hydrogen-bonding σ-profiles, PR+COSMOSAC provides the lowest RMS among the three methods and is capable to describe the upper critical solution temperature as shown in Figures 5.2-4, 5.2-5, and 5.2-6. It is noteworthy that, while the miscibility gaps predicted from the modified UNIFAC are in good agreement with the experimental data, it does so at the cost of introducing the temperature-dependent interaction parameters. The PR+COSMOSAC model can also reproduce the temperature dependence in the miscibility gap, however, without the need of using any ad-hoc temperature-dependent interaction parameters.

For ternary liquid-liquid equilibrium, the overall RMS from PR+COSMOSAC, modified UNIFAC, and UNIFAC-LLE are 0.0775 (or 72%), 0.0515 (or 53%), and 0.0492 (or 47%), respectively. While the PR+COSMOSAC EOS is the least accurate model seen here, it successfully predicts the existence of LLE for all the systems considered here. UNIFAC-LLE provides the lowest RMS because (1) much fewer systems can be predicted because of the issue of missing parameters, and (2) most of the remaining systems are in a small temperature range between 10 and 40 $^{\circ}$C. Figure 5.2-7 is an example of comparison of using PR+COSMOSAC, modified UNIFAC, and

UNIFAC-LLE in predicting tie-line of ternary mixture. The accuracy of PR+COSMOSAC for some systems is still far from accurate, but we believe that this accuracy is satisfactory for a predictive model with only few parameters and using the molecular structure as input.

It is useful to point out some of the limitations of the PR+COSMOSAC EOS in LLE predictions. The first, and most obvious, shortcoming is that it does not correctly describe the lower critical solution temperature, for example the 2-butanone/water system shown in Figure 5.2-5. The modified UNIFAC can produce both the upper and lower critical solution temperatures in this case. [Note that the modified UNIFAC may falsely generate a lower critical solution temperature when there should not be one. For example, see Figure 5.2-6.] Secondly, PR+COSMOSAC has a larger RMS for systems containing amines or compounds with amino groups such as N,N-dimethylformamide, aniline, and morpholine. This might be inherited from the original COSMO-SAC where it is known to be less accurate for N containing species [63-64]. Thirdly, it may fail to describe a system containing conformationally flexible molecules (such as 1,2-propanediol). The structure or conformation of molecule influences the predicted results because different conformation will provide different COSMO file and sigma profile [4, 123]. There are several possible ways to treat flexible molecules in the COSMO calculations [124-125], however, we consider this not the focus of this study.
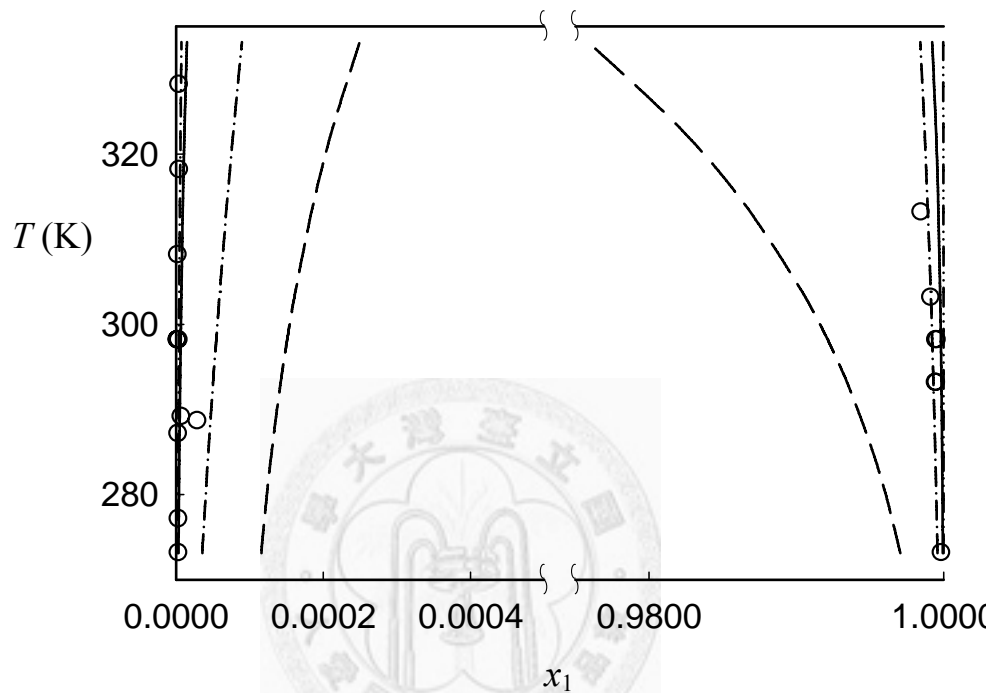
Figure 5.2-3. Comparison of predicted and experimental liquid-liquid equilibria for hexane (1) + water (2) (a type II system) [110]. The lines and symbols have the same meaning as in Figure 5.2-1.
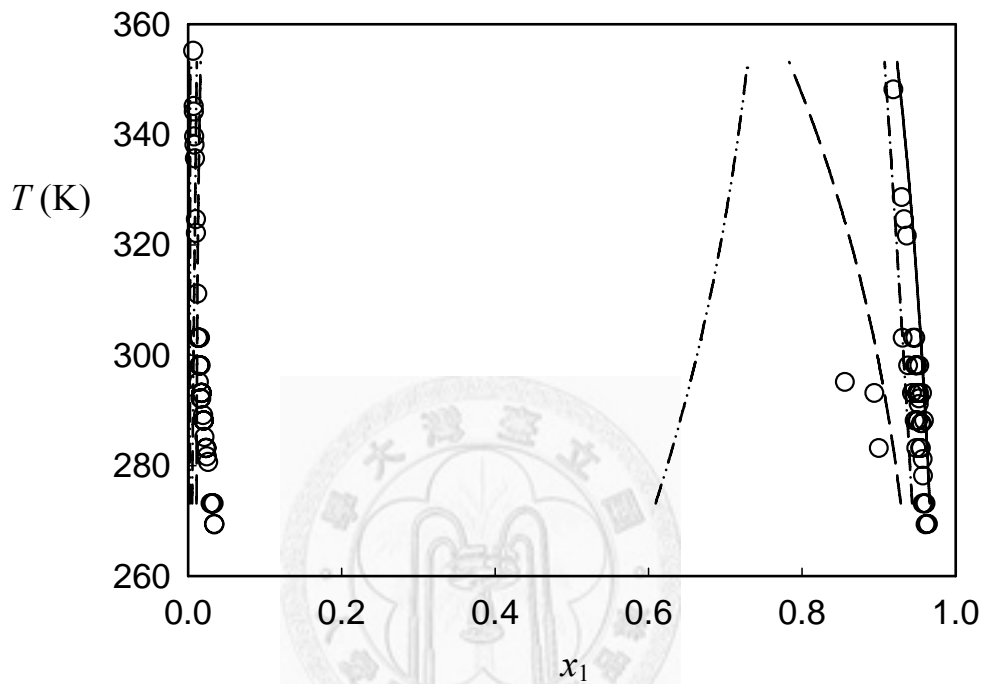
Figure 5.2-4. Comparison of predicted and experimental liquid-liquid equilibria for diethylether (1) + water (2) (a type III system) [110]. The lines and symbols have the same meaning as in Figure 5.2-1.
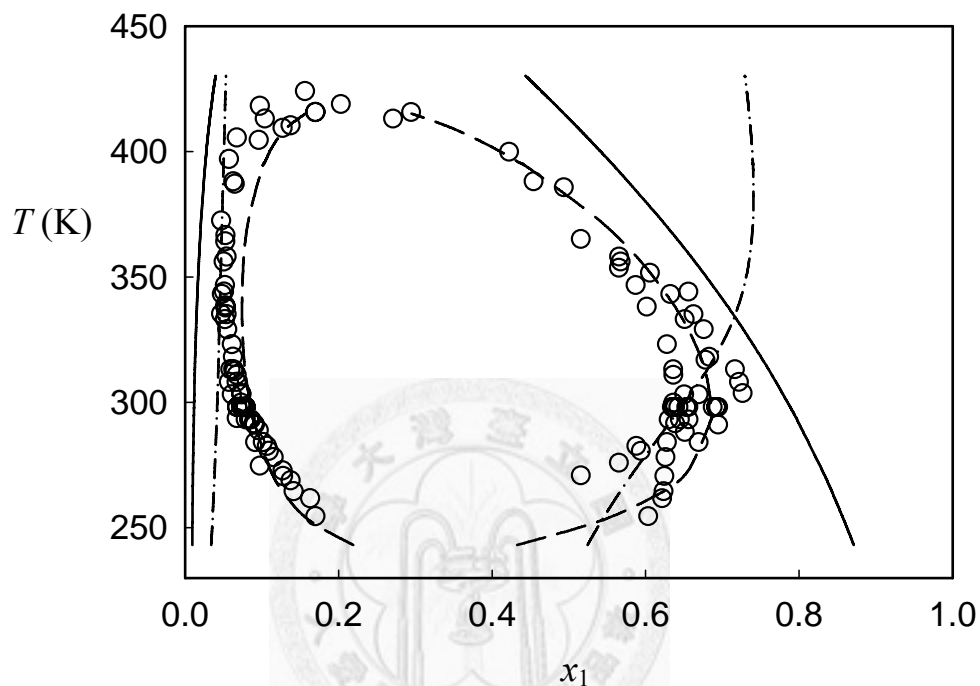
Figure 5.2-5. Comparison of predicted and experimental liquid-liquid equilibria for 2-butanone (1) + water (2) (a type III system) [110]. The lines and symbols have the same meaning as in Figure 5.2-1. COSMO-SAC predicts no miscibility gap of this system.
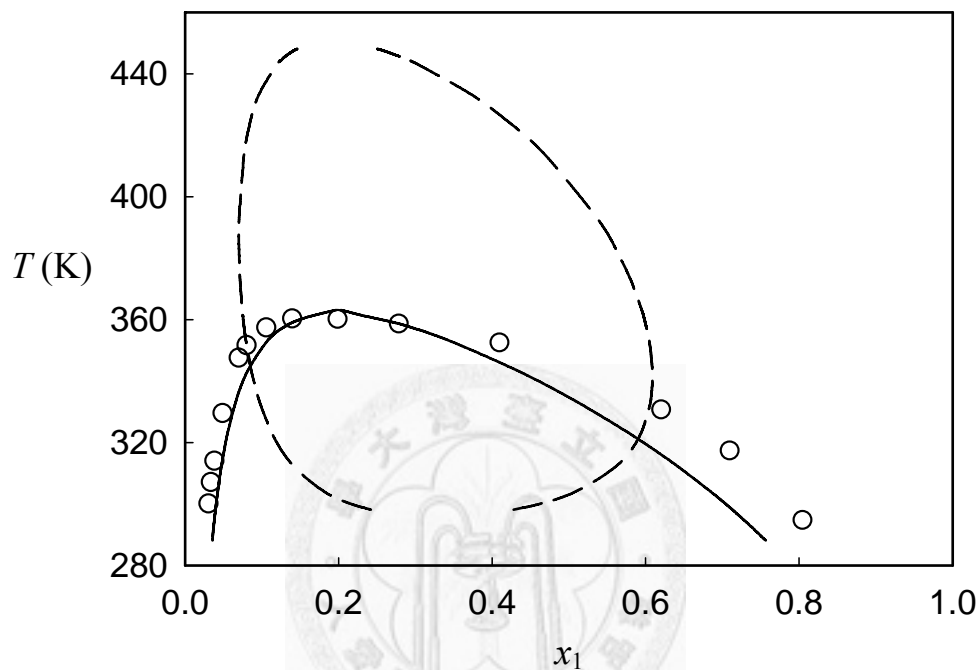
Figure 5.2-6. Comparison of predicted and experimental liquid-liquid equilibria for 2,4-pentanedione (1) + water (2) (a type III system) [110]. The lines and symbols have the same meaning as in Figure 5.2-1. UNIFAC-LLE and COSMO-SAC predicts no miscibility gap of this system.
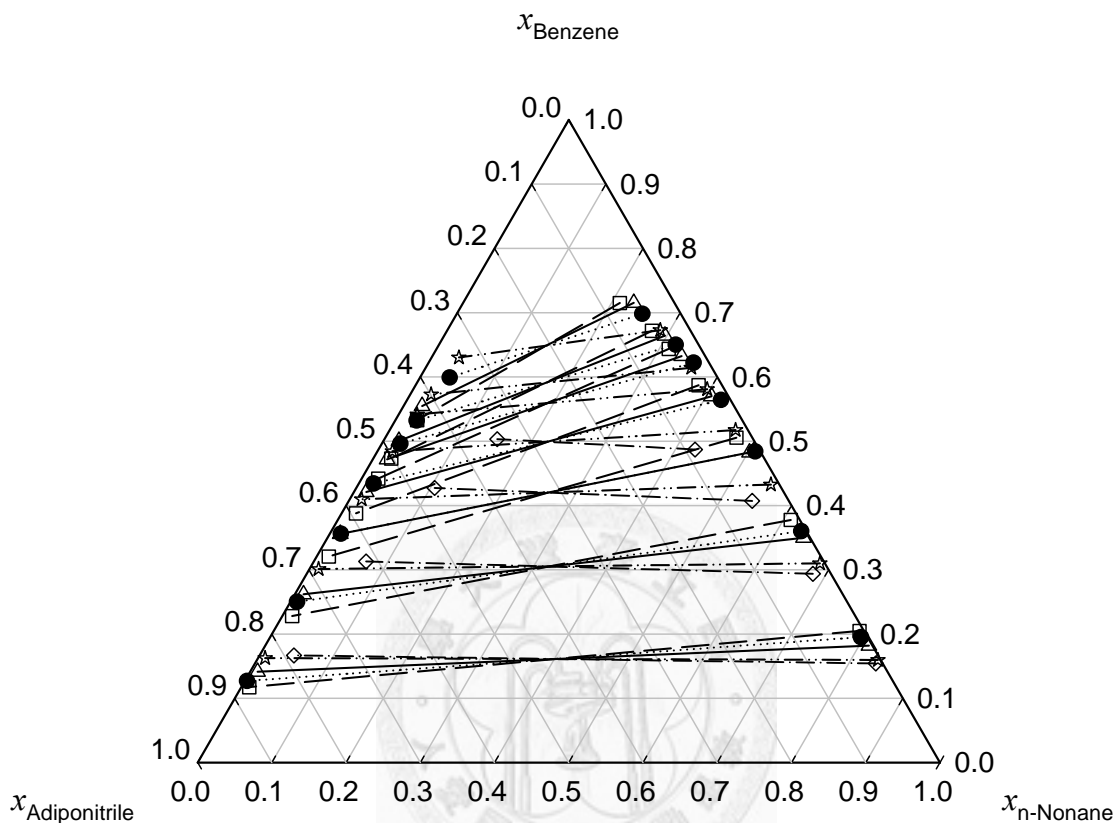
Figure 5.2-7. Comparison of predicted and experimental tie-lines of liquid-liquid equilibria for n-nonane + benzene + adiponitrile at 298.15 K (a type I system). The solid (open triangles), dashed (open squares), dotted-dashed (open diamonds), and dashed-dotted-dotted (open stars) lines are tie lines predicted from PR+COSMOSAC, modified UNIFAC, UNIFAC-LLE, and COSMO-SAC, respectively. The dotted (circles) lines are the tie lines from experiments [126].

5.3 Vapor-Liquid-Liquid Equilibrium (VLLE)

This section presents the application of PR+COSMOSAC for the prediction of VLLE. There are a total of 9 binary VLLE considered in this study, all of which are highly nonideal. The predicted results form PR+COSMOSAC, PR+COSMOSAC+$T_cP_c\omega$, and a widely used group contribution method, the modified UNIFAC model [55], are compared to experimental data.

The predictions of VLLE temperature and composition in three phases at atmospheric pressure for 8 binary mixtures are summarized in Table 5-3. The corresponding phase diagrams of isobaric VLE and LLE are illustrated in Figure 5.3-1. As shown in Figure 5.3-1, the PR+COSMOSAC, without use of any experimental data, captures the general features of VLLE, although it is least accurate among the three approaches considered in this study. The poor accuracy is a result of its inaccuracy in predicting the pure fluid vapor pressure. Therefore, when the critical properties and acentric factor are used (Eq. 2.4-2), i.e., the PR+COSMOSAC+$T_cP_c\omega$ model [36], the prediction accuracy is significantly improved. The accuracy in VLLE predictions from the modified UNIFAC model (required the use of tens of group interaction parameters and the use of experimental vapor pressures) is similar to that from PR+COSMOSAC+$T_cP_c\omega$. While PR+COSMOSAC gives the largest deviations, it is the only one approach that can successfully predict VLLE point for all 8 systems. The modified UNIFAC model fails to describe the LLE (or miscible gap) for water + acrolein [Figure 5.3-1 (f)] and PR+COSMOSAC+$T_cP_c\omega$ predicts a too low upper critical solution temperature for water + acrylonitrile [Figure 5.3-1 (h)]. Furthermore, the turning point (as defined by Iwakabe and Kosuge [67] and briefly explained in the section 3.4) was not found in the VLE calculations for water + acrolein using modified UNIFAC and for water + acrolein using PR+COSMOSAC+$T_cP_c\omega$. This confirms that

VLLE cannot be predicted using these two methods. In general, accurate VLLE can be predicted if a model is accurate on both VLE and LLE. This can be seen in the case of water + ethyl acetate using either PR+COSMOSAC+$T_c P_c \omega$ or modified UNIFAC [Figure 5.3-1 (e)]. Furthermore, good description on LLE helps in getting better liquid phase compositions; whereas good description on VLE helps in getting better equilibrium temperature and gas phase composition. For example, in Figure 5.3-1 (b), PR+COSMOSAC+$T_c P_c \omega$ has better description of LLE, but modified UNIFAC has better description on VLE.

The VLLE at different pressures for water + methyl propionate are studied and the predicted results are summarized in Table 5-4 and shown in Figure 5.3-2. The accuracy of VLLE predictions is very similar at different pressures. The predicted results are all acceptable from these three approaches (summarized in Table 5-4). The average errors in the equilibrium temperature and compositions are similar from the modified UNIFAC (vapor pressures are used in VLE calculations) and the PR+COSMOSAC+$T_c P_c \omega$ (critical properties and acentric factor are used). The error from PR+COSMOSAC is slightly higher; however, no experimental data is used in any of these calculations. Therefore, PR+COSMOSAC can serve as a complementary approach that provides an acceptable *ab initio* prediction for VLLE with the molecular structure as the only input.
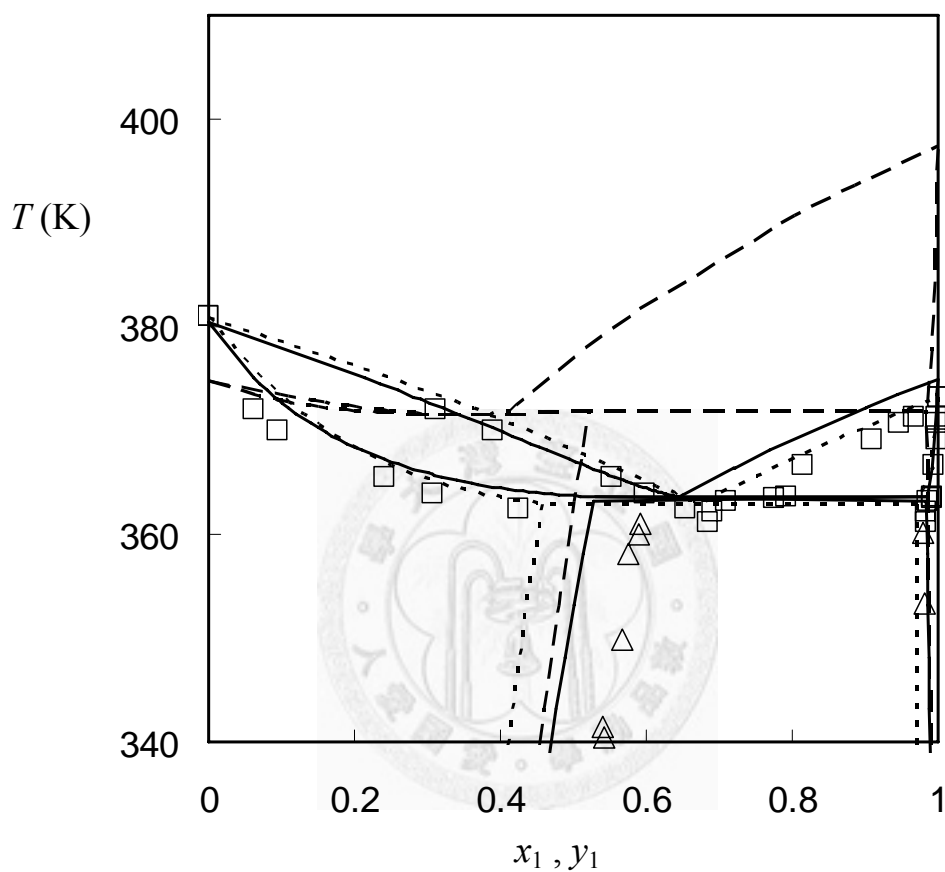
Figure 5.3-1(a). Comparison of VLLE from experiments and predictions for water(1) + 2-methyl-1-propanol(2). The open squares and triangles are experimental VLE and LLE [110, 118]. The dashed lines, solid lines, and dotted lines are results from PR+COSMOSAC, PR+COSMOSAC+$T_cP_c\omega$, and modified UNIFAC, respectively.
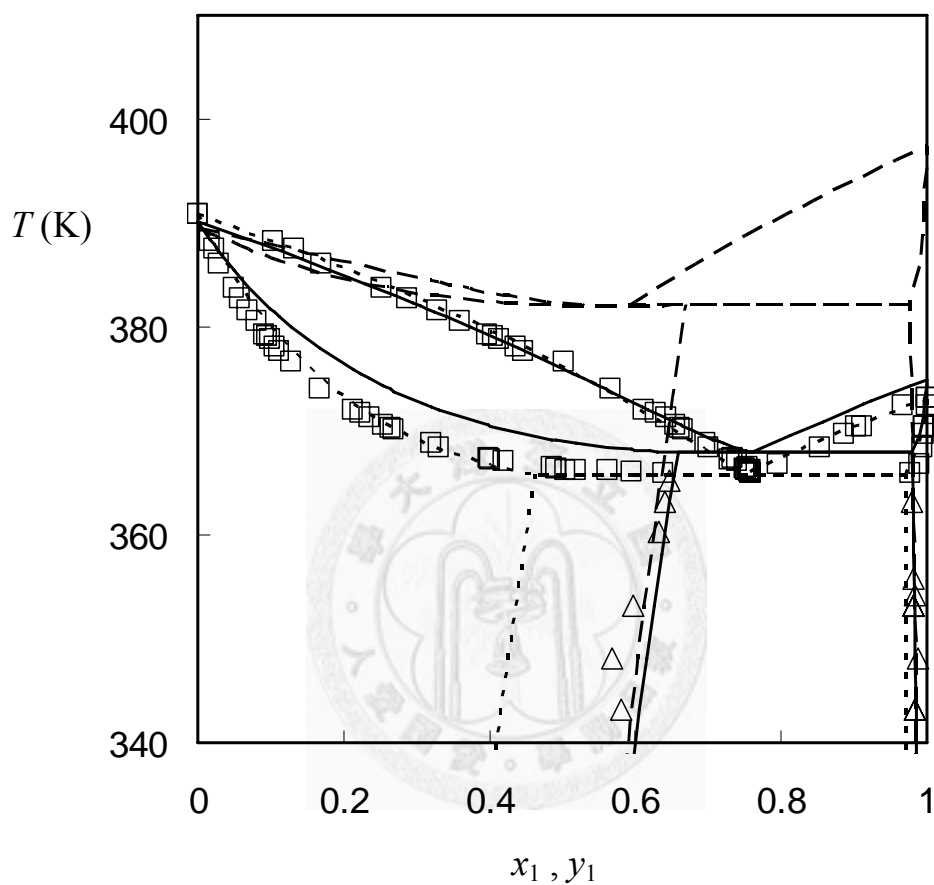
Figure 5.3-1(b). Comparison of VLLE from experiments and predictions for water(1) +

1-butanol(2) [110, 127]. The legends are the same as Figure 5.3-1(a).
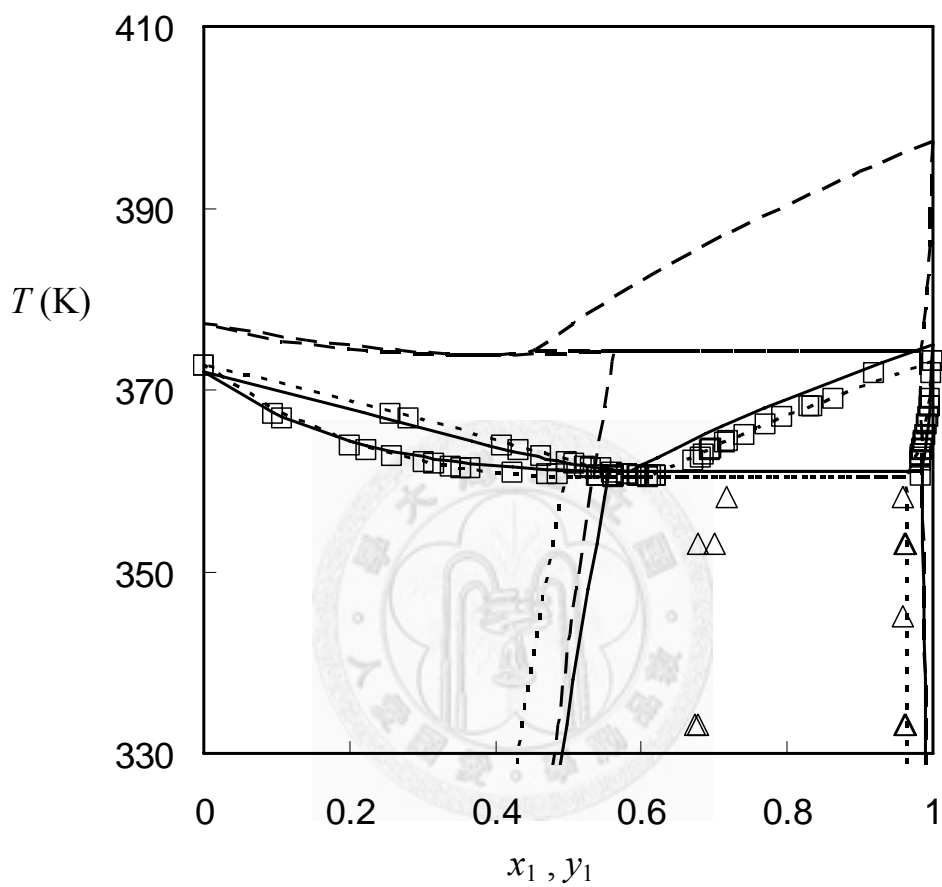
Figure 5.3-1(c). Comparison of VLLE from experiments and predictions for water(1) + 2-butanol(2) [110, 127]. The legends are the same as Figure 5.3-1(a).
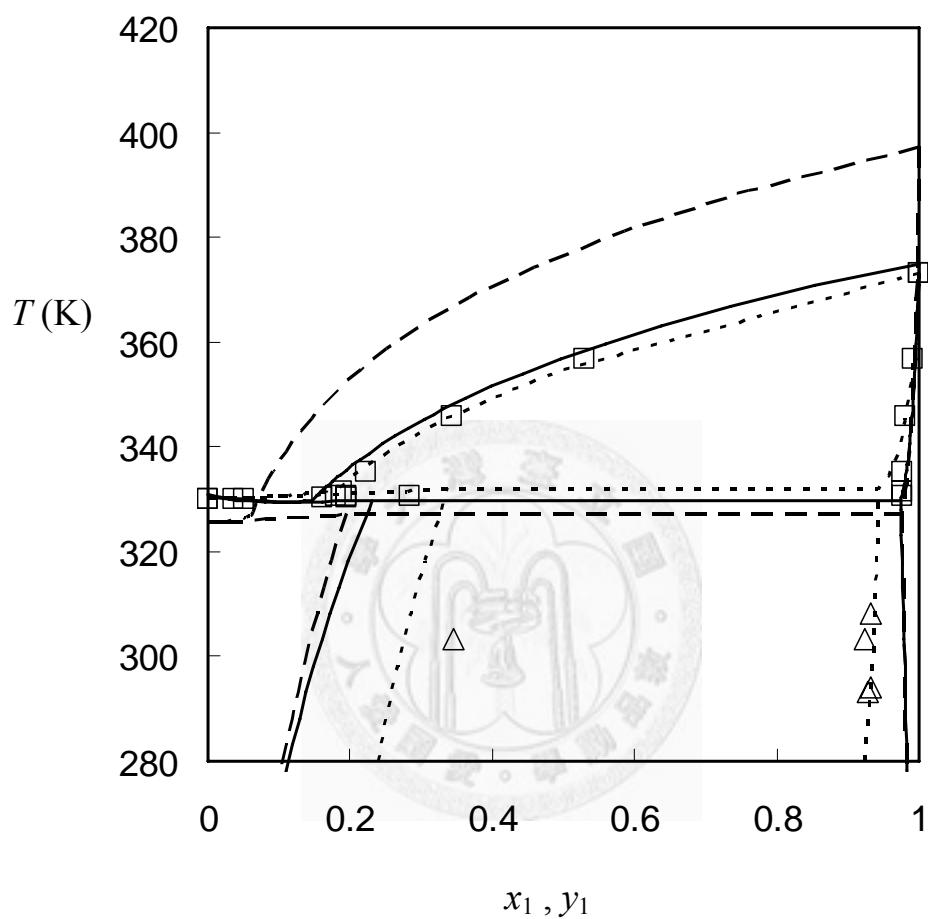
Figure 5.3-1(d). Comparison of VLLE from experiments and predictions for water(1) + methyl acetate(2) [110, 118]. The legends are the same as Figure 5.3-1(a).
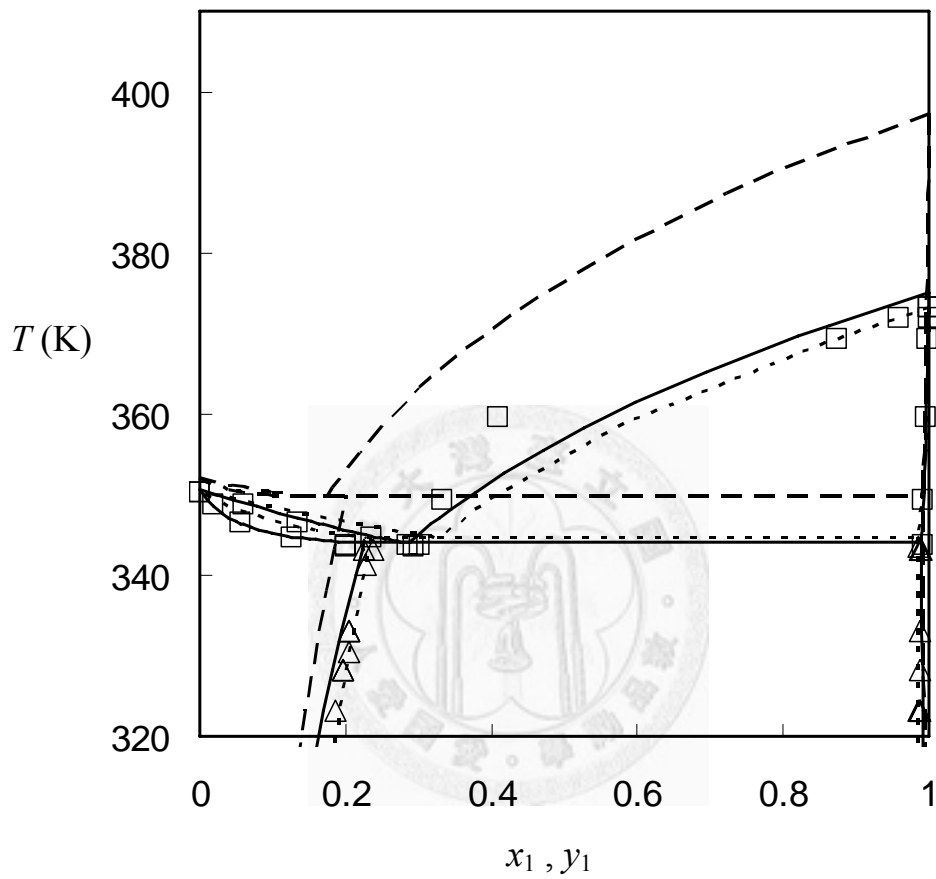
Figure 5.3-1(e). Comparison of VLLE from experiments and predictions for water(1) + ethyl acetate(2) [110, 118]. The legends are the same as Figure 5.3-1(a).
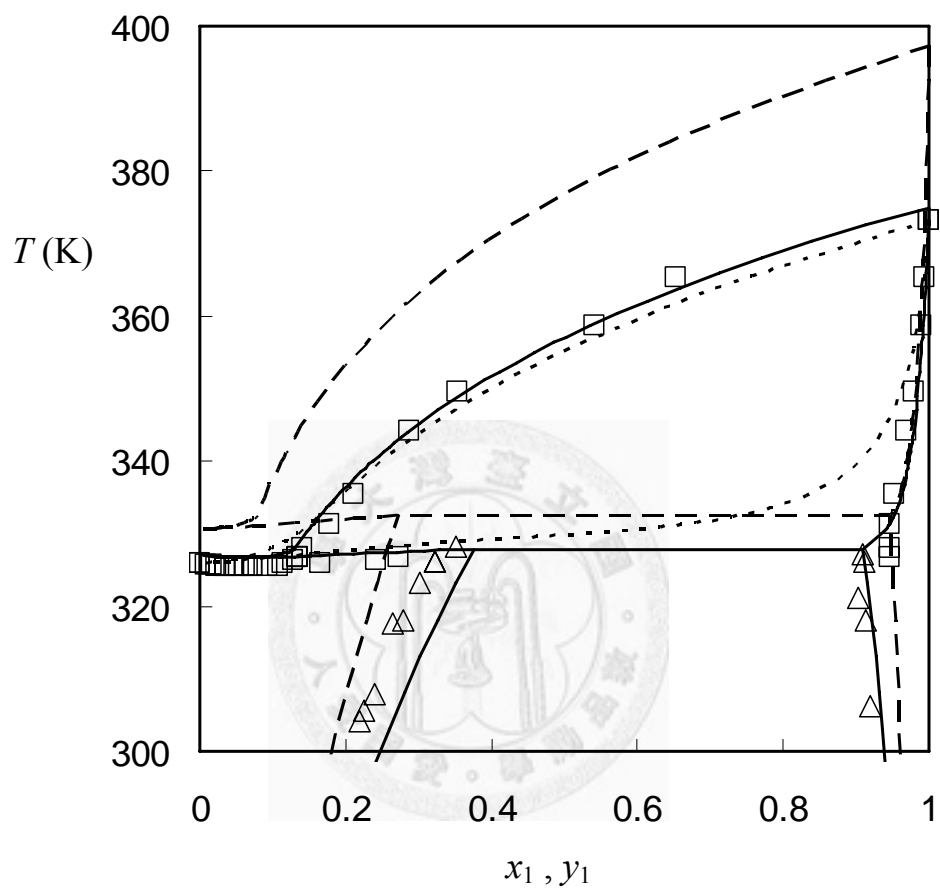
Figure 5.3-1(f). Comparison of VLLE from experiments and predictions for water(1) + acrolein(2) [110, 118]. The legends are the same as Figure 5.3-1(a).
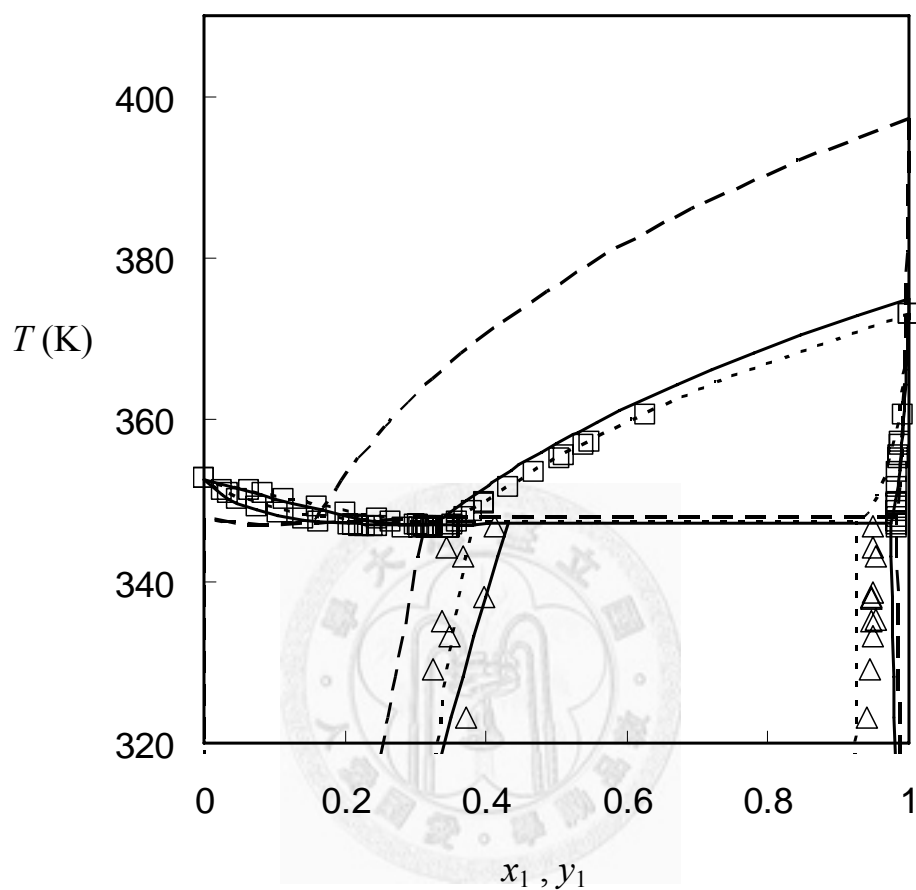
Figure 5.3-1(g). Comparison of VLLE from experiments and predictions for water(1) + 2-butanone(2) [110, 128]. The legends are the same as Figure 5.3-1(a).
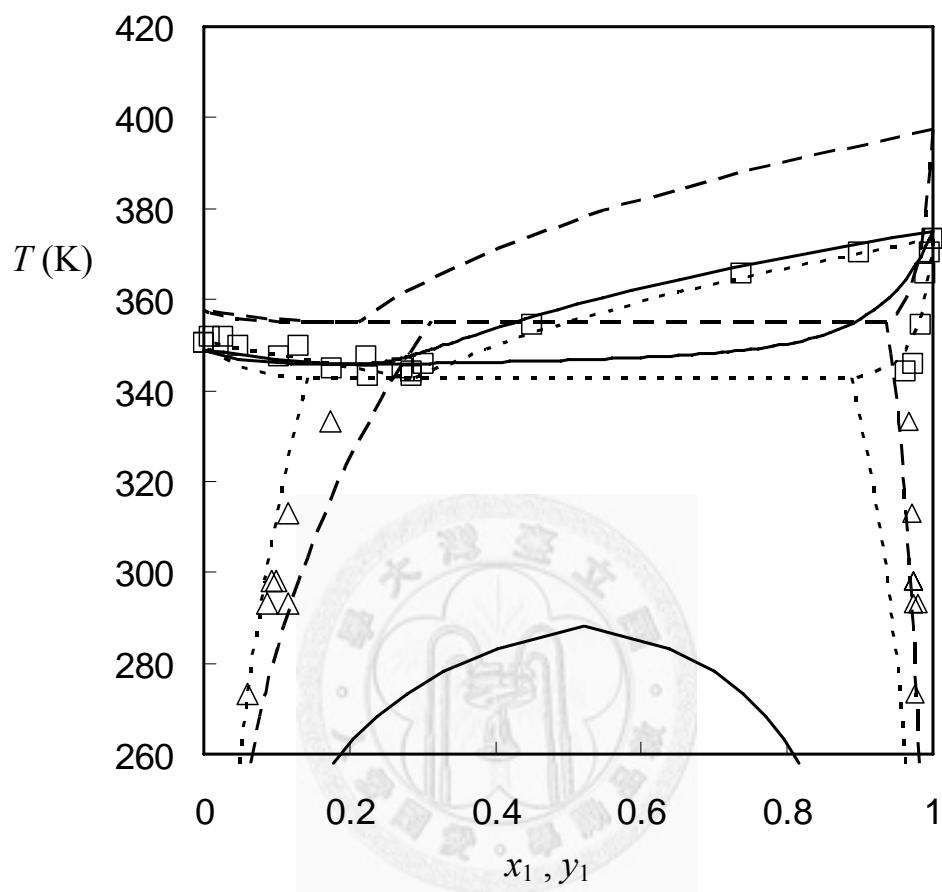
Figure 5.3-1(h). Comparison of VLLE from experiments and predictions for water(1) + acrylonitrile(2) [110, 118]. The legends are the same as Figure 5.3-1(a).
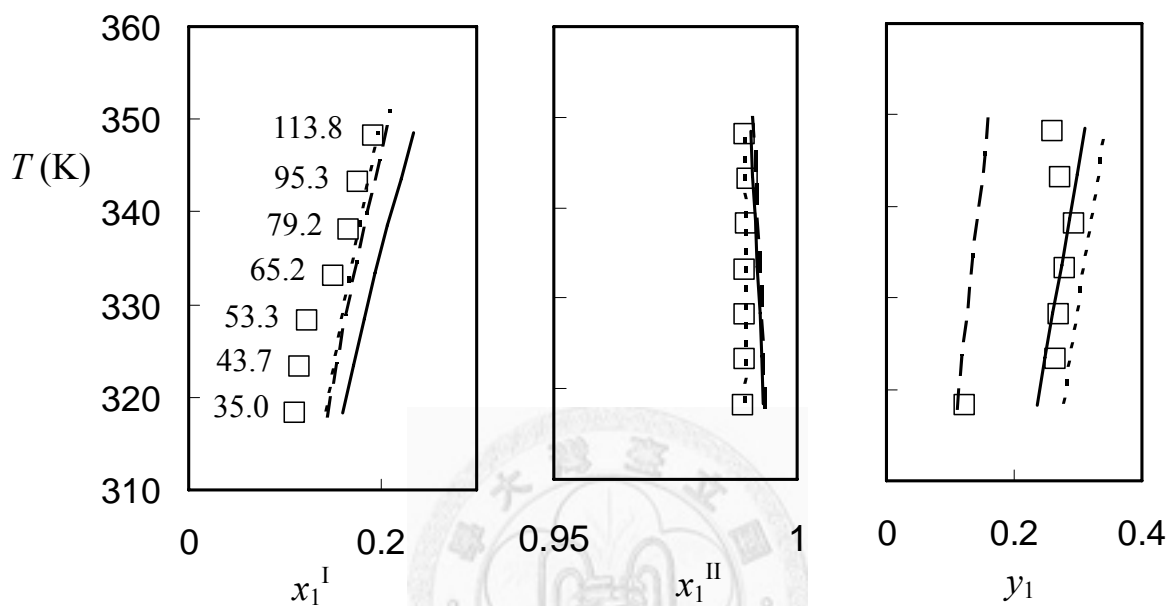
Figure 5.3-2. Comparison of VLLE from experiments and predictions for water (1) + methyl propionate (2) at pressures ranging from 35 kPa to 113.8 kPa. The open squares are experimental VLLE points [129]. The dashed lines, solid lines, and dotted lines are results from PR+COSMOSAC, PR+COSMOSAC+$T_cP_c\omega$, and modified UNIFAC, respectively.

Table 5-3. Comparison of predicted VLLE point at atmospheric pressure from different models

comp. 2†	Experimental data [127-128]				PR + COSMOSAC				PR + COSMOSAC + $T_cP_c\omega$				Modified UNIFAC			
	T_{expt} (K)	x_1^{I}	x_1^{II}	y_1	T_{calc} (K)	x_1^{I}	x_1^{II}	y_1	T_{calc} (K)	x_1^{I}	x_1^{II}	y_1	T_{calc} (K)	x_1^{I}	x_1^{II}	y_1
Acrylonitrile	344.05	0.9630	0.2260	0.2850	355.14	0.9365	0.3121	0.2102	--	--	--	--	342.72	0.8886	0.1434	0.2883
Acrolein	326.85	0.8980	0.3000	0.1340	332.48	0.9467	0.2718	0.0777	327.90	0.9101	0.3754	0.1301	--	--	--	--
Methyl acetate	--	--	--	--	327.05	0.9758	0.1941	0.0607	329.77	0.9739	0.2311	0.1463	331.96	0.9437	0.3377	0.1793
Ethyl acetate	344.25	0.9880	0.2240	0.3130	349.83	0.9909	0.1996	0.1736	344.03	0.9895	0.2256	0.2873	344.69	0.9854	0.2341	0.3248
2-Methyl-1-propanol	--	--	--	--	371.91	0.5212	0.9839	0.4140	363.58	0.5290	0.9843	0.6453	362.97	0.4571	0.9709	0.6728
2-Butanone	346.67	0.9498	0.4236	0.3478	348.02	0.9833	0.3159	0.1600	347.19	0.9735	0.4322	0.3273	347.32	0.9253	0.3826	0.3515
1-Butanol	365.92	0.6393	0.9481	0.7590	382.15	0.9763	0.6693	0.5952	367.91	0.6585	0.9791	0.7599	365.87	0.4638	0.9707	0.7504
2-Butanol	360.47	0.9590	0.7019	0.6201	374.27	0.9832	0.5619	0.4513	361.05	0.9848	0.5566	0.5846	360.34	0.9638	0.4955	0.6063
AAD-x AAD-y AARD-T					2.54%	7.88%	11.09%	13.18%	0.25%	1.65%	5.24%	1.73%	0.15%	5.64%	7.25%	0.82%

†component 1 is water in all 8 cases.

Table 5-4. Comparison of predicted VLLE point at different pressures for water (1) + methyl propionate (2)

	Experimental data [129]				PR + COSMOSAC				PR + COSMOSAC + $T_cP_c\omega$				Modified UNIFAC			
P (kPa)	T_{expt} (K)	x_1^{I}	x_1^{II}	y_1	T_{calc} (K)	x_1^{I}	x_1^{II}	y_1	T_{calc} (K)	x_1^{I}	x_1^{II}	y_1	T_{calc} (K)	x_1^{I}	x_1^{II}	y_1
35.0	318.24	0.1107	0.9890	0.1226	317.83	0.1445	0.9934	0.1101	318.27	0.1597	0.9930	0.2362	318.50	0.1424	0.9894	0.2765
43.7	323.24	0.1162	0.9891	0.2648	323.55	0.1546	0.9930	0.1186	323.53	0.1710	0.9927	0.2492	323.70	0.1508	0.9894	0.2877
53.3	328.24	0.1241	0.9892	0.2701	328.86	0.1644	0.9927	0.1267	328.39	0.1821	0.9923	0.2614	328.52	0.1589	0.9895	0.2981
65.2	333.15	0.1506	0.9893	0.2805	334.44	0.1752	0.9923	0.1354	333.49	0.1944	0.9919	0.2741	333.59	0.1680	0.9895	0.3093
79.2	338.15	0.1675	0.9894	0.2951	340.02	0.1866	0.9919	0.1443	338.57	0.2074	0.9914	0.2868	338.67	0.1775	0.9894	0.3205
95.3	343.15	0.1770	0.9899	0.2733	345.51	0.1982	0.9915	0.1533	343.57	0.2208	0.9909	0.2994	343.68	0.1874	0.9894	0.3316
113.8	348.15	0.1933	0.9891	0.2593	350.95	0.2103	0.9910	0.1623	348.52	0.2347	0.9904	0.3117	348.65	0.1976	0.9893	0.3428
AAD-x																
AAD-y					0.41%	2.78%	0.30%	11.64%	0.09%	4.72%	0.25%	3.30%	0.13%	2.05%	0.03%	5.72%
AARD-T																

5.4 The 1-Octanol-Water Partition Coefficient (K_{OW}) and the Infinite-Dilution Activity Coefficient (γ^∞) in Water

In the past decade, a series of industrial fluid properties simulation challenges has been organized to demonstrate the capabilities of modern methods, such as molecular simulation (including molecular dynamics and Monte Carlo simulations) and COSMO-based methods, to provide reasonable predictions of thermophysical properties of fluids for industrial applications. These simulation challenges are organized by an international collaboration (IFPSC) between industry, academia, and national laboratories (coordinated by the National Institute of Standards and Technology). Recently, the "5th Industrial Fluid Properties Simulation Challenge" was held in the 2008 Annual Meeting of American Institute of Chemical Engineers [130]. The challenge was to predict (1) the 1-octanol-water partition coefficient, K_{OW}, (in mole fraction units assuming neutral species) at 300 K and 101.325 kPa and (2) infinite-dilution activity coefficient (γ^∞) in water (mole fraction units with Lewis and Randall reference state) in water at 325 K and 13.5 kPa for two compounds, 1-ethylpropylamine (CAS# 616-24-0) and 3-methyl-1-pentanol (CAS# 589-35-5). The predictions from the PR+COSMOSAC model are summarized in Table 5-5.

In order to validate our predictions, we performed several additional calculations. The miscibility gap of 1-octanol and water from 280 K to 390 K is determined from PR+COSMOSAC and compared to those from original COSMOSAC and experimental data in Figure 5.4-1 As can be seen, the calculated miscibility gaps from PR+COSMOSAC are in good agreement with experiments over the whole temperature range. For example, at ambient conditions (300 K and 1 bar) the calculated mole fractions of water in the water-rich phase and the 1-octanol-rich phase are 0.9999 and 0.2909, compared to experimental results of 0.9999 and 0.275 [131].
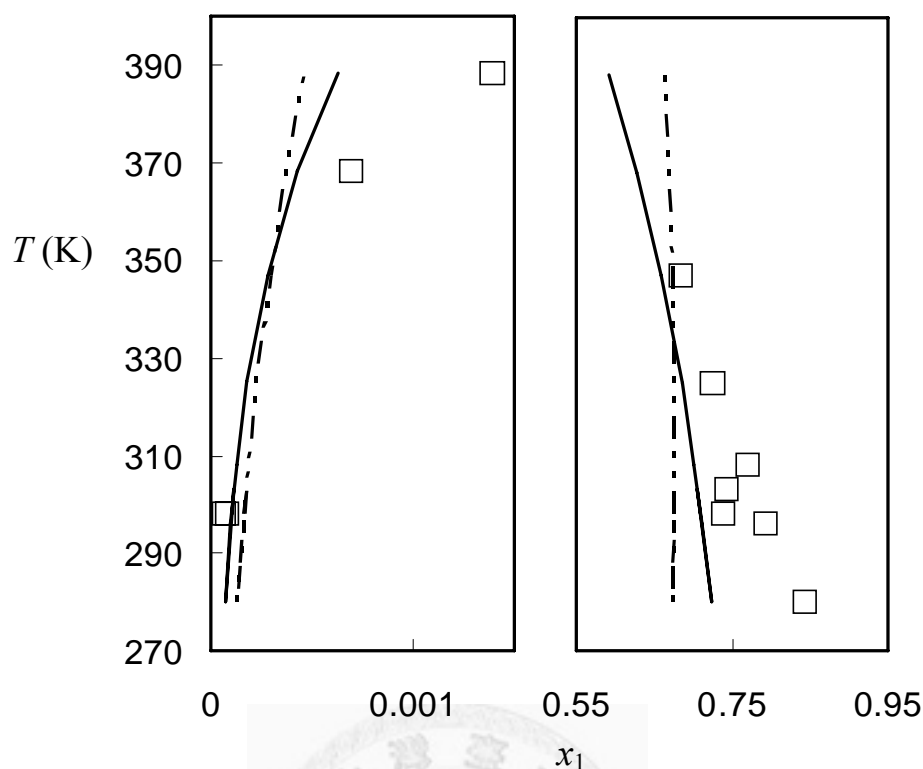
Figure 5.4-1. Predicted *T–x–x* phase diagram of liquid–liquid equilibrium for 1-octanol (1) + water (2). The open squares are experimental data [110, 132-134]. The solid and dashed-dotted-dotted lines are the results from PR+COSMOSAC and COSMO-SAC [64], respectively.

In order to examine the accuracy of the predicted results we have also calculated the values of 1-octanol-water partition coefficient (K_{OW}) and infinite dilution activity coefficient in water ($\gamma_{i/w}^{\infty}$) for amine and alcohol molecules for which experimental data are available. The predicted logK_{OW} from PR+COSMOSAC are compared to experiments in Table 5-6. The overall average absolute error for 43 selected compounds is 0.69 in logK_{OW}. While such an error is not negligible, it should be noted that all the predictions are obtained without using any experimental data specific to this problem

(e.g., the compositions of the water-rich and 1-octanol-rich phases, any activity coefficient data, etc). Furthermore, there is a good linear correlation between the predicted and experimental values as shown in Figure 5.4-2. The correlation is especially remarkable for compounds in the same homologous family, such as primary alcohols (squares in Figure 5.4-2) and primary amines (triangles in Figure 5.4-2)

For primary alcohols: $\log K_{OW}^{corr} = 1.2606 \log K_{OW}^{PR+COSMOSAC} - 0.6893$ (5.4-1a)

For primary amines: $\log K_{OW}^{corr} = 1.2001 \log K_{OW}^{PR+COSMOSAC} - 0.9211$ (5.4-1b)

We can thus improve our original predictions for K_{OW} with these correlation equations for the two compounds 1-ethylpropylamine and 3-methyl-1-pentanol. The corrected results are given in Table 5-5. The uncertainty is estimated based on predicted errors for compounds used to obtain the correlation equations.

The comparison of experimental and predicted $\log \gamma^{\infty}$ is shown in Table 5-6. The overall average absolute error for 43 selected compounds is 0.74 in $\log \gamma^{\infty}$. Similar to the previous case for K_{OW}, there exists a good correlation between the predicted and experimental γ^{∞} for compounds in the same homologous family as shown in Figure 5.4-3. The correlation equations are found to be

For primary alcohols: $\log \gamma_{i/W}^{\infty,corr} = 1.3432 \log \gamma_{i/W}^{\infty,PR+COSMOSAC} - 0.8275$ (5.4-2a)

For primary amines: $\log \gamma_{i/W}^{\infty,corr} = 1.3051 \log \gamma_{i/W}^{\infty,PR+COSMOSAC} - 0.7685$ (5,4-2b)

With these correlation equations, we have improved our predictions for γ^{∞} in water listed in Table 5-5.
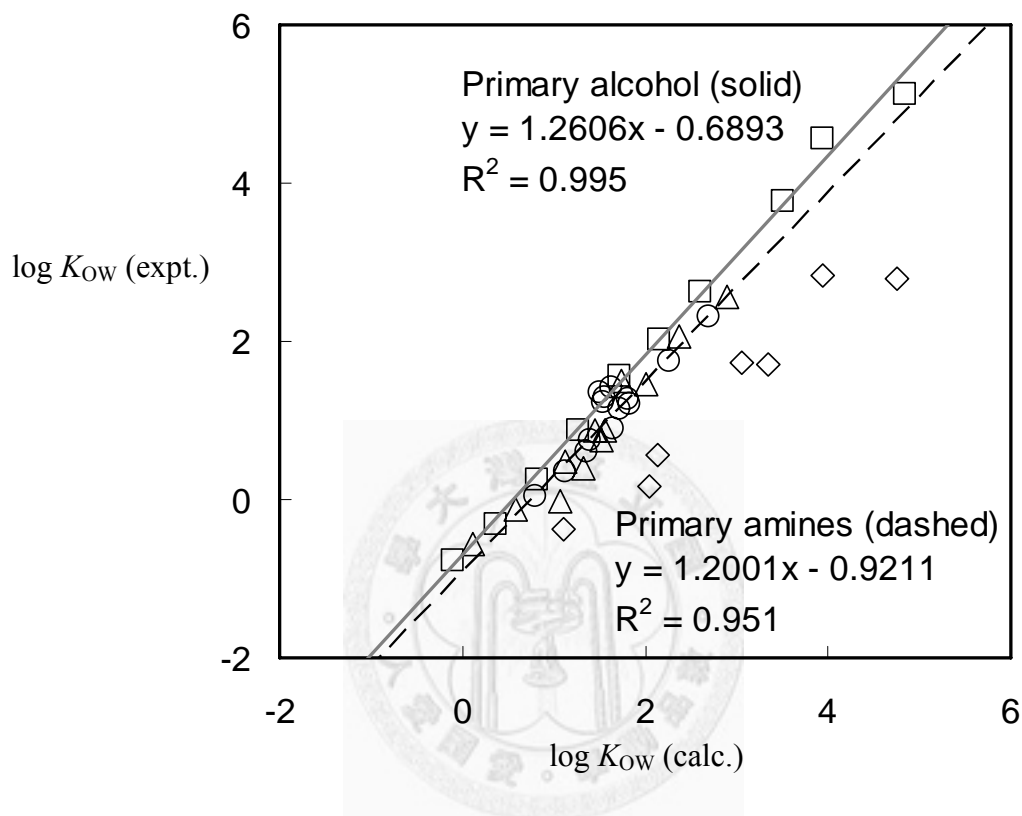
Figure 5.4-2. Comparisons of the predicted and experimental logK_{OW}. The squares, circles, triangles, and diamonds present primary alcohols, non-primary alcohols, primary amines, and non-primary amines, respectively. The solid and dashed lines are the linear regression lines for primary alcohols and primary amines.
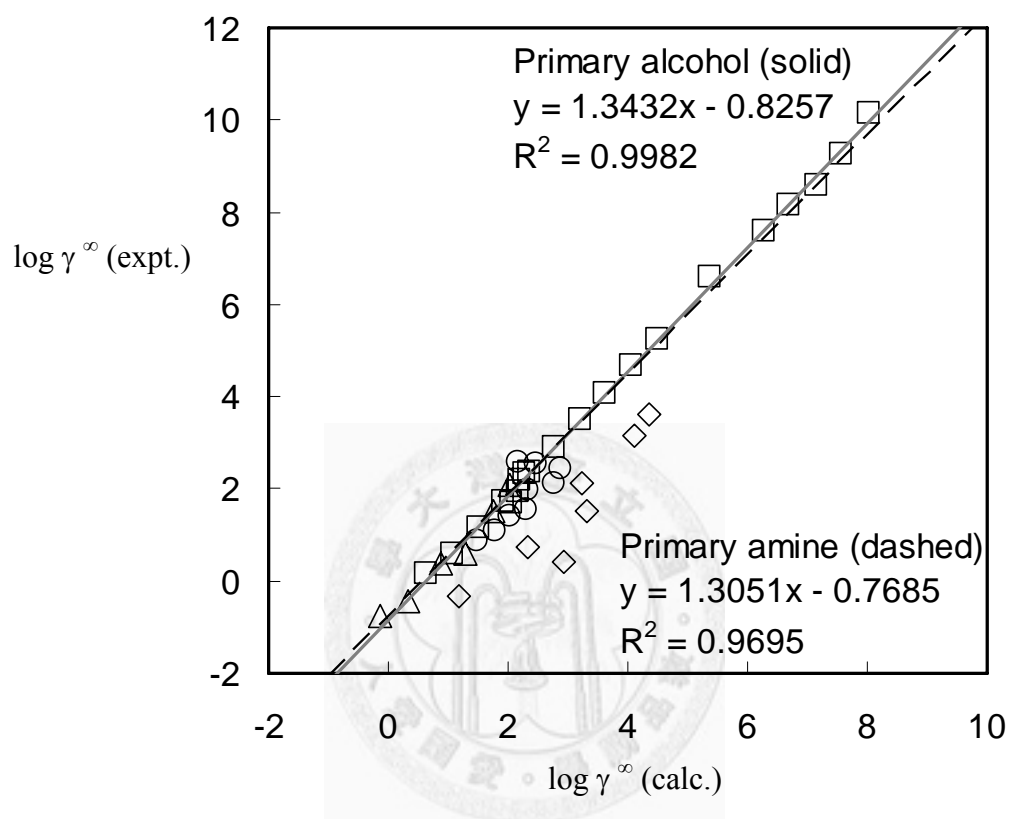
Figure 5.4-3. Comparisons of the predicted and experimental $\log\gamma^\infty$. The legends are the same as in Figure 5.4-2.

Table 5-5. Final results (in bold font, highlighted) for the 5th simulation challenge

	3-Methyl-1-pentanol			1-Ethylpropylamine		
	Calc.[a]	Corr.[b]	Expt.[c]	Calc.[a]	Corr.[b]	Expt.[c]
$\log K_{OW}$[d]	1.91	1.72	--	2.03	1.52	--
K_{OW}	81.3	52.3	--	107.2	32.7	--
$\log K_{OW,X}$[e]	2.74	2.55	2.50	2.86	2.35	2.20
$K_{OW,X}$	550	**354**	315±16	724	**221**	158±8
$\log \gamma^{\infty}$[f]	2.53	2.57	2.39	2.07	1.94	1.40
γ^{∞}	336.7	**369.0**	245.0±12	118.8	**87.0**	25.0±1.3

a. Predicted results from the PR+COSMOSAC model as described in the sections 3.5 and 3.6.

b. Corrected predictions using the linear correlation Eqs. (5.4-1) for K_{OW} and (5.4-2) for γ^{∞}.

c. Experimental data are taken from the work of Olsen et al. [135]

d. $\log K_{OW}$ in molar concentration units [Eq. (5.4-1)] evaluated at 300 K and 101.325 kPa.

e. The value of $\log K_{OW}$ on the mole fraction basis is converted from the molar concentration basis via $\log K_{OW,X,i} = \log K_{OW,i} + 0.830$ where the constant 0.83 is logarithm of total molar concentration ratio of the two phases. [131]

f. $\log \gamma^{\infty}$ evaluated at 325 K and 13.5 kPa.

Table 5-6. The 1-octanol-water partition coefficient and the infinite dilution activity coefficient in water from experiment (expt.), PR+COSMOSAC (calc.), and corrected PR+ COSMOSAC (corr.).

No.	Compound Name	$\log K_{OW}$			$\log \gamma^{\infty}$		
		calc.	corr.	expt.	calc.	corr.	expt.
1	Methanol	-0.10	-0.81	-0.77	0.64	0.02	0.16
2	Ethanol	0.36	-0.24	-0.31	1.06	0.59	0.58
3	Propanol	0.83	0.35	0.25	1.50	1.19	1.15
4	Butanol	1.26	0.90	0.88	1.92	1.75	1.73
5	Pentanol	1.72	1.48	1.56	2.36	2.34	2.35
6	Hexanol	2.16	2.03	2.03	2.77	2.89	2.90
7	Heptanol	2.61	2.60	2.62	3.21	3.48	3.51
8	Octanol	--	--	--	3.63	4.05	4.06
9	Nonanol	3.50	3.73	3.77	4.07	4.64	4.67
10	Decanol	3.94	4.28	4.57	4.49	5.22	5.25
11	Dodecanol	4.84	5.41	5.13	5.36	6.39	6.59
12	Tetradecanol	--	--	--	6.28	7.61	7.60
13	Pentadecanol	--	--	--	6.68	8.16	8.16
14	Hexadecanol	--	--	--	7.16	8.81	8.59
15	Heptadecanol	--	--	--	7.57	9.36	9.25
16	Octadecanol	--	--	--	8.02	9.96	10.16
17	Isobutanol	1.40	0.85	0.76	2.07	1.95	1.69
18	3-Methyl-1-butanol	1.64	1.12	1.42	2.28	2.24	2.32
19	2,2-Dimethylpropanol	1.50	0.97	1.36	2.17	2.09	1.94
20	2-Methyl-1butanol	1.55	1.02	1.29	2.19	2.11	2.21
21	2-Propanol	0.80	0.15	0.05	1.48	1.16	0.87
22	Secbutanol	1.37	0.81	0.61	2.04	1.91	1.42
23	Tertbutanol	1.13	0.53	0.35	1.78	1.57	1.08
24	3-Methy-2-butanol	1.82	1.33	1.28	--	--	--
25	2-Methyl-2-butanol	1.65	1.13	0.89	2.30	2.26	1.54
26	2-Pentanol	1.71	1.21	1.15	2.33	2.30	1.99
27	3-Pentanol	1.82	1.34	1.21	--	--	--

28	4-Methyl 2-pentanol	--	--	--	2.47	2.49	2.54
29	3-Methyl 3-pentanol	--	--	--	2.77	2.90	2.11
30	2-Hexanol	2.26	1.85	1.76	2.89	3.06	2.45
31	Cyclohexanol	1.54	1.00	1.23	2.16	2.07	2.58
32	2-Heptanol	2.70	2.36	2.31	--	--	--
33	Methylamine	0.11	-0.79	-0.57	-0.12	-0.93	-0.75
34	Ethylamine	0.58	-0.23	-0.13	0.32	-0.36	-0.43
35	Propylamine	1.12	0.42	0.48	0.89	0.39	0.37
36	Butylamine	1.55	0.94	0.88	1.30	0.92	0.60
37	Pentylamine	2.01	1.49	1.45	1.74	1.50	1.53
38	Hexylamine	2.36	1.92	2.06	2.04	1.89	2.10
39	Heptylamine	2.89	2.55	2.57	--	--	--
40	Isopropylamine	1.07	0.37	-0.03	--	--	--
41	Isobutylamine	1.44	0.81	0.88	--	--	--
42	Secbutylamine	1.52	0.91	0.74	--	--	--
43	Tertbutylamine	1.32	0.67	0.40	--	--	--
44	Cyclohexylamine	1.74	1.17	1.49	--	--	--
45	Dimethylamine	1.11	-0.44	-0.38	1.18	-0.74	-0.32
46	Diethylamine	2.14	0.59	0.57	2.32	0.68	0.73
47	Dipropylamine	3.05	1.48	1.73	3.22	1.81	2.11
48	Dibutylamine	3.94	2.35	2.83	4.10	2.92	3.15
49	Diisopropyl amine	--	--	--	3.30	1.92	1.52
50	Trimethylamine	2.04	0.49	0.16	2.92	1.44	0.43
51	Dimethylbutylamine	3.35	1.77	1.70	0.00	0.00	0.00
52	Triethylamine	--	--	--	4.35	3.23	3.62
53	Tripropylamine	4.76	3.16	2.79	--	--	--

1. These compounds are categorized in primary alcohols (1-20), non-primary alcohols (21-32), primary amines (33-44), and non-primary amines (45-53).

2. The experimental data for K_{OW} [136-140] and γ^{∞} [141-146] are taken from literatures.

Chapter 6. Prediction of Drug Solubility

The knowledge of drug solubility is important in the design of drug manufacturing processes because of the crystallization is the preferred method of purification in the pharmaceutical industry [147-148]. Experiments are performed to screen solvents and identify optimal operating conditions. However, it is time-intensive and costly to do these measurements because the crystallizations are often performed under mixed-solvent conditions. Furthermore, since the drug discovery techniques continue to improve, the number of potential drug candidates increases significantly. It is impractical to measure the solubility data for all drug candidates in all possible ranges of solvent combinations. Thus, a predictive thermodynamic model can help to overcome this obstacle. Numerous thermodynamic methods are used to predict the solubility of organic compounds in the literature [108, 124, 149-152]. In this section, the accuracy of PR+COSMOSAC in prediction of drug solubility is examined and compared with that of the COSMO-SAC model [64].

In this study, the solubility of 52 drug compounds [from 2 atoms (iodine), for the smallest, to 49 atoms (testosterone), for the largest] in 37 different pure solvents at the temperatures ranged from 273.15 K to 323.15 K are considered. There are a total of 171 drug-solvent pairs for drug solubility in pure solvent and 156 mixture solvent combinations (298 systems), including 3 ternary solvent mixtures (10 systems) and 1 quaternary solvent mixture (1 system). As discussed by Mullins et al. [108], the AARD and AAD cannot equally judge the over-prediction and under-prediction cases, especially in drug solubility prediction where the orders of experimental data are ranged from 10^{-1} to 10^{-6}, and the RMS error of logarithm of mole fraction solubility is the best way to evaluate the accuracy of drug solubility predictions,

$$\text{RMS error} = \left[\frac{1}{N} \sum_{j=1}^{N} \left(\log x_i^{\text{calc}} - \log x_i^{\text{expt}} \right)^2 \right]^{1/2} \tag{6.0-1}$$

where N is the number of data point per system [one drug in a (mixture or pure) solvent at a certain temperature].

As shown in Table 6-1, the overall RMS errors are 1.78 (corresponding to 495% in percentage error of solubility) and 1.92 (583%) from PR+COSMOSAC and COSMO-SAC, respectively. The RMS from COSMO-SAC model is essentially similar to that in Shu and Lin's work [152] (which is 1.96 for 400 data points containing for 33 drugs in 37 solvents) or in Mullins et al.'s work [108]. Figure 6-1 illustrates the comparison of solubility predictions from these two methods. As stated in Mullins et al.'s work [108], COSMO-SAC generally over-predicts the solubility. Similar tendency is observed in PR+COSMOSAC predictions, but overall the PR+COSMOSAC method can provide slightly better description of interaction between solutes and solvents than COSMO-SAC.

In the case of mixture solvents, as summarized in Table 6-2, the overall RMS errors from PR+COSMOSAC and COSMO-SAC are 1.40 (304%) and 1.61 (400%), respectively. Four examples for the comparison of predictions in mixture solvent systems from PR+COSMOSAC and COSMO-SAC are shown in Figures 6-2 to 6-5. Both PR+COSMOSAC and COSMO-SAC methods can capture the concentration dependence of drug solubility, and the accuracy in prediction of mixture solvent systems is strongly influenced by that of pure solvent. Since the PR+COSMOSAC model has a better accuracy in the case of pure solvent, its performance in the case of mixture solvents is superior to that of COSMO-SAC.

The prediction of solubility of a drug in the solution of mixture solvents can be greatly improved if the experimental solubility of the drug in the relevant pure solvent is

available. The dispersion free energy correction coefficient ($G^{\text{dsp,corr}}$) for drug-solvent pair can be determined from Eq. (2.5-7) and then used to improve the accuracy of prediction. This method is denoted as PR+COSMOSAC+$G^{\text{dsp,corr}}$. The overall RMS error is reduced to 0.65 (91%) from PR+COSMOSAC+$G^{\text{dsp,corr}}$ (Table 6-2), a reduction by more than 50% when compared with that (1.40) from PR+COSMOSAC. Figure 6-2 illustrates a typical example of the solubility prediction from COSMO-based methods. Since the PR+COSMOSAC model provides good solubility dependency on solvent compositions, very accurate predictions can be achieved for mixture solvent systems when the offsets on the two ends (pure solvents) in the Figure 6-2 are removed. The same phenomenon can be observed in Figures 6-3 to 6-5, especially for the system containing a maximum solubility (Figure 6-5). It should be noted that not all the $G^{\text{dsp,corr}}$ parameters can be determined for the 156 solvent mixtures studied in this work because of missing experimental solubility data for some drug-solvent pairs. In such case, the dispersion free energy correction coefficient for drug i and solvent k, $G_{ik}^{\text{dsp,corr}}$ is set to zero. As summarized in Table 6-2 (case B), there are 90 (out of the overall 298) systems where at least one of the needed experiment data is missing. It is interesting to note that the improvement is still significant [1.33 (278%) from PR+COSMOSAC to 1.00 (172%) from PR+COSMOSAC+$G^{\text{dsp,corr}}$] even when part of the experimental data are available.

Although the accuracy of PR+COSMOSAC in the prediction of drug solubility is still far from accurate, the ability to provide a priori predictions for compounds without binary interaction parameters and experimental data (the enthalpy of fusion and normal melting temperature of drug are needed). This is very useful for in the early stage of drug discovery and the design of purification processes in the pharmaceutical industry.

Table 6-1. Comparison of accuracy in drug solubility prediction in pure solvents from PR+COSMOSAC and COSMO-SAC models.

	Literature Points	Solute-Solvent Pairs	RMS Error[a]
PR+COSMOSAC	362	171	1.78 (495%)
COSMO-SAC	362	171	1.92 (583%)

a. The number in the parentheses are the corresponding percentage errors estimated from RMS errors.
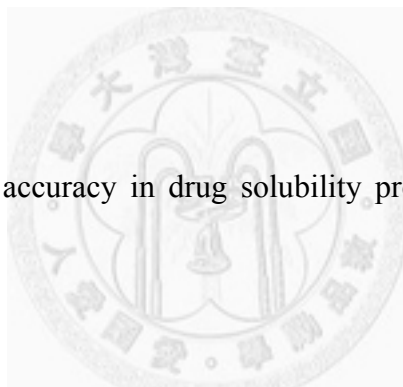
Table 6-2. Comparison of accuracy in drug solubility prediction in mixture solvents from different methods.

Cases [a]	Systems (data points)	COSMO-SAC	PR+COSMOSAC	PR+COSMOSAC $+G^{\text{dsporr}}$
A	208 (2480)	1.71 (450%)	1.43 (317%)	0.50 (64%)
B	90 (414)	1.39 (301%)	1.33 (278%)	1.00 (172%)
overall	298 (2894)	1.61 (400%)	1.40 (304%)	0.65 (91%)

a. Case A includes systems where solubility data in all needed pure solvents are available; case B includes systems where at least one of the pure solvent solubility data is not available.
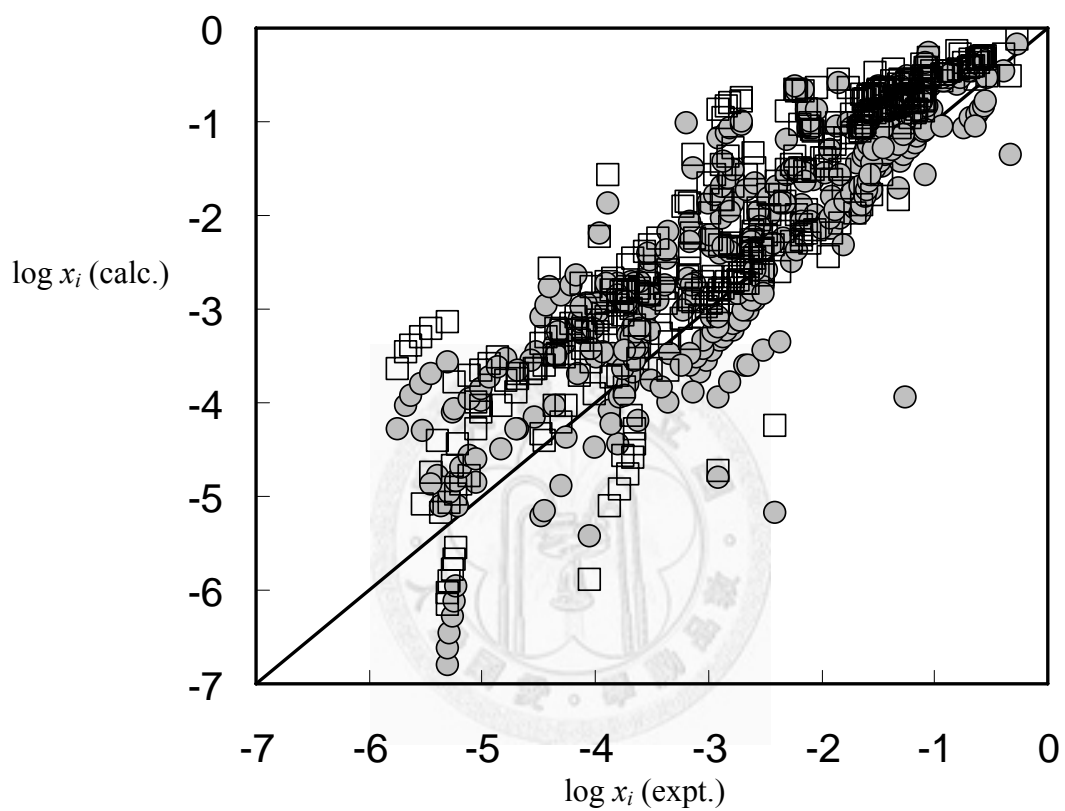
Figure 6-1. Comparison of the predicted and experimental drug solubility (in logarithm). The filled circles and open diamonds are predictions from PR+COSMOSAC and COSMO-SAC model, respectively.
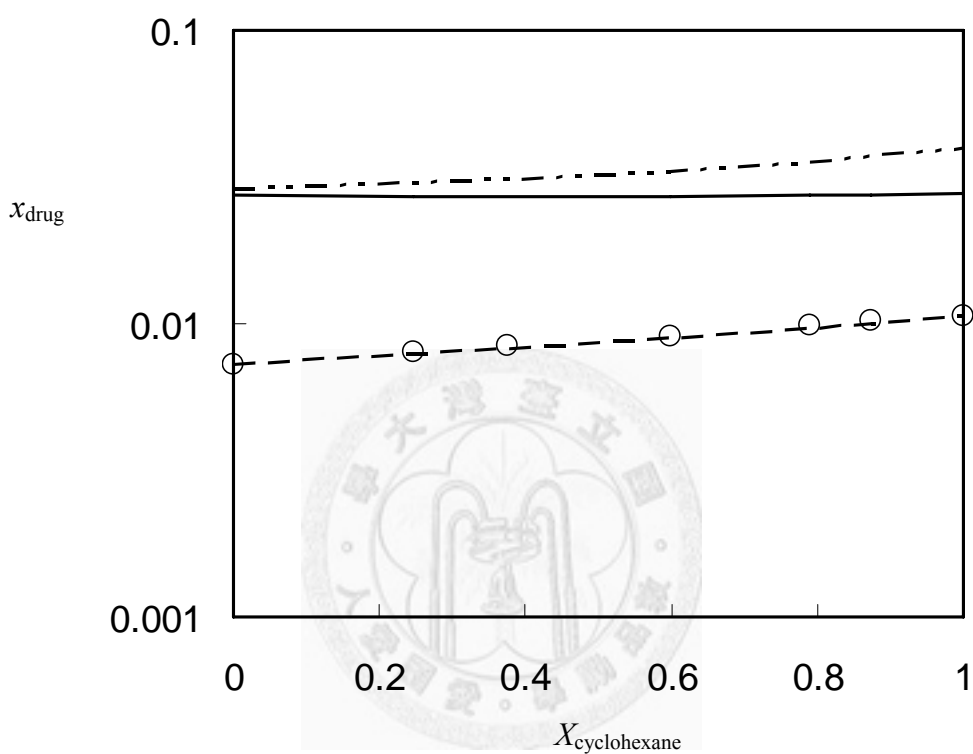
Figure 6-2. Solubility of benzil in the solvent of cyclohexane and n-octane at 298.15 K from PR+COSMOSAC (solid line), PR+COSMOSAC+G^{dsporr} (dashed line), and COSMO-SAC (dashed-dotted-dotted line). Experimental data [153] are shown in open circles. The x-axis X is the solvent fraction in the solute free solvent mixtures.
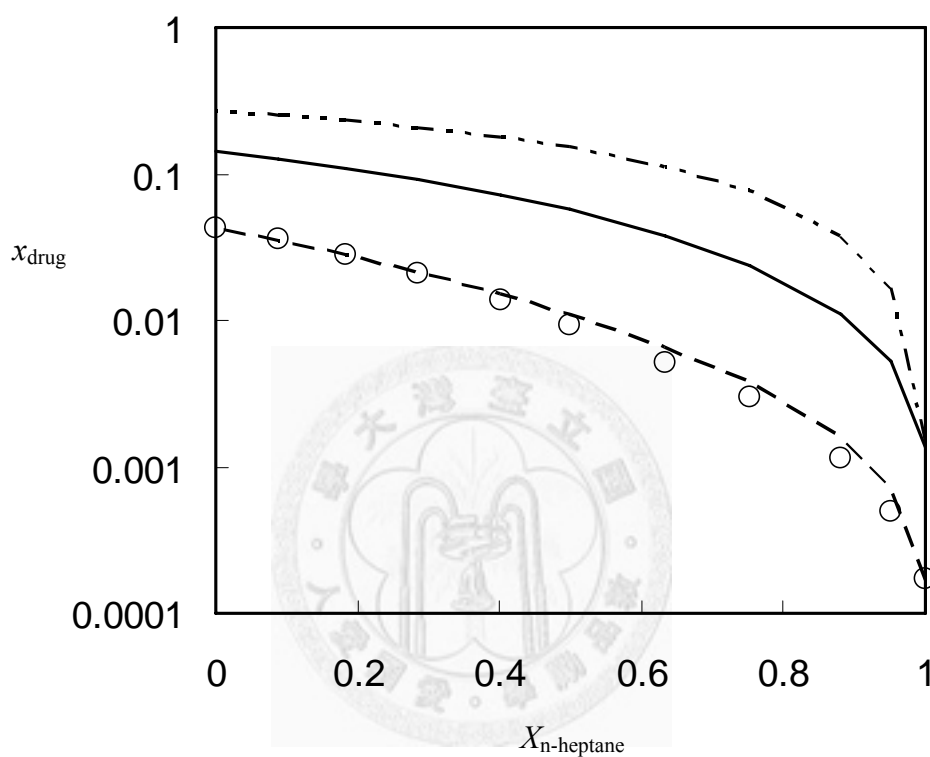
Figure 6-3. Solubility of carbazole in the solvent of n-heptane and tetrahydropyran at 298.15 K from PR+COSMOSAC (solid line), PR+COSMOSAC+G^{dsporr} (dashed line), and COSMO-SAC (dashed-dotted-dotted line). Experimental data [154] are shown in open circles. The x-axis X is the solvent fraction in the solute free solvent mixtures.
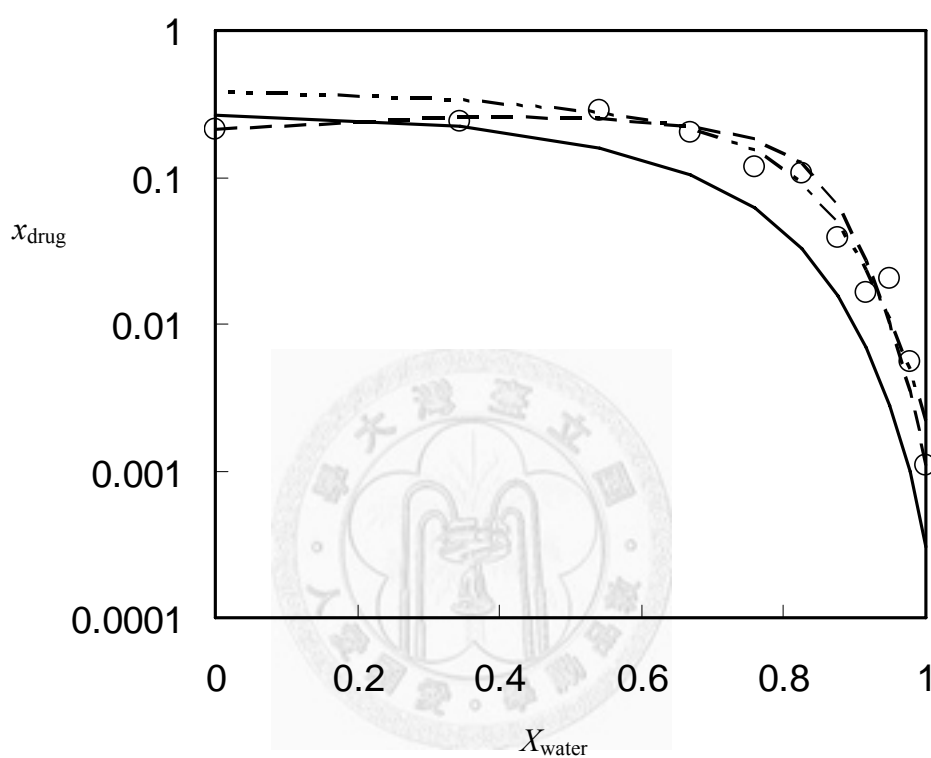
Figure 6-4. Solubility of acetanilide in the solvent of water and dioxane at 293.15 K from PR+COSMOSAC (solid line), PR+COSMOSAC+G^{dsporr} (dashed line), and COSMO-SAC (dashed-dotted-dotted line). Experimental data [155] are shown in open circles. The x-axis X is the solvent fraction in the solute free solvent mixtures.
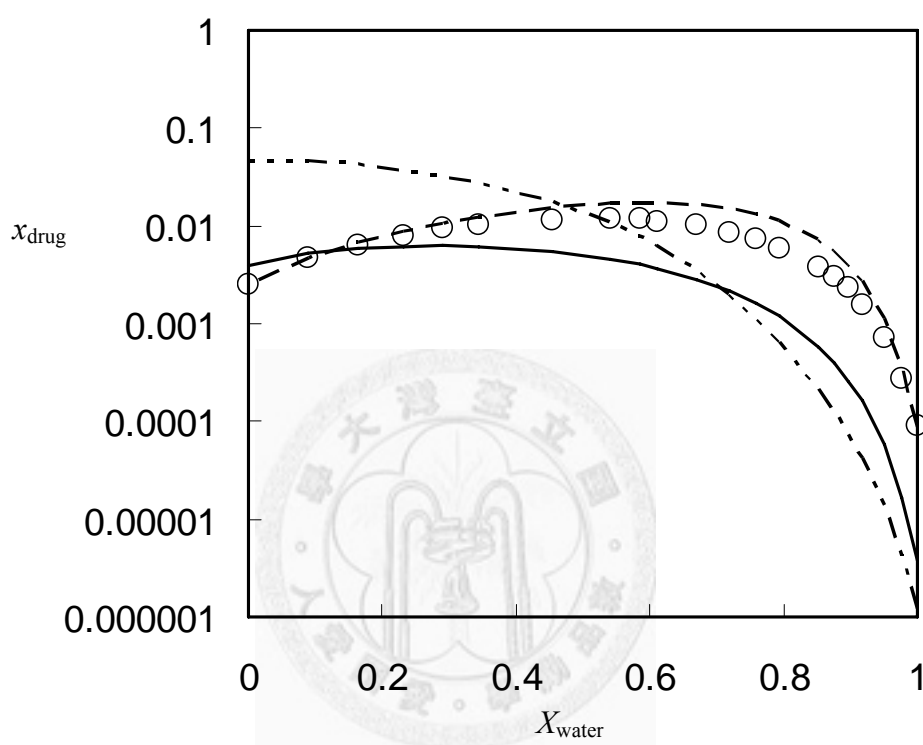
Figure 6-5. Solubility of sulphisomidine in the solvent of water and dioxane at 298.15 K from PR+COSMOSAC (solid line), PR+COSMOSAC+G^{dsporr} (dashed line), and COSMO-SAC (dashed-dotted-dotted line). Experimental data [156] are shown in open circles. The x-axis X is the solvent fraction in the solute free solvent mixtures.

Chapter 7. Conclusions

The employment of *ab initio* solvation calculation in determination of cubic equation of state parameters for pure and mixture fluids, denoted as PR+COSMOSAC, has led to a new way for describing fluid phase equilibria without input of experimental data such as critical properties. The solvation calculation presented in this work is capable of capturing the correct composition and temperature dependence of the interaction parameter $a(T,\underline{x})$, while the solvation cavity and mole-fraction weighted summation is a good estimate for volume parameter $b(\underline{x})$. The PR+COSMOSAC is able to provide reasonable predictions on vapor pressures, liquid densities and critical properties for pure fluids and vapor-liquid equilibrium (VLE), liquid-liquid equilibrium (LLE), vapor-liquid-liquid equilibrium (VLLE) for mixtures, and solid-liquid equilibrium (SLE) with a single model and a single set of parameters. The applications of this method in prediction of normal boiling temperature of environmentally important substances and the 1-octanol-water partition coefficients and infinite-dilution activity coefficients of some organics are demonstrated. The use of this method in the predictions of solubility of drugs in pure and mixture solvents is also validated. Although not shown here, this method can be used to determine other properties such as heat of vaporization, excess properties, etc.

Limited by the accuracy in vapor pressure predictions, this approach presently provides only qualitative results for VLE predictions; however, in the case of mixtures, the predicted accuracy can be improved significantly if the critical properties and acentric factor (PR+COSMOSAC+$T_cP_c\omega$) or the vapor pressure (PR+COSMOSAC+P^{vap}) are used. The accuracy from PR+COSMOSAC may, in some cases, be inferior to existing group contribution methods, e.g., PSRK or modified

UNIFAC. However, because of the proximity effects, methods based on concept of group contributions (e.g., PSRK) may fail badly if used for compounds that do not belong to the family of compounds used in the parameterization. Furthermore, unlike the group contribution methods (PSRK or modified UNIFAC) whose parameter matrix was optimized against a large set of experimental data, the PR+COSMOSAC contains only a few (about 33) non-species dependent, universal parameters. There is no issue of missing parameters if a new chemical species is involved. The time-consuming QM calculations have to be done only once for each chemical species and can be stored in a database. Once the database is established (e.g. the VT COSMO database), the time need for phase equilibrium calculations using PR+COSMOSAC is similar to that using group contribution methods on a modern personal computer. We consider the PR+COSMOSAC as an ideal complementary method when the existing models are not applicable or no experimental data are available.
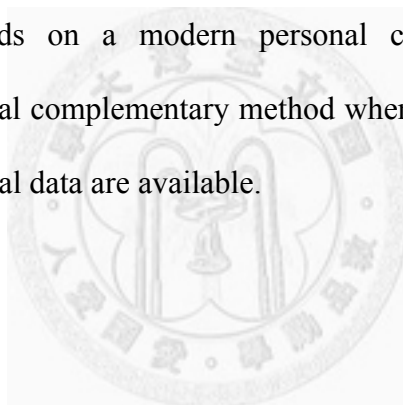
References

[1]   Cadoret, L.; Yu, C. C.; Huang, H. P.; Lee, M. J., Effects of physical properties estimation on process design: a case study using AspenPlus. *Asia-Pacific Journal of Chemical Engineering* **2009,** 4, (5), 729-734.

[2]   Wang, S. J.; Yu, C. C.; Huang, H. P., Plant-wide design and control of DMC synthesis process via reactive distillation and thermally coupled extractive distillation. *Computers & Chemical Engineering* **2010,** 34, (3), 361-373.

[3]   Fredenslund, A.; Gmehling, J.; Michelsen, M. L.; Rasmussen, P.; Prausnitz, J. M., Computerized design of multicomponent distillation-columns using UNIFAC group contribution method for calculation of activity-coefficients. *Industrial & Engineering Chemistry Process Design and Development* **1977,** 16, (4), 450-462.

[4]   Banerjee, T.; Sahoo, R. K.; Rath, S. S.; Kumar, R.; Khanna, A., Multicomponent liquid-liquid equilibria prediction for aromatic extraction systems using COSMO-RS. *Industrial & Engineering Chemistry Research* **2007,** 46, (4), 1292-1304.

[5]   Sandler, S. I., *Chemical and Engineering Thermodynamics*. 3rd ed.; John Weily & Sons: New York, 1999.

[6]   Prausnitz, J. M.; Lichtenthaler, R. N.; de Azevedo, E. G., *Molecular Thermodynamics of Fluid-Phase Equilibria*. 3rd ed.; Pearson Education Taiwan Ltd.: Taipei, 2004.

[7]   Smith, J. M.; Van Ness, H. C.; Abbott, M. M., *Introduction to Chemical Engineering Thermodynamics*. 6th ed.; McGraw-Hill: New York, 2000.

[8]   Higler, A.; Chande, R.; Taylor, R.; Baur, R.; Krishna, R., Nonequilibrium modeling of three-phase distillation. *Computers & Chemical Engineering* **2004,** 28, (10), 2021-2036.

[9]   Steyer, F.; Qi, Z. W.; Sundmacher, K., Synthesis of cylohexanol by three-phase reactive distillation: influence of kinetics on phase equilibria. *Chemical Engineering Science* **2002,** 57, (9), 1511-1520.

[10]   Gumus, Z. H.; Ciric, A. R., Reactive distillation column design with vapor/liquid/liquid equilibria. *Computers & Chemical Engineering* **1997,** 21, S983-S988.

[11]   Bekiaris, N.; Morari, M., Multiple steady states in distillation: infinity/infinity

Predictions, extensions, and implications for design, synthesis, and simulation. *Industrial & Engineering Chemistry Research* **1996,** 35, (11), 4264-4280.

[12]   Bekiaris, N.; Meski, G. A.; Morari, M., Multiple steady states in heterogeneous azeotropic distillation. *Industrial & Engineering Chemistry Research* **1996,** 35, (1), 207-227.

[13]   Redlich, O.; Kwong, J. N. S., On the thermodynamics of solutions .5. An equation of state - Fugacities of gaseous solutions. *Chemical Reviews* **1949,** 44, (1), 233-244.

[14]   Soave, G., Equilibrium constants from a modified Redlich-Kwong equation of state. *Chemical Engineering Science* **1972,** 27, (6), 1197-1203.

[15]   Peng, D.; Robinson, D. B., New 2-constant equation of state. *Industrial & Engineering Chemistry Fundamentals* **1976,** 15, (1), 59-64.

[16]   Coniglio, L.; Rauzy, E.; Peneloux, A.; Neau, E., Use of heat capacities for the estimation of cubic equation-of-state parameters - Application to the prediction of very low vapor pressures of heavy hydrocarbons. *Fluid Phase Equilibria* **2002,** 200, (2), 375-398.

[17]   Coniglio, L.; Trassy, L.; Rauzy, E., Estimation of thermophysical properties of heavy hydrocarbons through a group contribution based equation of state. *Industrial & Engineering Chemistry Research* **2000,** 39, (12), 5037-5048.

[18]   Figueira, F. L.; Lugo, L.; Olivera-Fuentes, C., Generalized parameters of the Stryjek-Vera and Gibbons-Laughton cohesion functions for use with cubic EOS of the van der Waals type. *Fluid Phase Equilibria* **2007,** 259, (1), 105-115.

[19]   Gasem, K. A. M.; Gao, W.; Pan, Z.; Robinson, R. L., A modified temperature dependence for the Peng-Robinson equation of state. *Fluid Phase Equilibria* **2001,** 181, (1-2), 113-125.

[20]   Kontogeorgis, G. M.; Smirlis, I.; Yakoumis, I. V.; Harismiadis, V.; Tassios, D. P., Method for estimating critical properties of heavy compounds suitable for cubic equations of state and its application to the prediction of vapor pressures. *Industrial & Engineering Chemistry Research* **1997,** 36, (9), 4008-4012.

[21]   Twu, C. H.; Coon, J. E.; Cunningham, J. R., A new generalized alpha-function for a cubic equation of state .1. Peng-Robinson equation. *Fluid Phase Equilibria* **1995,** 105, (1), 49-59.

[22]   Wu, D.; Sandler, S. I., Generalized temperature-dependent parameters for the

Peng-Robinson equation of state for normal-alkanes. *Industrial & Engineering Chemistry Research* **1989,** 28, (7), 1103-1106.

[23] Xu, Z.; Sandler, S. I., Temperature-dependent parameters and the Peng-Robinson equation of state. *Industrial & Engineering Chemistry Research* **1987,** 26, (3), 601-606.

[24] Zabaloy, M. S.; Vera, J. H., Cubic equation of state for pure compound vapor pressures from the triple point to the critical point. *Industrial & Engineering Chemistry Research* **1996,** 35, (3), 829-836.

[25] Hsieh, C. M.; Lin, S. T., Determination of cubic equation of state parameters for pure fluids from first principle solvation calculations. *AIChE Journal* **2008,** 54, (8), 2174-2181.

[26] Nichita, D. V., A new method for critical points calculation from cubic EOS. *AIChE Journal* **2006,** 52, (3), 1220-1227.

[27] Ahlers, J.; Gmehling, J., Development of an universal group contribution equation of state I. Prediction of liquid densities for pure compounds with a volume translated Peng-Robinson equation of state. *Fluid Phase Equilibria* **2001,** 191, (1-2), 177-188.

[28] Holderbaum, T.; Gmehling, J., PSRK - A group contribution equation of state based on UNIFAC. *Fluid Phase Equilibria* **1991,** 70, (2-3), 251-265.

[29] Jaubert, J. N.; Mutelet, F., VLE predictions with the Peng-Robinson equation of state and temperature dependent k(ij) calculated through a group contribution method. *Fluid Phase Equilibria* **2004,** 224, (2), 285-304.

[30] Lee, M. T.; Lin, S. T., Prediction of mixture vapor-liquid equilibrium from the combined use of Peng-Robinson equation of state and COSMO-SAC activity coefficient model through the Wong-Sandler mixing rule. *Fluid Phase Equilibria* **2007,** 254, (1-2), 28-34.

[31] Soave, G. S.; Bertucco, A.; Sponchiado, M., Avoiding the use of critical constants in cubic equations of state. *AIChE Journal* **1995,** 41, (8), 1964-1971.

[32] Stryjek, R.; Vera, J. H., PRSV - An improved Peng-Robinson equation of state with new mixing rules for strongly nonideal mixtures. *Canadian Journal of Chemical Engineering* **1986,** 64, (2), 334-340.

[33] Stryjek, R.; Vera, J. H., PRSV - An improved Peng-Robinson equation of state for pure compounds and mixtures. *Canadian Journal of Chemical Engineering* **1986,**

64, (2), 323-333.

[34] Twu, C. H.; Bluck, D.; Cunningham, J. R.; Coon, J. E., A cubic equation of state with a new alpha function and a new mixing rule. *Fluid Phase Equilibria* **1991,** 69, 33-50.

[35] Twu, C. H.; Coon, J. E.; Cunningham, J. R., A new cubic equation of state. *Fluid Phase Equilibria* **1992,** 75, 65-79.

[36] Hsieh, C. M.; Lin, S. T., First-principles predictions of vapor-liquid equilibria for pure and mixture fluids from the combined use of cubic equations of state and solvation calculations. *Industrial & Engineering Chemistry Research* **2009,** 48, (6), 3197-3205.

[37] Hsieh, C. M.; Lin, S. T., Prediction of liquid-liquid equilibrium from the Peng-Robinson+COSMOSAC equation of state. *Chemical Engineering Science* **2010,** 65, (6), 1955-1963.

[38] Hsieh, C. M.; Lin, S. T., Prediction of 1-octanol-water partition coefficient and infinite dilution activity coefficient in water from the PR plus COSMOSAC model. *Fluid Phase Equilibria* **2009,** 285, (1-2), 8-14.

[39] Chapman, W. G.; Gubbins, K. E.; Jackson, G.; Radosz, M., New reference equation of state for associating liquids. *Industrial & Engineering Chemistry Research* **1990,** 29, (8), 1709-1721.

[40] Chapman, W. G.; Jackson, G.; Gubbins, K. E., Phase-equilibria of associating fluids chain molecules with multiple bonding sites. *Molecular Physics* **1988,** 65, (5), 1057-1079.

[41] Gross, J.; Sadowski, G., Perturbed-chain SAFT: An equation of state based on a perturbation theory for chain molecules. *Industrial & Engineering Chemistry Research* **2001,** 40, (4), 1244-1260.

[42] Kontogeorgis, G. M.; Voutsas, E. C.; Yakoumis, I. V.; Tassios, D. P., An equation of state for associating fluids. *Industrial & Engineering Chemistry Research* **1996,** 35, (11), 4310-4318.

[43] *DIPPR801 Thermodynamic Properties Database*. Brigham Young University, Provo, 2008.

[44] Smith, B. D.; Srivastava, R., *Thermodynamic Data for Pure Compounds.   Part A. Hydrocarbons and Ketones*. Elsevier Amsterdam, 1986.

[45] Quadri, S. K.; Kudchadker, A. P., Measurement of the critical temperatures and

critical pressures of some thermally stable or mildly unstable esters, ketones, and ethers. *Journal of Chemical Thermodynamics* **1991,** 23, (2), 129-134.

[46] Poling, B. E.; Prausnitz, J. M.; O'Connell, J. P., *The Properties of Gases and Liquids* 5th ed.; McGraw-Hill: New York, 2001.

[47] Avaullee, L.; Trassy, L.; Neau, E.; Jaubert, J. N., Thermodynamic modeling for petroleum fluids - I. Equation of state and group contribution for the estimation of thermodynamic parameters of heavy hydrocarbons. *Fluid Phase Equilibria* **1997,** 139, (1-2), 155-170.

[48] Marrero, J.; Gani, R., Group-contribution based estimation of pure component properties. *Fluid Phase Equilibria* **2001,** 183, 183-208.

[49] Constantinou, L.; Gani, R., New group-contribution method for estimating properties of pure compounds. *AIChE Journal* **1994,** 40, (10), 1697-1710.

[50] Lin, S. T.; Sandler, S. I., Multipole corrections to account for structure and proximity effects in group contribution methods: Octanol-water partition coefficients. *Journal of Physical Chemistry A* **2000,** 104, (30), 7099-7105.

[51] Lin, S. T.; Hsieh, M. K.; Hsieh, C. M.; Hsu, C. C., Towards the development of theoretically correct liquid activity coefficient models. *Journal of Chemical Thermodynamics* **2009,** 41, (10), 1145-1153.

[52] Wilson, G. M., Vapor-liquid equilibrium.11. New expression for excess free energy of mixing. *Journal of the American Chemical Society* **1964,** 86, (2), 127-130.

[53] Renon, H.; Prausnitz, J. M., Local compositions in thermodynamic excess functions for liquid mixtures. *AIChE Journal* **1968,** 14, (1), 135-144.

[54] Abrams, D. S.; Prausnitz, J. M., Statistical thermodynamics of liquid-mixtures - new expression for excess Gibbs energy of partly or completely miscible systems. *AIChE Journal* **1975,** 21, (1), 116-128.

[55] Gmehling, J.; Lohmann, J.; Jakob, A.; Li, J. D.; Joh, R., A modified UNIFAC (Dortmund) model. 3. Revision and extension. *Industrial & Engineering Chemistry Research* **1998,** 37, (12), 4876-4882.

[56] Gmehling, J.; Li, J. D.; Schiller, M., A modified UNIFAC model .2. Present parameter matrix and results for different thermodynamic properties. *Industrial & Engineering Chemistry Research* **1993,** 32, (1), 178-193.

[57] Weidlich, U.; Gmehling, J., A modified UNIFAC model .1. Prediction of VLE,

He, and gamma-infinity. *Industrial & Engineering Chemistry Research* **1987,** 26, (7), 1372-1381.

[58] Jakob, A.; Grensemann, H.; Lohmann, J.; Gmehling, J., Further development of modified UNIFAC (Dortmund): Revision and extension 5. *Industrial & Engineering Chemistry Research* **2006,** 45, (23), 7924-7933.

[59] Gmehling, J.; Wittig, R.; Lohmann, J.; Joh, R., A modified UNIFAC (Dortmund) model. 4. Revision and extension. *Industrial & Engineering Chemistry Research* **2002,** 41, (6), 1678-1688.

[60] Klamt, A.; Jonas, V.; Burger, T.; Lohrenz, J. C. W., Refinement and parametrization of COSMO-RS. *Journal of Physical Chemistry A* **1998,** 102, (26), 5074-5085.

[61] Klamt, A., Conductor-like screening model for real solvents - A new approach to the quantitative calculation of solvation phenomena. *Journal of Physical Chemistry* **1995,** 99, (7), 2224-2235.

[62] Wang, S.; Sandler, S. I.; Chen, C. C., Refinement of COSMO-SAC and the applications. *Industrial & Engineering Chemistry Research* **2007,** 46, (22), 7275-7288.

[63] Lin, S. T.; Chang, J.; Wang, S.; Goddard, W. A.; Sandler, S. I., Prediction of vapor pressures and enthalpies of vaporization using a COSMO solvation model. *Journal Of Physical Chemistry A* **2004,** 108, (36), 7429-7439.

[64] Lin, S. T.; Sandler, S. I., A priori phase equilibrium prediction from a segment contribution solvation model. *Industrial & Engineering Chemistry Research* **2002,** 41, (5), 899-913.

[65] *Aspen Plus Unit Operation Models*, Aspen Technology Inc: Burlington, MA, 2007.

[66] Magnussen, T.; Rasmussen, P.; Fredenslund, A., UNIFAC parameter table for prediction of liquid-liquid equilibria. *Industrial & Engineering Chemistry Process Design and Development* **1981,** 20, (2), 331-339.

[67] Iwakabe, K.; Kosuge, H., A correlation method for isobaric vapor-liquid and vapor-liquid-liquid equilibria data of binary systems. *Fluid Phase Equilibria* **2008,** 266, (1-2), 202-210.

[68] Skjoldjorgensen, S.; Rasmussen, P.; Fredenslund, A., On the concentration-dependence of the UNIQUAC UNIFAC models. *Chemical*

Engineering Science **1982,** 37, (1), 99-111.

[69] Gupte, P. A.; Danner, R. P., Prediction of liquid-liquid equilibria with UNIFAC - A critical evaluation *Industrial & Engineering Chemistry Research* **1987,** 26, (10), 2036-2042.

[70] Huron, M. J.; Vidal, J., New mixing rules in simple equations of state for representing vapor-liquid-equilibria of strongly non-ideal mixtures. *Fluid Phase Equilibria* **1979,** 3, (4), 255-271.

[71] Vidal, J., Mixing rules and excess properties in cubic equations of state. *Chemical Engineering Science* **1978,** 33, (6), 787-791.

[72] Wong, D. S. H.; Sandler, S. I., A theoretically correct mixing rule for cubic equations of state. *Aiche Journal* **1992,** 38, (5), 671-680.

[73] Wong, D. S. H.; Orbey, H.; Sandler, S. I., Equation of state mixing rule for nonideal mixtures using available activity-coefficient model parameters and that allows extrapolation over large ranges of temperature and pressure. *Industrial & Engineering Chemistry Research* **1992,** 31, (8), 2033-2039.

[74] Michelsen, M. L., A modified Huron-Vidal mixing rule for cubic equations of state. *Fluid Phase Equilibria* **1990,** 60, (1-2), 213-219.

[75] Boukouvalas, C.; Spiliotis, N.; Coutsikos, P.; Tzouvaras, N.; Tassios, D., Prediction of vapor-liquid-equilibrium with the LCVM model - A linear combination of the Vidal and Michelsen mixing rules coupled with the original UNIFAC and the T-MPR equation of state. *Fluid Phase Equilibria* **1994,** 92, 75-106.

[76] Lin, S. T.; Hsieh, M. T., Improper matching of solvation energy components in Gex-based mixing rules *Fluid Phase Equilibria* **2008,** 269, (1-2), 139-142.

[77] Orbey, H.; Sandler, S. I., *Modelling Vapor-Liquid Equilibria. Cubic Equations of State and Their Mixing Rules*. Cambridge University Press: New York, 1998.

[78] Escobedo-Alvarado, G. N.; Sandler, S. I., Study of EOS-G(ex) mixing rules for liquid-liquid equilibria. *AIChE Journal* **1998,** 44, (5), 1178-1187.

[79] Matsuda, H.; Kurihara, K.; Ochi, K.; Kojima, K., Prediction of liquid-liquid equilibria at high pressure for binary systems using EOS-G(E) models: methanol plus hydrocarbon systems. *Fluid Phase Equilibria* **2002,** 203, (1-2), 269-284.

[80] Ben-Naim, A., *Solvation Thermodynamics*. Plenum Press: New York, 1987.

[81] Lin, S. T.; Hsieh, C. M.; Lee, M. T., Solvation and chemical engineering

thermodynamics. *Journal of the Chinese Institute of Chemical Engineers* **2007,** 38, (5-6), 467-476.

[82] Abbott, M. M.; Prausnitz, J. M., Generalized van der Waals theory: A classical perspective. *Fluid Phase Equilibria* **1987,** 37, 29-62.

[83] Tomasi, J.; Persico, M., Molecular-interactions in solution - An overview of methods based on continuous distributions of the solvent. *Chemical Reviews* **1994,** 94, (7), 2027-2094.

[84] Tomasi, J.; Mennucci, B.; Cammi, R., Quantum mechanical continuum solvation models. *Chemical Reviews* **2005,** 105, (8), 2999-3093.

[85] Lin, S. T.; Hsieh, C. M., Efficient and accurate solvation energy calculation from polarizable continuum models. *Journal of Chemical Physics* **2006,** 125, (12), 124103.

[86] Kollman, P., Free-energy calculations - Applications to chemical and biochemical phenomena. *Chemical Reviews* **1993,** 93, (7), 2395-2417.

[87] Cramer, C. J.; Truhlar, D. G., Implicit solvation models: Equilibria, structure, spectra, and dynamics. *Chemical Reviews* **1999,** 99, (8), 2161-2200.

[88] Wang, B. Z.; Ford, G. P., Molecular-orbital theory of a solute in a continuum with an arbitrarily shaped boundary represented by finite surface elements. *Journal of Chemical Physics* **1992,** 97, (6), 4162-4169.

[89] Miertus, S.; Tomasi, J., Approximate evaluations of the electrostatic free-energy and internal energy changes in solution processes. *Chemical Physics* **1982,** 65, (2), 239-245.

[90] Klamt, A.; Schuurmann, G., COSMO - A new approach to dielectric screening in solvents with explicit expressions for the screening energy and its gradient. *Journal Of The Chemical Society-Perkin Transactions 2* **1993**, (5), 799-805.

[91] Truong, T. N.; Stefanovich, E. V., Analytical first and 2nd energy derivatives of the generalized conductorlike screening model for free-energy of solvation. *Journal of Chemical Physics* **1995,** 103, (9), 3709-3717.

[92] Chipman, D. M., Simulation of volume polarization in reaction field theory. *Journal of Chemical Physics* **1999,** 110, (16), 8012-8018.

[93] Baldridge, K.; Klamt, A., First principles implementation of solvent effects without outlying charge error. *Journal of Chemical Physics* **1997,** 106, (16), 6622-6633.

[94]   Grensemann, H.; Gmehling, J., Performance of a conductor-like screening model for real solvents model in comparison to classical group contribution methods. *Industrial & Engineering Chemistry Research* **2005,** 44, (5), 1610-1624.

[95]   Lin, S. T.; Sandler, S. I., A priori phase equilibrium prediction from a segment contribution solvation model (vol 41, pg 903, 2004). *Industrial & Engineering Chemistry Research* **2004,** 43, (5), 1322-1322.

[96]   Pimentel, G. C.; McClellan, A. L., *The Hydrogen Bond*. W. H. Freeman and Company: New York, 1960.

[97]   Wang, S.; Lin, S. T.; Watanasiri, S.; Chen, C. C., Use of GAMESS/COSMO program in support of COSMO-SAC model applications in phase equilibrium prediction calculations. *Fluid Phase Equilibria* **2009,** 276, (1), 37-45.

[98]   Mu, T. C.; Rarey, J.; Gmehling, J., Performance of COSMO-RS with sigma profiles from different model chemistries. *Industrial & Engineering Chemistry Research* **2007,** 46, (20), 6612-6629.

[99]   Mu, T. C.; Rarey, J.; Gmehling, J., Group contribution prediction of surface charge density profiles for COSMO-RS(OI). *AIChE Journal* **2007,** 53, (12), 3231-3240.

[100]   Still, W. C.; Tempczyk, A.; Hawley, R. C.; Hendrickson, T., Semianalytical treatment of solvation for molecular mechanics and dynamics. *Journal of the American Chemical Society* **1990,** 112, (16), 6127-6129.

[101]   Cramer, C. J.; Truhlar, D. G., A universal approach to solvation modeling. *Accounts of Chemical Research* **2008,** 41, (6), 760-768.

[102]   Cramer, C. J.; Truhlar, D. G., General parameterized scf model for free-energies of solvation in aqueous-solution. *Journal of the American Chemical Society* **1991,** 113, (22), 8305-8311.

[103]   Marrero, J.; Abildskov, J., *Solubility and Related Properties of Large Complex Chemicals*. DECHEMA: Frankfurt am Main, 2003; Vol. XV.

[104]   NIST http://webbook.nist.gov/chemistry/.

[105]   Chickos, J. S.; Acree, W. E., Estimating solid-liquid phase change enthalpies and entropies. *Journal of Physical and Chemical Reference Data* **1999,** 28, (6), 1535-1673.

[106]   Chickos, J. S.; Acree, W. E., Total phase change entropies and enthalpies - An update on their estimation and applications to the estimations of amphiphillic

fluorocarbon-hydrocarbon molecules. *Thermochimica Acta* **2003,** 395, (1-2), 59-113.

[107]   Mullins, E.; Oldland, R.; Liu, Y. A.; Wang, S.; Sandler, S. I.; Chen, C. C.; Zwolak, M.; Seavey, K. C., Sigma-profile database for using COSMO-based thermodynamic methods. *Industrial & Engineering Chemistry Research* **2006,** 45, (12), 4389-4415.

[108]   Mullins, E.; Liu, Y. A.; Ghaderi, A.; Fast, S. D., Sigma profile database for predicting solid solubility in pure and mixed solvent mixtures for organic pharmacological compounds with COSMO-based thermodynamic methods. *Industrial & Engineering Chemistry Research* **2008,** 47, (5), 1707-1725.

[109]   http://www.design.che.vt.edu/VT-Databases.html

[110]   Sørensen, J. M.; Arlt, W., *Liquid-Liquid Equilibrium Data Collection*. DECHEMA: Frankfurt, 1979; Vol. 1.

[111]   Lin, S. T., Thermodynamic equations of state from molecular solvation. *Fluid Phase Equilibria* **2006,** 245, (2), 185-192.

[112]   Katritzky, A. R.; Slavov, S. H.; Dobchev, D. A.; Karelson, M., Rapid QSPR model development technique for prediction of vapor pressure of organic compounds. *Computers & Chemical Engineering* **2007,** 31, (9), 1123-1130.

[113]   Eckert, F.; Klamt, A., Fast solvent screening via quantum chemistry: COSMO-RS approach. *AIChE Journal* **2002,** 48, (2), 369-385.

[114]   Emami, F. S.; Vahid, A.; Elliott, J. R.; Feyzi, F., Group contribution prediction of vapor pressure with statistical associating fluid theory, perturbed-chain statistical associating fluid theory, and Elliott-Suresh-Donohue equations of state. *Industrial & Engineering Chemistry Research* **2008,** 47, (21), 8401-8411.

[115]   Wang, S.; Lin, S. T.; Chang, J.; Goddard, W. A.; Sandler, S. I., Application of the COSMO-SAC-BP solvation model to predictions of normal boiling temperatures for environmentally significant substances. *Industrial & Engineering Chemistry Research* **2006,** 45, (16), 5426-5434.

[116]   Psutka, S.; Wichterle, I., Vapor-liquid equilibria in the binary and ternary systems composed of 2-methylpentane, 3-methyl-2-butanone and 3-methyl-2-butanol. *Journal of Chemical and Engineering Data* **2005,** 50, (4), 1338-1342.

[117]   Campbell, S. W.; Wilsak, R. A.; Thodos, G., Isothermal

106

Vapor-Liquid-Equilibrium Measurements for the Normal-Pentane Acetone System at 372.7-K, 397.7-K, and 422.6-K. *Journal of Chemical and Engineering Data* **1986,** 31, (4), 424-430.

[118] Gmehling, J.; Onken, U.; Arlt, W., *Vapor-Liquid Equilibrium Data Collection* Dechema: Frankfurt, 1977.

[119] Hwang, S. M.; Lee, M. J.; Lin, H. M., Isothermal vapor-liquid equilibria for mixtures of 4-methoxyphenol, catechol, and p-cresol. *Fluid Phase Equilibria* **2000,** 172, (2), 183-196.

[120] Bobbo, S.; Fedele, L.; Camporese, R.; Stryjek, R., Isothermal vapor-liquid equilibrium for the three binary systems 1,1,1,2,3,3-hexafluoropropane with dimethyl ether or propane, and 1,1,1,3,3,3-hexafluoropropane with dimethyl ether. *Fluid Phase Equilibria* **2000,** 174, (1-2), 3-12.

[121] Barr-David, F.; Dodge, B. F., Vapor-liquid equilibrium at high pressures. The systems ethanol-water and 2-propanol-water. *Journal of Chemical and Engineering Data* **1959,** 4, (2), 107 - 121.

[122] Sada, E.; Morisue, T., Isothermal vapor-liquid equilibrium data of isopropanol-water system. *Journal of Chemical Engineering of Japan* **1975,** 8, (3), 191-195.

[123] Wang, S.; Stubbs, J. M.; Siepmann, J. I.; Sandler, S. I., Effects of conformational distributions on sigma profiles in COSMO theories. *Journal of Physical Chemistry A* **2005,** 109, (49), 11285-11294.

[124] Klamt, A.; Eckert, F.; Hornig, M.; Beck, M. E.; Burger, T., Prediction of aqueous solubility of drugs and pesticides with COSMO-RS. *Journal of Computational Chemistry* **2002,** 23, (2), 275-281.

[125] Klamt, A., *COSMO-RS from Quantum Chemistry to Fluid Phase Thermodynamics and Drug Design*. Elsevier: Amsterdam, 2005.

[126] Letcher, T. M.; Naicker, P. K., Liquid-liquid equilibria for mixtures of an alkane plus an aromatic hydrocarbon+1,4-dicyanobutane at 298.15 K. *Journal of Chemical and Engineering Data* **2000,** 45, (1), 104-109.

[127] Iwakabe, K.; Kosuge, H., Isobaric vapor-liquid-liquid equilibria with a newly developed still. *Fluid Phase Equilibria* **2001,** 192, (1-2), 171-186.

[128] Moon, H. M.; Ochi, K.; Kojima, K., Vapor-liquid-equilibria for the ethyl methyl ketone + water - system with limited miscibility. *Journal of Chemical and*

Engineering Data **1995,** 40, (2), 468-471.

[129]   Hsieh, C. T.; Lee, M. J.; Lin, H. M., Vapor-liquid -liquid equilibria for aqueous systems with methyl acetate, methyl propionate, and methanol. *Industrial & Engineering Chemistry Research* **2008,** 47, (20), 7927-7933.

[130]   Case, F. H.; Chaka, A.; Moore, J. D.; Mountain, R. D.; Olson, J. D.; Ross, R. B.; Schiller, M.; Shen, V. K.; Stahlberg, E. A., The fifth industrial fluid properties simulation challenge. *Fluid Phase Equilibria* **2009,** 285, (1-2), 1-3.

[131]   Lin, S. T.; Sandler, S. I., Prediction of octanol-water partition coefficients using a group contribution solvation model. *Industrial & Engineering Chemistry Research* **1999,** 38, (10), 4081-4091.

[132]   Butler, J. A. V.; Thomson, D. W.; Maclennan, W. H., The free energy of the normal aliphatic alcohols in aqueous solution - Part I The partial vapour pressures of aqueous solutions of methyl, n-propyl, and n-butyl alcohols - Part II The solubilities of some normal aliphatic alcohols in water - Part III The theory of binary solutions, and its application to aqueous-alcoholic solutions. *Journal of the Chemical Society* **1933**, 674-686.

[133]   Kinoshita, K.; Ishikawa, H.; Shinoda, K., Solubility of alcohols in water determined by the surface tension measurements. *Bulletin of the Chemical Society of Japan* **1958,** 31, (9), 1081-1082.

[134]   Zhuravleva, I. K.; Zhuravlev, E. F.; Lomakina, N. G., Structural diagrams of ternary liquid-systems, having 3 binary laminations with upper-critical temperatures of dissolution. *Zhurnal Fizicheskoi Khimii* **1977,** 51, (7), 1700-1707.

[135]   Olson, J. D.; Morrison, R. E.; Wilson, L. C., Benchmarks for the fifth industrial fluid properties simulation challenge. *Fluid Phase Equilibria* **2009,** 285, (1-2), 4-7.

[136]   Suzuki, T.; Kudo, Y., Automatic Log P-Estimation based on combined additive modeling methods. *Journal of Computer-Aided Molecular Design* **1990,** 4, (2), 155-198.

[137]   Sangster, J., *Octanol-Water Partition Coefficients: Fundamentals and Physical Chemistry*. Wiley and Sons: New York, 1997.

[138]   Isnard, P.; Lambert, S., Aqueous solubility and normal-octanol water partition-coefficient correlations. *Chemosphere* **1989,** 18, (9-10), 1837-1853.

[139] Mennucci, B.; Cances, E.; Tomasi, J., Evaluation of solvent effects in isotropic and anisotropic dielectrics and in ionic solutions with a unified integral equation method: Theoretical bases, computational implementation, and numerical applications. *Journal of Physical Chemistry B* **1997,** 101, (49), 10506-10517.

[140] Kamlet, M. J.; Doherty, R. M.; Abraham, M. H.; Marcus, Y.; Taft, R. W., Linear solvation energy relationships .46. An improved equation for correlation and prediction of octanol water partition-coefficients of organic nonelectrolytes (Including strong hydrogen-bond donor solutes). *Journal of Physical Chemistry* **1988,** 92, (18), 5244-5255.

[141] Tiegs, D.; Gmehling, J.; Medina, A.; Soares, M.; Bastos, J.; Alessi, P.; Kicic, I., *Activity Coefficients at Infinite Dilution*. DECHEMA: Frankfurt, 1986; Vol. IX.

[142] Hait, M. J.; Liotta, C. L.; Eckert, C. A.; Bergmann, D. L.; Karachewski, A. M.; Dallas, A. J.; Eikens, D. I.; Li, J. J. J.; Carr, P. W.; Poe, R. B.; Rutan, S. C., Space predictor for infinite dilution activity-coefficients. *Industrial & Engineering Chemistry Research* **1993,** 32, (11), 2905-2914.

[143] Kojima, K.; Zhang, S. J.; Hiaki, T., Measuring methods of infinite dilution activity coefficients and a database for systems including water. *Fluid Phase Equilibria* **1997,** 131, (1-2), 145-179.

[144] Mackay, D.; Shiu, W. Y., A Critical review of Henry's law constants for chemicals of environmental interest. *Journal of Physical and Chemical Reference Data* **1981,** 10, (4), 1175-1199.

[145] Meylan, W. M.; Howard, P. H., Bond contribution method for estimating Henry's law constants. *Environmental Toxicology and Chemistry* **1991,** 10, (10), 1283-1293.

[146] Yaws, C.; Yang, H. C.; Xiang, P., Henry's law constants for organic 362 compounds in water. *Chemical Engineering* **1991,** 98, (11), 179-185.

[147] Modarresi, H.; Conte, E.; Abildskov, J.; Gani, R.; Crafts, P., Model-based calculation of solid solubility for solvent selection - A review. *Industrial & Engineering Chemistry Research* **2008,** 47, (15), 5234-5242.

[148] Constable, D. J. C.; Jimenez-Gonzalez, C.; Henderson, R. K., Perspective on solvent use in the pharmaceutical industry. *Organic Process Research & Development* **2007,** 11, (1), 133-137.

[149] Chen, C. C.; Simoni, L. D.; Brennecke, J. F.; Stadtherr, M. A., Correlation and

prediction of phase behavior of organic compounds in ionic liquids using the nonrandom two-liquid segment activity coefficient model. *Industrial & Engineering Chemistry Research* **2008,** 47, (18), 7081-7093.

[150]   Chen, C. C.; Crafts, P. A., Correlation and prediction of drug molecule solubility in mixed solvent systems with the Nonrandom Two-Liquid Segment Activity Coefficient (NRTL-SAC) model. *Industrial & Engineering Chemistry Research* **2006,** 45, (13), 4816-4824.

[151]   Tung, H. H.; Tabora, J.; Variankaval, N.; Bakken, D.; Chen, C. C., Prediction of pharmaceutical solubility via NRTL-SAC and COSMO-SAC. *Journal of Pharmaceutical Sciences* **2008,** 97, (5), 1813-1820.

[152]   Shu, C. C.; Lin, S. T., Prediction of drug solubility in mixed solvent systems using the COSMO-SAC activity coefficient model. *Industrial & Engineering Chemistry Research* **2010,** in press.

[153]   Acree, W. E.; Rytting, J. H., Solubility in binary solvent systems. 1. Specific versus nonspecific interactions. *Journal of Pharmaceutical Sciences* **1982,** 71, (2), 201-205.

[154]   Acree, W. E.; McCargar, J. W.; Zvaigzne, A. I.; Teng, I. L., Mathematical representation of thermodynamic properties - Carbazole solubilities in binary alkane + dibutyl ether and alkane + tetrahydropyran solvent mixtures. *Physics and Chemistry of Liquids* **1991,** 23, (1), 27-35.

[155]   Bustamante, P.; Romero, S.; Pena, A.; Escalera, B.; Reillo, A., Enthalpy-entropy compensation for the solubility of drugs in solvent mixtures: Paracetamol, acetanilide, and nalidixic acid in dioxane-water. *Journal of Pharmaceutical Sciences* **1998,** 87, (12), 1590-1596.

[156]   Martin, A.; Wu, P. L.; Velasquez, T., Eetended Hildebrand solubility approach - Sulfonamides in binary and ternary solvents. *Journal of Pharmaceutical Sciences* **1985,** 74, (3), 277-282.

Appendix

Appendix A. Method for calculation of the critical properties

In the P-V diagram, the critical point is the inflection point of $T = T_c$ isotherm [5] , i.e.,

$$\left(\frac{\partial P}{\partial \underline{V}}\right)_T\bigg|_{T_c,P_c,\underline{V}_c} = \left(\frac{\partial^2 P}{\partial \underline{V}^2}\right)_T\bigg|_{T_c,P_c,\underline{V}_c} = 0 \tag{A-1}$$

For the Peng-Robinson EOS, we have

$$\left(\frac{\partial P}{\partial \underline{V}}\right)_T\bigg|_{T_c,P_c,\underline{V}_c} = \frac{-RT_C}{(\underline{V}_C - b)^2} + \frac{2a(\underline{V}_C + b)}{(\underline{V}_C^2 + 2b\underline{V}_C - b^2)^2} = 0 \tag{A-2}$$

and

$$\left(\frac{\partial^2 P}{\partial \underline{V}^2}\right)_T\bigg|_{T_c,P_c,\underline{V}_c} = \frac{2RT}{(\underline{V}_C - b)^3} + \frac{2a(\underline{V}_C^2 + 2b\underline{V}_C - b^2) - 8a(\underline{V}_C^2 + 2b\underline{V}_C + b^2)}{(\underline{V}_C^2 + 2b\underline{V}_C - b^2)^3} = 0 \tag{A-3}$$

Solving the Eqs (A-2) and (A-3), we obtain the critical volume expressed in terms of the volume parameter b,

$$\underline{V}_C = b\left[1 + (4 + 2\sqrt{2})^{1/3} + (4 - 2\sqrt{2})^{1/3}\right] \tag{A-4}$$

Rewriting eqn. 24, we obtain the expression for energy parameter a at the critical point,

$$a(T_C) = \frac{RT_C}{(\underline{V}_C - b)^2} \frac{(\underline{V}_C^2 + 2b\underline{V}_C - b^2)^2}{2(\underline{V}_C + b)} \tag{A-5}$$

Thus, the critical temperature T_c can be evaluated numerically, e.g., by the Newton-Rapson method. Once we have T_c and V_c, the critical pressure P_c can be easily calculated from the original Peng-Robinson EOS

$$P_C = \frac{RT_C}{\underline{V}_C - b} - \frac{a(T_C)}{\underline{V}_C(\underline{V}_C + b) + b(\underline{V}_C - b)} \tag{A-6}$$

or, equivalently,

$$P_C = \frac{z_C R T_C}{\underline{V}_C} \qquad\qquad \text{(A-7)}$$

where z_c=0.307 is a constant in Peng-Robinson EOS. As mentioned in the context, most chemical species have a value of $z_c(=P_c\underline{V}_c/RT_c)$ around 0.26. Therefore, it is recommended that, for better accuracy, z_c=0.26 be used in Eq. (A-7) for P_c.

Appendix B. List for systems used in parameter optimization

Parameter	System used in optimization
$A_{dsp,C}$, $B_{dsp,C}$, $A_{dsp,H}$, and $B_{dsp,H}$	linear alkanes from ethane to dodecane without any branches
$A_{dsp,O}$ and $B_{dsp,O}$,	6 aldehydes, 11 ketones, 6 ethers, and 8 esters without branches
$A_{dsp,N}$ and $B_{dsp,N}$,	3 nitros and 3 nitriles
$A_{dsp,Cl}$ and $B_{dsp,Cl}$	4 chlorine containing alkyl halides: (1) chloroethane (2) 1-chloropropane (3) 1-chlorobutane (4) 1-chloropentane
$A_{dsp,F}$ and $B_{dsp,F}$	6 fluorine containing alkyl halides: (1) ethylfluoride (2) hexafluoroethane (3) carbontetrafluoride (4) octafluorocyclobutane (5) fluorobenzene (6) hexafluorobenzene
$A_{dsp,RING}$ and $B_{dsp,RING}$	49 cycloalkane and aromatic compounds containing C and H atoms
$A_{dsp,HB}$, $B_{dsp,HB}$, $C_{dsp,HB}$, c_{HH}, and c_{OO}	14 linear alcohols from 1-propanol (C_3) to 1-octadecanol (C_{18}) except 1-undecanol (C_{11}) and 1-tridecanol (C_{13})
c_{HO}	LLE of 9 systems: (1) succinonitrile + 1-pentanol (2) acrylonitrile + water (3) nitroethane + water (4) 2-methyl-propanal + water (5) isobutyric acid + water (6) diethylether + water

	(7) propyl formate + water (8) 2-butanone + water (9) 3-pentanone + water
c_{AA}	vapor pressures of 20 selected amines: (1) ethylamine (2) propylamine (3) butylamine (4) pentylamine (5) hexylamine (6) heptylamine (7) octylamine (8) nonylamine (9) decylamine (10) allylamine (11) iso-butylamine (12) dimethylamine (13) tert-butylamine (14) sec-butylamine (15) diethylamine (16) dipropylamine (17) ethylenediamine (18) hexamethylenediamine (19) 1,2-propanediamine (20) 1,3-propanediamine
c_{HA}	LLE systems of two systems: (1) ethanol, 2-amino + benzene (2) ethanol, 2-amino + heptane
c_{AO}	vapor pressures of 12 selected compounds (1) 2-methylacrylamide (2) acrylamide (3) formamide (4) N-methylformamide (5) acetamide (6) dicyandiamide (7) tert-butylformamide (8) N-methylacetamide (9) 6-aminocapronitrile (10) aminoacetonitrile (11) 2-amino ethoxyethanol (12) 1-methoxy-2-propanamine

Appendix C. List for Comparison of T_b Prediction

		PR+COSMOSAC			COSMO-SAC-BP		
Overall deviation		17.69	3.82		21.98	4.59	
Compound	T_b^{expt} (K)	T_b^{calc} (K)	ΔT (K)	AARD (%)	T_b^{calc} (K)	ΔT (K)	AARD (%)
formic acid	373.90	348.88	25.02	6.69	384.50	10.60	2.83
dichloroacetic acid	467.20	416.68	50.52	10.81	465.67	1.53	0.33
triethanolamine	608.55	611.18	2.63	0.43	668.41	59.86	9.84
2,2'-diethanolamine	541.54	551.93	10.39	1.92	542.74	1.20	0.22
ethylformate	327.00	323.87	3.13	0.96	322.60	4.40	1.35
methylacrylate	354.00	350.89	3.11	0.88	356.55	2.55	0.72
methylmethacrylate	373.50	366.11	7.39	1.98	371.71	1.79	0.48
propylformate	354.10	348.33	5.77	1.63	348.32	5.78	1.63
ethylacrylate	372.75	372.99	0.24	0.06	387.35	14.60	3.92
2,2,5-trimethylhexane	397.00	407.47	10.47	2.64	423.59	26.59	6.70
2-methylheptane	390.70	393.51	2.81	0.72	409.62	18.92	4.84
isobutylene	266.70	270.79	4.09	1.53	249.67	17.03	6.39
2-methyl-2-butene	311.00	298.00	13.00	4.18	292.54	18.46	5.94
2-methyl-1-butene	304.30	300.32	3.98	1.31	297.09	7.21	2.37
cis-2-pentene	309.80	302.08	7.72	2.49	300.66	9.14	2.95
trans-2-pentene	309.40	302.65	6.75	2.18	300.05	9.35	3.02
2,6-dimethylphenol	474.22	463.28	10.94	2.31	458.19	16.03	3.38
2,4-dimethylphenol	484.13	472.73	11.40	2.35	461.82	22.31	4.61
3,4-dimethylphenol	500.15	483.49	16.66	3.33	491.58	8.57	1.71
phthalic acid	598.00	587.76	10.24	1.71	711.17	113.17	18.92
diphenylamine	575.15	585.63	10.48	1.82	585.91	10.76	1.87
ethylbenzoate	485.00	476.85	8.15	1.68	502.94	17.94	3.70
benzylbenzoate	596.20	607.41	11.21	1.88	649.16	52.96	8.88
propylbenzoate	503.70	507.04	3.34	0.66	548.28	44.58	8.85
hexachlorobenzene	582.55	506.89	75.66	12.99	607.76	25.21	4.33
trans-1,4-dimethylcyclohexane	392.60	397.75	5.15	1.31	401.97	9.37	2.39
propylcyclopentane	404.10	407.12	3.02	0.75	397.74	6.36	1.57

cyclopentene	317.00	306.45	10.55	3.33	293.56	23.44	7.39
cyclohexene	356.00	340.76	15.24	4.28	336.01	19.99	5.62
1,4-cyclohexadiene	360.15	344.93	15.22	4.23	344.35	15.80	4.39
cycloheptene	387.00	377.67	9.33	2.41	373.11	13.89	3.59
1,2,3,4-tetrahydronaphthalene	490.00	469.63	20.37	4.16	465.16	24.84	5.07
D-limonene	450.00	448.43	1.57	0.35	453.41	3.41	0.76
isoprene	307.00	304.18	2.82	0.92	300.89	6.11	1.99
1-decene	440.00	447.64	7.64	1.74	469.90	29.90	6.80
methylchloromethylether	332.65	341.55	8.90	2.68	345.22	12.57	3.78
epichlorohydrin	389.60	364.10	25.50	6.55	360.87	28.73	7.37
bis-(2-chloroethyl)ether	451.00	414.31	36.69	8.14	437.78	13.22	2.93
1,1-dichloroethylene	304.55	287.48	17.07	5.60	304.73	0.18	0.06
vinylchloride	259.30	260.94	1.64	0.63	256.67	2.63	1.01
cis-1,2-dichloroethylene	333.00	306.50	26.50	7.96	336.67	3.67	1.10
trans-1,2-dichloroethylene	321.00	288.69	32.31	10.07	309.57	11.43	3.56
tetrachloroethylene	394.20	347.11	47.09	11.95	419.33	25.13	6.37
1,1,2,2-tetrachloro- 1,2-difluoroethane	365.75	347.09	18.66	5.10	368.90	3.15	0.86
2-chloro-1,3-butadiene	333.00	325.17	7.83	2.35	335.12	2.12	0.64
perchlorocyclopentadiene	512.20	497.18	15.02	2.93	565.78	53.58	10.46
hexachlorobutadiene	488.20	453.44	34.76	7.12	547.26	59.06	12.10
diphenylenimine	628.20	591.15	37.05	5.90	599.55	28.65	4.56
acridine	618.70	580.44	38.26	6.18	615.17	3.53	0.57
2-methyl-propylbenzene	444.00	458.84	14.84	3.34	473.56	29.56	6.66
dimethylphthalate	555.00	551.84	3.16	0.57	550.28	4.72	0.85
diethylphthalate	571.00	587.76	16.76	2.94	667.06	96.06	16.82
dibutylphthalate	613.20	662.76	49.56	8.08	738.64	125.44	20.46
acenaphthylene	543.15	510.30	32.85	6.05	517.23	25.92	4.77
fluoranthene	655.95	613.59	42.36	6.46	650.42	5.53	0.84
pyrene	667.95	604.05	63.90	9.57	652.30	15.65	2.34
2-ethylnaphthalene	527.00	522.84	4.16	0.79	527.04	0.04	0.01
trans-1,2-diphenylethene	579.15	593.78	14.63	2.53	598.88	19.73	3.41
pentachlorobenzene	550.20	490.19	60.01	10.91	574.38	24.18	4.39

1,1,3-trimethylcyclopentane	378.10	399.65	21.55	5.70	386.62	8.52	2.25
tetrahydropyran	361.00	346.39	14.61	4.05	342.40	18.60	5.15
2-chlorobiphenyl	547.20	562.71	15.51	2.83	597.93	50.73	9.27
3-chlorobiphenyl	557.70	565.08	7.38	1.32	596.73	39.03	7.00

作 者 簡 介

Education:

Ph.D. in Chemical Engineering (Sep. 2004 – Jul. 2010**)**
    National Taiwan University, Taiwan, Republic of China
    Advisor: Dr. Lin, Shiang-Tai

B.S. in Chemical Engineering (Sep. 2000 – Jun. 2004)
    National Taiwan University, Taiwan, Republic of China

Experience:

Teaching Assistant (Sep. 2005 – Jun. 2006)

Exchange Student (Mar. 2009 - Jan. 2010)
    University of Delaware, U.S.A.
    Supervisor: Professor Dr. Sandler, Stanley I.

Journal Articles:

1. Lin, Shiang-Tai*; **Hsieh, Chieh-Ming**, 2006, September, "Efficient and accurate solvation energy calculation from polarizable continuum models," Journal of Chemical Physics, volume 125, issue 12, article number 124103. (SCI, EI)

2. Lin, Shiang-Tai*; **Hsieh, Chieh-Ming**; Lee, Ming-Tsung, 2007, August, "Solvation and chemical engineering thermodynamics," Journal of the Chinese Institute of Chemical Engineers, volume 38, issue 5-6, pages 467-476. (SCI, EI)

3. **Hsieh, Chieh-Ming;** Lin, Shiang-Tai*, 2008, June, "Determination of cubic equation of state parameters for pure fluids from first principle solvation calculations," AIChE Journal, volume 54, issue 8, pages 2174-2181. (SCI, EI)

4. **Hsieh, Chieh-Ming**; Lin, Shiang-Tai*, 2009, March, "First Principle Prediction of Vapor-Liquid Equilibria for Pure and Mixture Fluids from Combined Use of Cubic Equation of State and Solvation Calculations," Industrial & Engineering Chemistry Research, volume 48, issue 6, pages 3197-3205. (SCI, EI)

5. Lin, Shiang-Tai*; Hsieh, Min-Kang; **Hsieh, Chieh-Ming;** Hsu, Chan-Chia, 2009, October, "Towards the development of theoretically correct liquid activity coefficient models," Journal of Chemical Thermodynamics, volume 41, issue 10, pages 1145-1153. (SCI, EI)

6. Lin, Shiang-Tai*; Hsieh, Min-Kang; **Hsieh, Chieh-Ming;** Hsu, Chan-Chia; Huang, Shao-Nung, 2009, November, "Reply to "Comment on "Towards the development of theoretically correct liquid activity coefficient models,""" Journal of Chemical Thermodynamics, volume 41, issue 11, pages 1314-1316. (SCI, EI)

7. **Hsieh, Chieh-Ming;** Lin, Shiang-Tai*, 2009, November, "Prediction of 1-octanol-water partition coefficient and infinite dilution activity coefficient in

water from the PR+COSMOSAC model," Fluid Phase Equilibria, volume 285, issue 1-2, pages 8-14. (SCI, EI)

8. **Hsieh, Chieh-Ming**; Lin, Shiang-Tai*, 2010, "Prediction of liquid–liquid equilibrium from the Peng–Robinson+COSMOSAC equation of state," Chemical Engineering Science, volume 65, issue 6, 1955-1963. (SCI, EI)

9. **Hsieh, Chieh-Ming**; Lin, Shiang-Tai*, 2010, "First-Principles Prediction of Vapor-Liquid-Liquid Equilibrium from the PR+COSMOSAC Equation of State," Industrial & Engineering Chemistry Research, in press.

10. **Hsieh, Chieh-Ming**; Sandler, Stanley I.; Lin, Shiang-Tai*, 2010, "Improvements of COSMO-SAC for vapor-liquid and liquid-liquid equilibrium predictions," Fluid Phase Equilibria, in press.

Conference Articles:

1. **Hsieh, Chieh-Ming**; Lin, Shiang-Tai, 2005, November, "Multiscale Computer Simulations for Prediction of Thermophysical Properties and Phase Equilibrium" in ChiChE Annual Meeting. Miao-Li, Taiwan.

2. **Hsieh, Chieh-Ming**; Lin, Shiang-Tai, 2008, November, "Determination of cubic equation of state parameters for pure and mixture fluids from first principle solvation calculations" in 2008 AIChE Annual Meeting. Philadelphia, PA, USA.

3. **Hsieh, Chieh-Ming**; Lin, Shiang-Tai, 2009, November, "Combination of Peng-Robinson equation of state and first principle solvation calculations in phase equilibrium prediction of pure and mixture fluids" in 2009 AIChE Annual Meeting. Nashville, TN, USA.

4. **Hsieh, Chieh-Ming**; Lin, Shiang-Tai, 2010, May, "Prediction of VLE, LLE, and VLLE using the Peng-Robinson+COSMOSAC equation of state" in 2010 The 12th international conference on Properties and Phase Equilibria for Product and Process Design (PPEPPD). Suzhou, Jiangsu, People Republic of China

Awards:

1. **Hsieh, Chieh-Ming**; Lin, Shiang-Tai, Champions in the 5th Industrial Fluid Properties Simulation Challenge, American Institute of Chemical Engineers Annual Meeting, Philadelphia, PA, U.S.A.. (2008/11/21)

2. **Hsieh, Chieh-Ming**, Graduate Students Study Abroad Program (2009), National Science Council (NSC) of Taiwan R.O.C.. (NSC 97-2917-I-002-118)